

Material Properties of Organic Liquids, Ices, and Hazes on Titan

XINTING YU (余馨婷)^{1,2}, YUE YU (于越)², JULIA GARVER,³ JIALIN LI (李嘉霖)³,
ABIGALE HAWTHORN,³ ELLA SCIAMMA-O'BRIEN,⁴ XI ZHANG,² AND ERIKA BARTH⁵

¹*Department of Physics and Astronomy, University of Texas at San Antonio
1 UTSA Circle
San Antonio, TX 78249, USA*

²*Department of Earth and Planetary Sciences, University of California Santa Cruz
1156 High St
Santa Cruz, CA 95064, USA*

³*Department of Physics, University of California Santa Cruz
1156 High St
Santa Cruz, CA 95064, USA*

⁴*NASA Ames Research Center, Space Science & Astrobiology Division, Astrophysics Branch
Moffett Field, CA 94035, USA*

⁵*Southwest Research Institute
1050 Walnut St Suite 300, Boulder, CO 80302, USA*

(Received September 6, 2022; Accepted March 14, 2023)

Submitted to ApJS

ABSTRACT

Titan has a diverse range of materials in its atmosphere and on its surface: the simple organics that reside in various phases (gas, liquid, ice) and the solid complex refractory organics that form Titan's haze layers. These materials all actively participate in various physical processes on Titan, and many material properties are found to be important in shaping these processes. Future in-situ exploration on Titan would likely encounter a range of materials, and a comprehensive database to archive the material properties of all possible material candidates will be needed. Here we summarize several important material properties of the organic liquids, ices, and the refractory hazes on Titan that are available in the literature and/or that we have computed. These properties include thermodynamic properties (phase change points, sublimation and vaporization saturation vapor pressure, and latent heat), physical property (density), and surface properties (liquid surface tensions and solid surface energies). We have developed a new database to provide a repository for these data and make them available to the science community. These data can be used as inputs for various theoretical models to interpret current and future remote sensing and in-situ atmospheric and surface measurements on Titan. The material properties of the simple organics may also

be applicable to giant planets and icy bodies in the outer solar system, interstellar medium, protoplanetary disks, and exoplanets.

Keywords: Titan — Saturnian satellites — Planetary atmospheres — Dwarf planets — Natural satellites (Solar system) — Surface ices — Planetary surfaces — Interstellar medium — Protoplanetary disks — Exoplanets

1. INTRODUCTION

The methane (CH_4) and nitrogen (N_2) in Titan’s upper atmosphere enable rich photochemistry, creating numerous organic molecules in Titan’s atmosphere. At least 18 organic species have been detected with space- and ground-based observations (for a list of the observed gaseous molecules, see Table 1 and Figure 1). The simple organic molecules that have been detected typically have six heavy atoms or less (C or N) and include a range of hydrocarbons and nitriles, e.g., ethane (C_2H_6), acetylene (C_2H_2), benzene (C_6H_6), hydrogen cyanide (HCN), cyanoacetylene (C_2N_2). Most of the simple organic molecules are in the gas phase when produced in the upper atmosphere. During their descent through the atmosphere, Titan’s unique temperature profile allows these gaseous organic molecules to condense into liquids or solids in its stratosphere, forming liquid or ice clouds (Sagan & Thompson 1984; Curtis et al. 2005; Anderson et al. 2018). Various types of organic clouds have been detected in Titan’s atmosphere through both ground-based and spacecraft observations by Voyager 1 and Cassini (Anderson et al. 2018; Vinatier et al. 2018, and references therein). The simple organic molecules in Titan’s atmosphere can further coagulate and react to form the complex refractory organic particles that constitute Titan’s thick haze layers (Tomasko et al. 2005).

It is expected that the organics in Titan’s atmosphere will eventually fall towards the surface of Titan. If they land on dry surfaces, species that are able to remain in the solid form will become surface sediments (see Figure 1). For example, Titan’s equatorial regions are largely covered by dunes (Lorenz et al. 2006), and the sand particles are likely derived from complex organic hazes falling from the atmosphere (Soderblom et al. 2007). Simple organics in the solid form have been detected on Titan’s surface, such as acetylene ice (Singh et al. 2016). At the same time, atmospheric species that remain in liquid forms, when they land on Titan’s dry surface, can modify and wet the surface by rainfalls and storms (e.g., Turtle et al. 2011). For organics that land on the surfaces of lakes and seas, the ones in liquid form would become part of the lake liquids, while the ones in solid form could either dissolve in the lake liquids, float on the lake surfaces, or sink and form lakebed sediments (Cordier & Carrasco 2019; Yu et al. 2020a). After the lake dries, the dissolved organics could precipitate as solids and form evaporites on Titan’s surface (Barnes et al. 2011; MacKenzie et al. 2014).

Because of the diverse range of temperature and pressure regimes that can exist on Titan, from its atmosphere to the base of its lakes and seas, it is anticipated that many organic species are present in multiple phases (gas, liquid, and solid phases). Lots of these species actively participate in various processes such as cloud formation, lake interaction, and sediment transport. The unique material properties of each species are found to play an important role in shaping these different processes (e.g., Barth & Toon 2003, 2006; Barth 2017; Lavvas et al. 2011; Anderson et al. 2018; Yu et al. 2018; Cordier & Carrasco 2019; Yu et al. 2020a,b; Comola et al. 2022; Lapôtre et al. 2022; Gunn & Jerolmack 2022; Li et al. 2022) and therefore represent critical input parameters to perform the required calculations to model these processes and prepare for the future in-situ explorations of Titan.

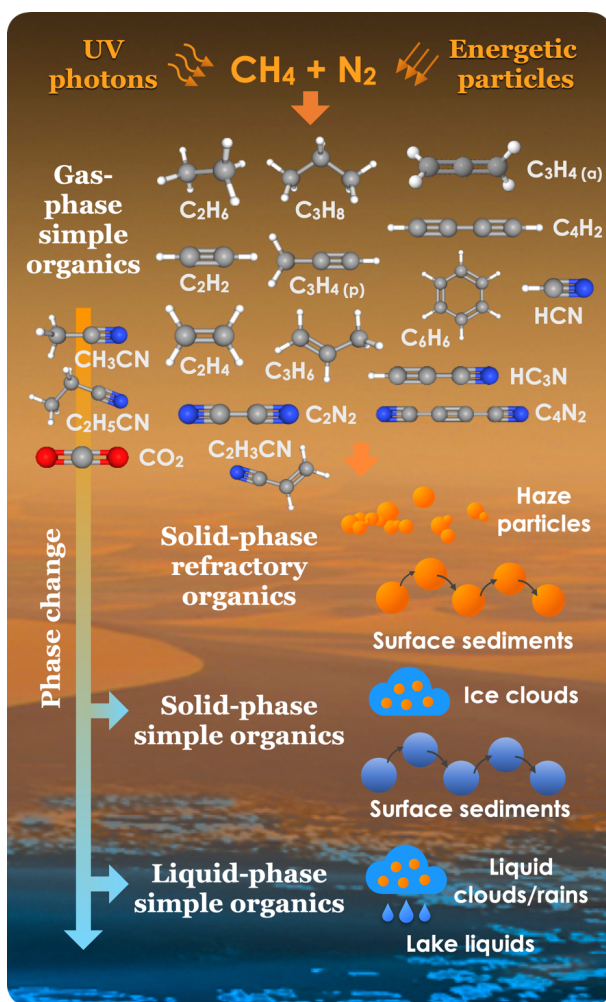


Figure 1. Photochemistry in Titan's upper atmosphere leads to the creation of numerous organic molecules, from simple organics in the gas phase to complex refractory organic solids that form Titan's thick haze layers. The simple organics could undergo phase changes, along with the complex organics, participate in various atmospheric and surface processes on Titan.

For example, the NASA New Frontiers mission Dragonfly, due to arrive at Titan in 2034, will be capable of investigating some of the material properties of the substances it will encounter through in-situ measurements (Barnes et al. 2021). Various material properties are also found to be crucial for the design of the rotorcraft to ensure its success in operation (Benkoski et al. 2019; Zacny et al. 2019). Thus, a comprehensive database to archive the material properties for all possible material candidates is timely and necessary to better model these processes and support the mission.

So far, there has been no consolidated database that is dedicated to summarizing the material properties of organics on Titan. For the simple organics, many of their material properties have been measured in the laboratory and can be found in published studies. However, these datasets have been scattered in the literature for over a century. Due to the sparseness of the data and the expansiveness of the literature involved, modern research studies often assume or estimate values for the material properties like, e.g., the density of simple organics (e.g., Brunetto et al. 2008; Lavvas et al. 2021), even though there are density measurements for many of the organic ices. Moreover, many properties

measured and published in the early 1900s do not have digitized copies, which makes the efforts to utilize these data even more difficult. We have developed a database that will serve as a repository for these published material properties of simple organics, and enable the use of more representative material properties in models. This database will also help identify the gaps between existing material property measurements and those needed for simple organics at Titan-relevant conditions, which will be crucial to guide future laboratory work.

For the complex organics, such as the atmospheric haze particles and the parent material for the organic sands on Titan’s surface, no sample returned from Titan is available. Therefore, laboratory-made organic aerosol analogs (“tholins”) have been used as the model material. The issue with the material properties of these tholins is different from that of the simple organics. Many laboratory facilities have been synthesizing tholins since the 1970s and have characterized them to different extents (see reviews by [Cable et al. \(2012\)](#) and [Hörst \(2017\)](#), and references therein; [Sciamma-O’Brien et al. \(2017\)](#); [He et al. \(2017\)](#); [Sebree et al. \(2018\)](#)). Even though most of the tholins are usually produced from the dominant gas constituents in Titan’s atmosphere, N_2 and CH_4 , a broad range of experimental conditions are used that can influence the material properties, including different energy sources, pressures, temperatures, gas exposure times, and gas flow rates. However, modern research studies often adopt the properties of tholins from one particular laboratory (e.g., [Witek & Czechowski 2015](#); [Schurmeier & Dombard 2018](#)). A recent comparative study has demonstrated that tholin samples indeed have varying properties based on their experimental production conditions ([Li et al. 2022](#)). In view of this recent comparative study, there remain several open questions about 1) whether or which tholins are representative of the actual complex organics on Titan; and 2) whether we can use the properties of tholins to constrain processes involving complex organics. Given that there will be no direct sample from Titan in the near future and that the Dragonfly mission will arrive and take measurements on Titan’s surface in the 2030s, we need to provide some material properties as baseline comparisons to the atmospheric hazes and the surface sediments on Titan. We think the best way to enable future science and prepare for Dragonfly is to archive all previously measured material properties of tholins along with their experimental production conditions. This will help us identify whether or not and which laboratory-produced tholins mimic the actual organic hazes/sediments on Titan. Before we find the best analog of Titan aerosols/sediments, it will be important for future modeling studies to include the uncertainty of material properties of tholins produced under different experimental conditions.

In this work, we summarize several important material properties of the simple and complex organics relevant to Titan’s exploration that we have aggregated from the literature or newly computed. For the simple organics, we focus on molecules that have already been detected in Titan’s stratosphere in the gas phase and may experience phase change on Titan. We also choose to include dicyanoacetylene (C_4N_2), which has been detected in the solid phase ([Khanna et al. 1987](#); [Anderson et al. 2016](#)), but only an upper limit was established for its gas phase ([Samuelson et al. 1997](#); [Jolly et al. 2015](#)). Some organic species are predicted by photochemical models to form in Titan’s atmosphere, but they have either not been detected (e.g., 1,3-butadiene, [Vuitton et al. \(2019\)](#); [Willacy et al. \(2016\)](#)) or only upper limits of their abundances are established (e.g., butane, [Steffens et al. \(2022\)](#), pyridine and pyrimidine, [Nixon et al. \(2020\)](#)). In this work, we choose not to include these molecules. Table 1 lists the molecules included in this work, their observed abundance ranges, and the associated references.

For the complex organics, we include existing material property measurements for tholins, their experimental production conditions, and measuring techniques. From here on, to differentiate between the simple organics in various phases and the complex refractory materials, analogs of solid haze particles, we will call the simple organics in the liquid and solid phases, “organic liquids” and “organic ices,” respectively, and the complex refractory materials as “organic solids.” The material properties investigated in this study include 1) thermodynamic properties (phase change pressure and temperature, saturation vapor pressure for organic liquids and ices, latent heat for vaporization for organic liquids, and latent heat for sublimation for organic ices); 2) physical property (density of organic liquids, ices, and solids), and 3) surface properties (liquid surface tensions for organic liquids and solid surface energies for organic ices and solids). These datasets can be used by the scientific community for modeling, data analysis, comparison to and interpretation of spacecraft observations and in-situ measurements, and preparation/development of future instrumentation.

Table 1. The 18 detected simple organic compounds included in this work and their stratospheric mixing ratios. The mixing ratios of gaseous organic compounds fluctuate seasonally in Titan’s atmosphere (e.g., Teanby et al. 2019). Here we adopt the largest possible range of mixing ratios encompassing past Cassini and ground-based observations. References: [1] Lellouch et al. (2014); [2] Niemann et al. (2010); [3] Teanby et al. (2019); [4] Lombardo et al. (2019); [5] Nixon et al. (2013); [6] Coustenis et al. (2016); [7] Coustenis et al. (2020); [8] Thelen et al. (2019); [9] Sylvestre et al. (2020); [10] Palmer et al. (2017); [11] Cordiner et al. (2015); [12] Jolly et al. (2015).

Compound name	CAS number	Mixing ratio range	Reference
Methane (CH ₄)	74-82-8	$1 \times 10^{-2} - 6 \times 10^{-2}$	[1,2]
Ethane (C ₂ H ₆)	74-84-0	$7 \times 10^{-6} - 3 \times 10^{-5}$	[3]
Ethylene (C ₂ H ₄)	74-85-1	$7 \times 10^{-8} - 6 \times 10^{-6}$	[3]
Acetylene (C ₂ H ₂)	74-86-2	$2 \times 10^{-6} - 1 \times 10^{-5}$	[3]
Diacetylene (C ₄ H ₂)	460-12-8	$9 \times 10^{-10} - 1 \times 10^{-7}$	[3]
Benzene (C ₆ H ₆)	71-43-2	$6 \times 10^{-11} - 2 \times 10^{-7}$	[6,7]
Propane (C ₃ H ₈)	74-98-6	$2 \times 10^{-7} - 3 \times 10^{-6}$	[6,7]
Propene (C ₃ H ₆)	115-07-1	$1 \times 10^{-9} - 6 \times 10^{-9}$	[5]
Allene (C ₃ H ₄ -a)	463-49-0	$6.9 \pm 0.8 \times 10^{-10}$	[4]
Propyne (C ₃ H ₄ -p)	74-99-7	$5 \times 10^{-9} - 1 \times 10^{-7}$	[3]
Hydrogen cyanide (HCN)	74-90-8	$4 \times 10^{-8} - 3 \times 10^{-4}$	[6]
Cyanoacetylene (HC ₃ N)	68010-34-4	$6 \times 10^{-11} - 9 \times 10^{-7}$	[3,7]
Carbon dioxide (CO ₂)	124-38-9	$1 \times 10^{-8} - 3 \times 10^{-8}$	[3]
Acetonitrile (CH ₃ CN)	75-05-8	$4 \times 10^{-10} - 1 \times 10^{-8}$	[8]
Propionitrile (C ₂ H ₅ CN)	107-12-0	$8 \times 10^{-10} - 3 \times 10^{-9}$	[11]
Acrylonitrile (C ₂ H ₃ CN)	107-13-1	$2 \times 10^{-10} - 8 \times 10^{-10}$	[10]
Cyanogen (C ₂ N ₂)	460-19-5	$5 \times 10^{-11} - 7 \times 10^{-9}$	[9]
Dicyanoacetylene (C ₄ N ₂)	1071-98-3	$< 5 \times 10^{-10}$	[12]

Recent experimental works have shown that a new class of minerals, the co-crystals, could form by co-condensing two or more molecules in Titan’s atmosphere or by co-precipitation on Titan’s

surface (see a review of Cable et al. 2021). While the co-crystals could also be important components of Titan, the associated laboratory studies are still in their infancy. Thus, in this work, we only include the material properties of pure substances. In the following sections, we describe the efforts associated with archiving and calculating each material property.

2. THERMODYNAMIC PROPERTIES

In the subsequent sections, we review and compute several important thermodynamic properties of organic liquids and ices for the 18 species detected on Titan. In Section 2.1, we summarize several phase change points of these substances. These phase change points allow us to determine what the physical state of these substances would be at a given pressure and temperature on Titan. In Section 2.2, we summarize and compute the sublimation saturation vapor pressure (s-g SVP) of the organic solids and the vaporization saturation vapor pressure (l-g SVP) of the organic liquids as a function of temperature, for each of the 18 organic species detected on Titan. The SVP can help determine the transformation of substances, e.g., when do a vapor reach saturation and form clouds (or when do a species transform from the gaseous state to the liquid or the solid state)? What is the humidity of a certain substance given the temperature and pressure of the location? Lastly, in Section 2.3, we compute the sublimation latent heats of the organic ices and the vaporization latent heats of the organic liquids for each of the 18 species at their triple point temperatures. The latent heats of these substances can not only help us understand the energy release/uptake during the phase transformation, but they are also useful in predicting other material properties of these substances (e.g., the surface energies of organic ices in Section 4.2).

2.1. Phase change points of organics liquids and ices for species detected on Titan

In Table 2, we summarize several phase change temperatures and pressures for the 18 simple organics listed in Table 1: the triple point temperature and pressure (T_{tri} and P_{tri}), the critical point temperature and pressure (T_{cri} and P_{cri}), and the crystalline ice phase transition temperature (T_{tran}) for applicable species. The triple point of a substance is defined as the temperature (T_{tri}) and pressure (P_{tri}) where the solid, liquid, and gas (vapor) phases can coexist, and it is also the intersection of the sublimation, fusion, and vaporization curves. The critical point of a substance is the temperature (T_{cri}) and pressure (P_{cri}) where the boundary between two phases vanishes. All the critical points in Table 2 represent the liquid-gas critical points, and beyond which a substance can be both in the liquid and the gas phase, or the so-called supercritical liquid. Note that on Titan, none of the 18 detected substances can reach their critical point. For organic ices, we only consider phase changes in the crystalline phase, when there is a sudden change in a crystal lattice structure. These phase transition temperatures are also summarized in Table 2 for selected crystal transitions. We do not take into consideration the amorphous-crystalline phase transitions in this table. For the known amorphous-crystalline transition information of the ices, see Table 18 in the Appendix section. Note that in Table 2, except for the few data points that are direct experimentally determined (Dannhauser & Flueckinger 1963; Putnam et al. 1965; Weber & Kilpatrick 1962; Finke et al. 1972), most of the phase transition temperatures are directly pulled from the published NIST/TRC Web Thermo Tables (WTT) database (Kroenlein et al. 2011), which are “determined using an average of a series of accepted experimental and predicted values, weighted by uncertainties.”

2.2. Saturation vapor pressures of organic liquids and ices for species detected on Titan

Table 2. Triple point temperature (T_{tri}) and pressure (P_{tri}), critical temperature (T_{cri}) and pressure (P_{cri}), and crystalline phase transition temperature (T_{tran}) for the 18 species detected on Titan include in this work (Table 1). Most of the triple point temperature, all of the critical point temperature and pressure, and most of the crystalline phase transition temperature data are from Kroenlein et al. (2011), which are averages of a series of accepted experimental and predicted values. The triple point temperature of HC_3N is estimated using experimental data from Dannhauser & Flueckinger (1963). The triple point pressures are calculated using saturation vapor pressure functions in Table 3. The crystalline phase transition temperatures of CH_3CN , $\text{C}_2\text{H}_5\text{CN}$, and $\text{C}_2\text{H}_3\text{CN}$ are experimental data from Putnam et al. (1965), Weber & Kilpatrick (1962), and Finke et al. (1972).

Species	T_{tri} (K)	P_{tri} (bar)	T_{cri} (K)	P_{cri} (bar)	T_{tran} (K)	Phase transition note
CH_4	90.686±0.010	0.117±0.001	190.564±0.010	45.992±0.073	20.509±0.047	crystal II-crystal I
C_2H_6	90.3560 ± 0.0050	$(1.1 \pm 0.1) \times 10^{-5}$	305.322±0.035	48.72±0.23	89.816±0.027 89.726±0.050	crystal II-crystal I crystal III-crystal II
C_2H_4	103.966±0.016	$(1.2 \pm 0.1) \times 10^{-3}$	282.350±0.025	50.417±0.068	N/A	N/A
C_2H_2	191.66±0.94	1.2±0.1	308.39±0.35	62.06±0.67	133.0±1.0	crystal II-crystal I
C_4H_2	237.7±2.5	0.13 ± 0.01	410±16	26.0±10.0	N/A	N/A
C_6H_6	278.6877±0.0023	$(4.7 \pm 0.1) \times 10^{-2}$	562.02±0.13	49.06±0.20	N/A	N/A
C_3H_8	85.400±0.054	$(1.8 \pm 0.2) \times 10^{-9}$	369.89±0.14	42.51±0.21	80.40±0.10	metastable crystal-crystal I
C_3H_6	87.850±0.020	$(8 \pm 1) \times 10^{-9}$	364.21±0.26	45.55±0.76	N/A	N/A
$\text{C}_3\text{H}_4\text{-a}$	136.70±0.53	$(1.8 \pm 0.1) \times 10^{-4}$	393.9±4.0	62.80±4.40	N/A	N/A
$\text{C}_3\text{H}_4\text{-p}$	169.87±0.77	$\sim 3.8 \times 10^{-3}$	402.7±1.5	56.58±0.81	N/A	N/A
HCN	259.871±0.091	0.1865 ± 0.0015	456.65±0.50	49.70±3.90	170.40±0.50	crystal II-crystal I
HC_3N	280±1	~ 0.25	527±11	52.00±27.00	N/A	N/A
CO_2	216.5890±0.0077	5.18 ± 0.01	304.128±0.038	73.77±0.20	N/A	N/A
CH_3CN	229.349±0.053	$\sim 1.9 \times 10^{-3}$	545.41±0.40	48.66±0.27	216.9±0.1	crystal II-crystal I
$\text{C}_2\text{H}_5\text{CN}$	180.4±1.2	$\sim 1.7 \times 10^{-6}$	561.26±0.20	42.60±0.89	176.964±0.005	crystal II-crystal I
$\text{C}_2\text{H}_3\text{CN}$	189.642±0.050	$(3.5 \pm 0.5) \times 10^{-5}$	540.0±2.0	46.50±2.80	162.50±0.10	crystal II-crystal I
C_2N_2	245.29±0.10	0.77 ± 0.03	397.1±3.0	62.50±4.00	N/A	N/A
C_4N_2	293.0±1.3	1.7×10^{-1}	496±22	66.00±55.00	N/A	N/A

In Table 3, we summarize the sublimation and vaporization saturation vapor pressures (SVPs) as functions of temperature for the gas-phase species observed in Titan’s atmosphere (Table 1). For consistency with previous work (Fray & Schmitt 2009), all the saturation vapor pressures (P_{sat}) are listed in units of bar, and the temperature in K. Most of the applicable temperature range starts (for vaporization equilibrium, or l-g) or ends (for sublimation equilibrium, or s-g) with the material’s triple point (see also Table 2). For the vaporization equilibrium (l-g), most of the applicable temperature range ends with the material’s critical point (see also Table 2). For each saturation vapor pressure function, we define the applicable temperature range as such: temperature values without brackets have existing laboratory measurement data, and temperature values with brackets apply for extrapolated SVPs beyond the laboratory-measured range. The idea is that users should be cautious when using extrapolated SVPs in the bracketed temperature range, as actual SVPs may significantly deviate from the extrapolated values. We use such notation hoping to provide directions for future laboratory efforts to fill in the gaps of the existing SVP measurements. Specifically, there are no reliable sublimation vapor pressure measurements for $\text{C}_3\text{H}_4\text{-p}$, C_3H_6 , C_3H_8 , CH_3CN , $\text{C}_2\text{H}_5\text{CN}$, and $\text{C}_2\text{H}_3\text{CN}$ ices, and more laboratory work is needed to directly measure the sublimation vapor pressure

of these ices at low temperatures. We attempt to establish sublimation vapor pressure functions for these species using thermodynamic and empirical approaches.

In this work, a total of six empirical mathematical functions are used to express SVPs (in bar) as a function of temperature (in K):

- The Antoine equation (Antoine 1888, used in Yaws 2015), where A , B , and C are empirically fitted for each compound:

$$P_{sat}(T) = 10^{A-B/(T+C)} \quad (1)$$

- The extended Antoine equation (Dykyj et al. 1999), where A , B , C , n , E , and F are empirically fitted for each compound, T_0 is the lower bound of the temperature, and T_{cri} is the critical temperature:

$$P_{sat}(T) = 10^{A-B/(T+C)+0.43429[(T-T_0)/T_{cri}]^n+E[(T-T_0)/T_{cri}]^8+F[(T-T_0)/T_{cri}]^{12}} \quad (2)$$

- The polynomial equation (used in Brown & Ziegler 1980; Fray & Schmitt 2009), where A_i s ($i = 0, 1, \dots, n$) are empirically fitted for each compound:

$$P_{sat}(T) = e^{A_0+\sum_{i=1}^n A_i/T^i}. \quad (3)$$

- The Kirchoff-Rankine equation (Kirchhoff 1858; Rankine 1966; Kroenlein et al. 2011), where A , B , and C are empirically fitted for each compound:

$$P_{sat}(T) = e^{A+B/T+C\ln T}. \quad (4)$$

- The Wagner equation (Wagner 1973, used in Kroenlein et al. 2011), where A_i s ($i = 1, 2, 3, 4$) are empirically fitted for each compound, and P_{cri} is the critical pressure:

$$P_{sat}(T) = P_{cri}e^{T_{cri}/T[A_1(1-T/T_{cri})+A_2(1-T/T_{cri})^{1.5}+A_3(1-T/T_{cri})^{2.5}+A_4(1-T/T_{cri})^5]}. \quad (5)$$

- The extended polynomial equation used in this work, where A_i s ($i = 0, 1, 2, \dots, 7$) are empirically fitted for each compound:

$$P_{sat}(T) = e^{A_0+A_1/T+A_2\ln(T)+A_3T+A_4T^{1.5}+A_5T^2+A_6T^3+A_7T^4}. \quad (6)$$

Most vapor pressure expressions are directly extracted from literature reviews or existing chemical databases (Brown & Ziegler 1980; Dykyj et al. 1999; Fray & Schmitt 2009; Kroenlein et al. 2011; Yaws 2015). Note that we only select to present one set of vapor pressure functions for each phase change of each species. Among existing SVP expressions for a given species, we typically select the one that has the largest applicable temperature range or that best fits the experimental measurements in a broad range of temperatures (see Figures 3-6 in the Appendix section). For example, for the sublimation SVP of C_6H_6 ice, we choose to present the expression by Dykyj et al. (1999), not the others (Fray & Schmitt 2009; Kroenlein et al. 2011; Růžička et al. 2014; Dubois et al. 2021; Hudson et al. 2022), as Dykyj et al. (1999)'s expression best fits the most recent low-temperature measurements of Hudson et al. (2022), the adjusted low-temperature measurements of Dubois et al. (2021) ($130 < T < 160$ K), and previous high-temperature measurements ($T > 150$ K). We also rated the approximate order of

accuracy of the adopted SVP functions in Table 3. The SVP expressions with ratings of A⁺, A, and B typically have good agreements with laboratory-measured data (<10 %) within the temperature range without brackets. The accuracy of SVP expressions with ratings of C and D are lower (>10 %), due to the larger spread and/or the large uncertainties of the existing laboratory data. More laboratory measurements are needed to help improve the accuracy of these SVPs.

Table 3. Adopted saturation vapor pressure expressions (P_{sat}) as functions of temperature (T) for species in Table 1, s-g represents solid-gas transitions and l-g represents liquid-gas transitions. The “Temp. (K)” column indicates the temperature range for which the SVP functions can be applied. Note that temperature ranges with brackets correspond to temperatures for which only extrapolated SVPs are available, and temperatures without brackets have experimentally determined SVPs in the temperature range. References: [a] Dykyj et al. (1999); [b] Yaws (2015); [c] Fray & Schmitt (2009); [d] Kroenlein et al. (2011); [e] Orton et al. (2014); [f] this work; [g] Dannhauser & Flueckinger (1963); [h] Duschek et al. (1990). The “Accuracy” column gives the accuracy rating of the fittings within the temperature range where experimental data exist in the form of a rating. The ratings consist of five letters. Each letter corresponds to the rough order of accuracy of the fittings to the experimental data: A⁺ (0.1-1 %), A (1-5 %), B (5-10 %), C (10-50 %), D (>50 %).

Species	Type	Saturation vapor pressure expressions $P_{sat}(T)$ (bar)	Temp. (K)	Ref.	Accuracy
CH ₄	s-g	$10^{4.31972-451.64/(T-4.66)}$	[20.509]-48-90.686 (T_{tri})	[a]	48-70 K, C 70 K- T_{tri} , A
	l-g	$10^{3.96867-435.453/(T-1.789)}$	90.686-190.564 (T_{cri})	[b]	A
C ₂ H ₆	s-g	$10^{6.6388-1009.6/(T-3.15)}$	[<]71-90.3560 (T_{tri})	[a]	C
	l-g	$10^{4.0768-698.93/(T-12.886)}$	90.3560-305.322 (T_{cri})	[b]	B
C ₂ H ₄	s-g	$e^{15.4-2206/T-1.216\times 10^4/T^2+2.843\times 10^5/T^3-2.203\times 10^6/T^4}$	[<]77.3-103.966 (T_{tri})	[c]	C
	l-g	$10^{3.82898-581.901/(T-17.787)}$	103.966-122	[a]	C
	l-g	$10^{3.91382-596.526/(T-16.78)}$	122-174	[a]	B
	l-g	$10^{3.91382-596.526/(T-16.78)+0.43429((T-174)/T_{cri})^{2.79132}+9.717((T-174)/T_{cri})^8+52.77((T-174)/T_{cri})^{12}}$	174-282.350 (T_{cri})	[a]	A
C ₂ H ₂	s-g	$e^{13.4-2536/T}$	[<]98.55-191.66 (T_{tri})	[c]	B
	l-g	$62.06e^{T_{cri}/T[-7.5718(1-T/T_{cri})+3.1025(1-T/T_{cri})^{1.5}-3.4594(1-T/T_{cri})^{2.5}+0.32221(1-T/T_{cri})^5]}$	191.66-308.39 (T_{cri})	[d]	A
C ₄ H ₂	s-g	$10^{7.3757-1958.25/T}$	[<]127-237.7 (T_{tri})	[e]	D
	l-g	$e^{10.600-3007.6/T}$	237.7-410 (T_{cri})	[d]	C
C ₆ H ₆	s-g	$10^{6.72391-2107.85/(T-16.45)}$	[<]134.8-278.6877 (T_{tri})	[a]	B
	l-g	$10^{3.98523-1184.236/(T-55.623)}$	278.6877-376	[a]	C
	l-g	$10^{3.98523-1184.236/(T-55.623)+0.43429((T-376)/T_{cri})^{2.3835}+12.283((T-376)/T_{cri})^8+664.01((T-376)/T_{cri})^{12}}$	376-562.02 (T_{cri})	[a]	B
C ₃ H ₈	s-g	$e^{17.802-2985/T-3.423\times 10^4/T^2+1.163\times 10^6/T^3-1.488\times 10^7/T^4}$	[50.0]-[85.400] (T_{tri})	[f]	N/A
	l-g	$10^{4.1451-889.864/(T-16.066)}$	85.400-369.89 (T_{cri})	[b]	B
C ₃ H ₆	s-g	$e^{16.425-2691/T-5.291\times 10^4/T^2+1.858\times 10^6/T^3-2.481\times 10^7/T^4}$	[50.0]-[87.850] (T_{tri})	[f]	N/A
	l-g	$10^{4.1322-859.722/(T-17.255)}$	87.850-364.21 (T_{cri})	[b]	B
C ₃ H ₄ -a	s-g	$10^{6.7534-1434.94/T}$	[<]106-136.70 (T_{tri})	[a]	B
	l-g	$62.80e^{T_{cri}/T[-8.4862(1-T/T_{cri})+5.4394(1-T/T_{cri})^{1.5}-5.3149(1-T/T_{cri})^{2.5}+0.70544(1-T/T_{cri})^5]}$	136.70-393.9 (T_{cri})	[d]	C
C ₃ H ₄ -p	s-g	$e^{16.795-3799.6/T}$	[<]169.87] (T_{tri})	[f]	N/A
	l-g	$10^{4.2817-923.311/(T-32.071)}$	169.87-402.7	[b]	B
HCN	s-g	$e^{54.889-5969.5/T-6.0411\ln T}$	[<]194.565-259.871 (T_{tri})	[d]	A
	l-g	$10^{4.8607-1432.7/(T-3.7358)}$	259.871-456.65 (T_{cri})	[f]	A
HC ₃ N	s-g	$10^{9.0744-3046.5/(T+36.176)}$	[<]164.9-280 (T_{tri})	[f]	B
	l-g	$10^{4.6649-1470/T}$	280-315-527] (T_{cri})	[g]	C
CO ₂	s-g	$e^{20.0456-3274.96/T-0.6102\ln(T)}$	[<]69.697-216.5890 (T_{tri})	[d]	B
	l-g	$73.77e^{T_{cri}/T[-7.0206(1-T/T_{cri})+1.5072(1-T/T_{cri})^{1.5}-2.1863(1-T/T_{cri})^{2.5}-3.0645(1-T/T_{cri})^5]}$	216.5890-304.128 (T_{cri})	[h]	A ⁺
CH ₃ CN	s-g	$e^{21.542-5853.5/T-6.9785\times 10^{-3}T-1.9407\times 10^{-4}T^{1.5}}$	[20]-[216.9]	[f]	N/A
	s-g	$e^{23.405-5655.0/T-0.72971\ln(T)-1.6902\times 10^{-3}T-1.9407\times 10^{-4}T^{1.5}}$	[216.9]-[229.349] (T_{tri})	[f]	N/A
	l-g	$10^{4.6691-1583.4/(T-15.263)}$	229.349-545.41 (T_{cri})	[b]	B
C ₂ H ₅ CN	s-g	$e^{25.869-6428.6/T-2.1410\times 10^{-2}T-2.0625\times 10^{-4}T^{1.5}+2.7238\times 10^{-5}T^2}$	[15]-[176.964]	[f]	N/A
	s-g	$e^{-366.46+436.73/T+75.442\ln(T)-0.22541T-2.0625\times 10^{-4}T^{1.5}}$	[176.964]-[180.4] (T_{tri})	[f]	N/A
	l-g	$42.60e^{T_{cri}/T[-8.1477(1-T/T_{cri})+2.4460(1-T/T_{cri})^{1.5}-2.5323(1-T/T_{cri})^{2.5}-2.4144(1-T/T_{cri})^5]}$	180.4-561.26 (T_{cri})	[d]	B
C ₂ H ₃ CN	s-g	$e^{23.485-5879.0/T-1.1719\times 10^{-2}T-1.0523\times 10^{-5}T^2+5.0429\times 10^{-9}T^3-1.1612\times 10^{-12}T^4}$	[12.5]-[162.5]	[f]	N/A
	s-g	$e^{20.897-5583.8/T-4.1416\times 10^{-2}\ln(T)-5.6792\times 10^{-3}T-1.0523\times 10^{-5}T^2+5.0429\times 10^{-9}T^3-1.1612\times 10^{-12}T^4}$	[162.5]-[189.642] (T_{tri})	[f]	N/A
	l-g	$10^{4.5332-1477.29/(T-24.71)}$	189.642-540.0 (T_{cri})	[b]	B
C ₂ N ₂	s-g	$e^{16.53-4109/T}$	[<]156.3-245.29 (T_{tri})	[c]	B
	l-g	$62.50e^{T_{cri}/T[-7.0700(1-T/T_{cri})+0.019087(1-T/T_{cri})^{1.5}-0.13088(1-T/T_{cri})^{2.5}-3.7467(1-T/T_{cri})^5]}$	245.29-397.1 (T_{cri})	[d]	B
C ₄ N ₂	s-g	$e^{19.09-6036/T}$	[125.0]-147.0-273.2-[293.0] (T_{tri})	[c]	D
	l-g	$10^{3.6326-1156.9/(T-30.398)}$	[293.0]-296.0-349.7-[496] (T_{cri})	[f]	A ⁺

Note that extra caution is always needed when using any SVP expressions beyond the temperature range for which measurements are available, as those are extrapolations to the existing data to estimate the behavior of the material at lower temperatures. By comparing the existing SVP functions in Table 3 and in the Appendix Table 15, we found that the different SVP functions typically agree well with each other within the temperature range with laboratory measurements and start to deviate (up to orders of magnitude) towards lower temperatures, where no or few SVP measurements have been made. Barth (2019, submitted) also summarizes a comprehensive sublimation SVP and latent heat database that compares adopted vapor pressure functions from various literature sources, focusing on a range of general hydrocarbons and nitriles in the outer solar system; while the work presented here focuses on all the already detected gas-phase species in Titan’s atmosphere.

In this work, we also introduce new SVP functions for C_3H_8 (s-g), C_3H_6 (s-g), C_3H_4 -p (s-g), HCN (l-g), HC_3N (s-g), CH_3CN (s-g), C_2H_5CN (s-g), C_2H_3CN (s-g), and C_4N_2 (l-g). Some of these new SVP functions are fitted using more comprehensive experimental data (HCN l-g, HC_3N s-g, and C_4N_2 l-g) using the Antoine equation 1, and some are theoretically calculated using thermodynamic and empirical approaches as no direct SVP measurements at cryogenic temperatures are available in the literature (C_3H_8 s-g, C_3H_6 s-g, C_3H_4 -p s-g, CH_3CN s-g, C_2H_3CN s-g, and C_2H_5CN s-g).

- For HCN, we least-square fit its l-g SVP expression using data from Bredig & Teichmann (2005); Perry & Porter (1926); Sinozaki et al. (1926).
- For HC_3N , we least-square fit its s-g SVP expression using data from Dannhauser & Flueckinger (1963); Benilan et al. (1994); Rumble (2020).
- For C_4N_2 , we least-square fit its l-g SVP expression using data from Saggiomo (1957).
- For C_3H_6 and C_3H_8 , Yarbrough & Tsai (1978) theoretically computed the sublimation vapor pressure and latent heat from 50 K up to the triple points of the two species using the thermodynamic approach. This allows us to derive the s-g SVP functions for C_3H_6 and C_3H_8 , by least-square fitting the computed data using fourth-degree polynomials.
- For CH_3CN , C_2H_5CN , and C_2H_3CN , we are able to derive their sublimation vapor pressure as a function of temperature using the thermodynamic approach presented in Fray & Schmitt (2009). The phase equilibrium for a pure substance is given by the Clausius-Clapeyron equation:

$$\frac{dP_{sub}(T)}{dT} = \frac{L_{sub}(T)}{T(V_v - V_s)}, \quad (7)$$

where $P_{sub}(T)$ is the sublimation saturation vapor pressure of a species, $L_{sub}(T)$ is the molar sublimation latent heat or enthalpy as a function of temperature (with a unit of $J \cdot mol^{-1}$). The latent heat is the heat absorbed when a pure substance transfers from the solid to the vapor phase at constant pressure. V_v and V_s are the molar volumes of the vapor and the solid phase. The volume of the condensed phase is typically much less significant compared to the volume of the vapor phase, thus, we may assume $V_v \gg V_s$. If we also assume the gas follows perfect gas behavior, the volume of the vapor phase can be expressed using the ideal gas law ($V_v = RT/P$), where R is the universal gas constant ($8.314 J \cdot K^{-1} mol^{-1}$). The Clausius-Clapeyron equation can be approximated as:

$$\frac{dP_{sub}(T)}{P_{sub}} = \frac{L_{sub}(T)dT}{RT^2}, \quad (8)$$

This allows us to integrate Equation 8 to obtain the sublimation vapor pressure of a species:

$$\ln(P_{sub}(T)) = \int_{T_0}^T \frac{L_{sub}(T')}{RT'^2} dT' + \ln(P_{sub}(T_0)). \quad (9)$$

If we know the sublimation vapor pressure at a certain temperature T_0 and the sublimation latent heat as a function of temperature $L_{sub}(T)$, we can compute the sublimation pressure of a species as a function of temperature. For CH_3CN , $\text{C}_2\text{H}_5\text{CN}$, and $\text{C}_2\text{H}_3\text{CN}$, we choose the triple point temperature and pressure calculated using the vaporization vapor pressure function, then we need to determine their latent heat of sublimation as a function of temperature, which can be written as:

$$L_{sub}(T) = H_v(T) - H_s(T), \quad (10)$$

where $H_v(T)$ and $H_s(T)$ are the enthalpies of the species in the gas and solid phase. For an ideal gas, $H_v(T) = \int_{T_0}^T C_{p,v}(T') dT' + H_v(T_0)$, and for the solid $H_s(T) = \int_{T_0}^T C_{p,s}(T') dT' + H_s(T_0)$, where $C_{p,v}(T)$ and $C_{p,s}(T)$ are the molar heat capacities of the gas and the solid (with a unit of $\text{J}\cdot\text{K}^{-1}\text{ mol}^{-1}$). Thus we can rewrite the latent heat as:

$$L_{sub}(T) = \int_{T_0}^T (C_{p,v}(T') - C_{p,s}(T')) dT' + L_{sub}(T_0). \quad (11)$$

For CH_3CN , $\text{C}_2\text{H}_5\text{CN}$, and $\text{C}_2\text{H}_3\text{CN}$, we are able to find their solid molar heat capacity data ($C_{p,s}(T)$) measured at cryogenic temperatures below the triple point and the computed gas molar heat capacity data ($C_{p,v}(T)$). These data are least-square fitted to facilitate integration in Equation 11. We also need the latent heat of sublimation at a certain temperature in Equation 11. In this case, we choose the triple point of CH_3CN , $\text{C}_2\text{H}_5\text{CN}$, and $\text{C}_2\text{H}_3\text{CN}$. Because the latent heat of sublimation is the summation of the latent heat of fusion and vaporization, $L_{sub} = L_{fus} + L_{vap}$, we can use the latent heat of fusion measured at the triple point $L_{fus}(T_{tri})$ and the latent heat of vaporization $L_{vap}(T_{tri})$ computed using the vaporization vapor pressure function to obtain the latent heat of sublimation at the triple point $L_{sub}(T_{tri})$. The fitted molar heat capacity functions and latent heat data needed to perform the s-g SVP integration for CH_3CN , $\text{C}_2\text{H}_5\text{CN}$, and $\text{C}_2\text{H}_3\text{CN}$ are summarized in Table 4.

- For $\text{C}_3\text{H}_4\text{-p}$, the only existing sublimation vapor pressure measurement for its solid phase is likely measured upon supercooled C_3H_4 liquid (see discussion in [Fray & Schmitt 2009](#)). We are unable to locate any heat capacity data for solid $\text{C}_3\text{H}_4\text{-p}$. Thus, we cannot use the above thermodynamic approach to calculate its sublimation saturation vapor pressure. [Daubert & Danner \(1989\)](#) estimated the latent heat of fusion of $\text{C}_3\text{H}_4\text{-p}$ using the method of [Chickos et al. \(1991\)](#). This allows us to empirically derive the sublimation saturation vapor pressure function of $\text{C}_3\text{H}_4\text{-p}$. We start with Equation 9, where we choose the triple point temperature and pressure calculated using the vaporization vapor pressure function. Then by assuming a constant latent heat of sublimation independent of temperature $L_{sub}(T) = L_{sub}(T_{tri})$, we can directly integrate Equation 9 using the sum of the latent heat of fusion (L_{fus}) provided by [Daubert & Danner \(1989\)](#) and the latent heat of vaporization (L_{vap}) calculated by using the vaporization SVP function of [Yaws \(2015\)](#) ($L_{sub} = L_{fus} + L_{vap}$).

Table 4. Selected property values for CH₃CN, C₂H₅CN, and C₂H₃CN for s-g SVP calculations through the thermodynamic approach and for C₃H₄-p through the empirical approach. The notations in the “Acc” (accuracy) column are the same as Table 3.

CH ₃ CN selected property value	Unit	Reference	Acc.
$C_{p,s1}(T) = 0.30962T + 6.0668, 216.9 < T < 229.349 (T_{tri})$	J·K ⁻¹ mol ⁻¹	Putnam et al. (1965)	A ⁺
$C_{p,s2}(T) = 0.39755T, 20 < T < 216.9$	J·K ⁻¹ mol ⁻¹	Putnam et al. (1965)	C
$C_{p,v}(T) = -6.0507 \times 10^{-3}T^{1.5} + 0.28151T, 0 < T < 900$	J·K ⁻¹ mol ⁻¹	Krishna Pillai & Cleveland (1961)	B
$L_{vap}(T_{tri}) = 34.79$	kJ·mol ⁻¹	Yaws (2015)	
$L_{fus}(T_{tri}) = 8.17$	kJ·mol ⁻¹	Putnam et al. (1965)	
$T_{tran} = 216.9$	K	Putnam et al. (1965)	
$L_{trans}(T_{transition}) = 0.898$	kJ·mol ⁻¹	Putnam et al. (1965)	
C ₂ H ₅ CN selected property value	Unit	Reference	
$C_{p,s1}(T) = 4.1003T - 627.22, 176.964 < T < 180.4 (T_{tri})$	J·K ⁻¹ mol ⁻¹	Weber & Kilpatrick (1962)	A ⁺
$C_{p,s2}(T) = -1.3588 \times 10^{-3}T^2 + 0.70822T, 15 < T < 176.964$	J·K ⁻¹ mol ⁻¹	Weber & Kilpatrick (1962)	C
$C_{p,v}(T) = -6.4302 \times 10^{-3}T^{1.5} + 0.35221T, 0 < T < 600$	J·K ⁻¹ mol ⁻¹	Duncan & Janz (1955)	A ⁺
$L_{vap}(T_{tri}) = 42.36$	kJ·mol ⁻¹	Kroenlein et al. (2011)	
$L_{fus}(T_{tri}) = 5.05$	kJ·mol ⁻¹	Weber & Kilpatrick (1962)	
$T_{tran} = 176.964$	K	Weber & Kilpatrick (1962)	
$L_{trans}(T_{transition}) = 1.71$	kJ·mol ⁻¹	Weber & Kilpatrick (1962)	
C ₂ H ₃ CN selected property value	Unit	Reference	
$C_{p,s1}(T) = 0.42969T + 0.34433, 162.50 < T < 189.642 (T_{tri})$	J·K ⁻¹ mol ⁻¹	Finke et al. (1972)	A
$C_{p,s2}(T) = 0.53012T, 12.5 < T < 162.50$	J·K ⁻¹ mol ⁻¹	Finke et al. (1972)	C
$C_{p,v}(T) = -1.9309 \times 10^{-10}T^4 + 5.0312 \times 10^{-7}T^3 - 5.2491 \times 10^{-4}T^2 + 0.33526T, 0 < T < 1000$	J·K ⁻¹ mol ⁻¹	Finke et al. (1972)	A
$L_{vap}(T_{tri}) = 37.39$	kJ·mol ⁻¹	Yaws (2015)	
$L_{fus}(T_{tri}) = 6.23$	kJ·mol ⁻¹	Finke et al. (1972)	
$T_{tran} = 162.50$	K	Finke et al. (1972)	
$L_{tran}(T_{transition}) = 1.19$	kJ·mol ⁻¹	Finke et al. (1972)	
C ₃ H ₄ -p selected property value	Unit	Reference	
$L_{vap}(T_{tri}) = 26.24$	kJ·mol ⁻¹	Yaws (2015)	
$L_{fus}(T_{tri}) = 5.35$	kJ·mol ⁻¹	Daubert & Danner (1989)	

Using the saturation vapor pressure functions in Table 3 and species abundances in Table 1, we can now construct condensation curves for all the detected gas-phase species in Titan’s atmosphere. We plot the condensation curves using the ratio between the saturation vapor pressure expressions ($P_{sat}(T)$) and the mixing ratios of each species (X). In Figure 2, we show the condensation curves for all 18 detected gas-phase organic species (Table 1). Condensation occurs when the condensation curve of one species intersects the pressure-temperature (P-T) profile. To account for the seasonal and latitudinal changes on Titan, in addition to the mean P-T profile (shown as the solid black curve in Figure 2), we also include the possible range of P-T profile using the retrieved Cassini/Composite Infrared Spectrometer (CIRS) data (see the supporting information of Teanby et al. 2019), which is marked as the shaded grey region. Note that the P-T profile measured by the Huygens-Atmospheric Structure Instrument (HASI) (Fulchignoni et al. 2005) is closer to the lower limit of the P-T profiles of Teanby et al. (2019). We choose to present the data of Teanby et al. (2019) because Cassini/CIRS measurements are most sensitive to the stratospheric temperature (10^{-2} to 10^{-4} bar), and the data covers the entire Cassini mission, taking into account temporal and latitudinal variations of the P-T profiles. Solid condensation curves represent solid-gas (s-g) transitions, and dashed lines represent liquid-gas (l-g) transitions. We also include the possible seasonal/latitudinal variations of the abundances of each species by using the largest possible range of stratospheric mixing ratios of each species, as provided in Table 1, to compute the condensation curves. The variation of the condensa-

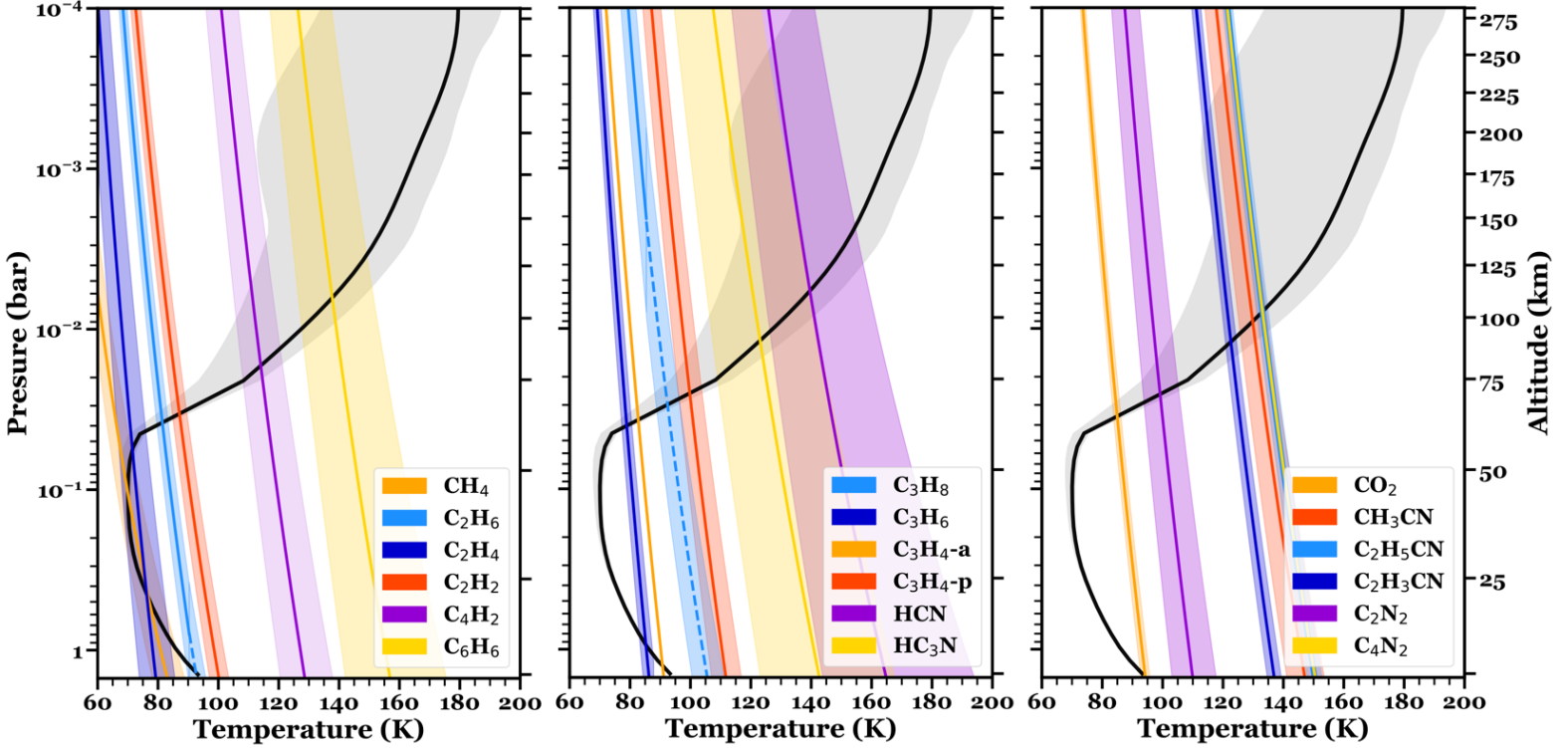


Figure 2. Condensation curves for detected gaseous organic species in Titan’s atmosphere. The black line in each panel represents Titan’s mean temperature profile, and the shaded grey area represents the range of retrieved temperature profiles using Cassini/CIRS data throughout the Cassini mission (Teanby et al. 2019). Note that the altitude axis on the right represents the altitude for the mean temperature-pressure profile. The solid condensation curves are plotted with the average mixing ratio, and the shaded regions are plotted using the observed upper and lower bond mixing ratios listed in Table 1. Solid condensation curves represent solid-gas (s-g) transitions and dash lines represent liquid-gas transitions (l-g). (left) Condensation curves for CH_4 , C_2H_6 , C_2H_4 , C_2H_2 , C_4H_2 , and C_6H_6 . (center) Condensation curves for C_3H_6 , C_3H_8 , C_3H_4 -a (allene), C_3H_4 -p (propyne), HCN , and HC_3N . (right) Condensation curves for CO_2 , CH_3CN , $\text{C}_2\text{H}_5\text{CN}$, $\text{C}_2\text{H}_3\text{CN}$, C_2N_2 , and C_4N_2 .

tion curves is represented by the shaded regions with the same color as the condensation curve for each compound. Note that we used vertically constant mixing ratios to plot these condensation curves. However, since most of the species condense in and below the stratosphere, the stratospheric mixing ratios ($\sim 10^{-2}$ - 10^{-3}) we used should closely reflect the mixing ratio of each species before condensation. Based on Figure 2, all the 18 observed gas-phase species would condense in the stratosphere of Titan’s atmosphere. While most species would condense as ices (with the solid black condensation curves intersecting the P-T profile), C_3H_8 from the upper atmosphere and evaporated C_2H_6 from Titan’s surface would condense as liquids (with their dashed condensation curve intersecting the P-T profile).

In Table 5, we summarize the mean condensation temperature (T_{cond}) and pressure (P_{cond}) for each species, i.e., the intersecting temperature and pressure of the mean P-T profile and condensation curve constructed with the mean mixing ratio of a species. We also summarize the maximum and minimum condensation temperature, pressure, and altitude given the varying P-T profile and condensation curves due to the variation of species abundances. Note that in this work, we only consider the

Table 5. Condensation temperatures, pressures, and altitudes for each species identified on Titan (Table 1). We extract the mean-, min-, and max condensing temperatures (T_{cond}), pressures (P_{cond}), and altitudes (h_{cond}) at the intersections of the condensation curves and Titan’s mean-, min-, and max P-T profile in Figure 2, respectively.

Species	T_{cond} (K)			P_{cond} (mbar)			h_{cond} (km)		
	Mean	Min	Max	Mean	Min	Max	Mean	Min	Max
CH ₄	70.0	69.1	71.9	1.1×10^2	0.45×10^2	1.8×10^2	44.8	36.1	57.3
	76.9	71.9	86.4	0.48×10^3	0.18×10^3	1.0×10^3	20.3	6.14	36.1
C ₂ H ₆ (ice)	81.5	79.2	83.4	38	30	41	61.5	60.7	64.4
C ₂ H ₆ (liquid)	92.5	89.3	93.0	1.4×10^3	1.2×10^3	1.4×10^3	0.998	0.000	3.99
C ₂ H ₄	71.6	67.7	76.1	0.57×10^2	0.38×10^2	1.5×10^2	54.6	39.2	60.2
C ₂ H ₂	87.1	84.3	89.5	34	25	37	63.8	62.5	68.4
C ₄ H ₂	114	106	121	17	2.8	23	80.2	72.9	122
C ₆ H ₆	138	119	151	6.4	0.077	13	109	89.0	234
C ₃ H ₈ (liquid)	91.6	87.6	95.6	30	20	35	66.0	63.9	73.0
C ₃ H ₆	78.9	77.1	80.6	40	33	43	60.5	59.8	62.8
C ₃ H ₄ -a	82.7	82.1	83.0	37	30	39	62.0	61.7	64.3
C ₃ H ₄ -p	99.7	95.2	104	25	12	30	70.0	67.3	84.5
HCN	140	117	157	5.8	0.058	14	112	87.8	244
HC ₃ N	123	106	141	12	0.19	23	89.8	73.3	204
CO ₂	85.0	83.3	86.3	35	27	38	62.9	62.2	66.3
CH ₃ CN	130	117	135	9.0	0.21	14	98.1	87.1	200
C ₂ H ₅ CN	133	122	136	7.9	0.20	11	102	93.1	202
C ₂ H ₃ CN	123	113	125	12	0.41	16	89.4	82.5	180
C ₂ N ₂	99.2	93.1	105	26	11	31	69.7	66.2	87.0
C ₄ N ₂	133	123	134	7.9	0.22	11	102	94.9	199

condensation curves of pure species. It has been shown that nitrogen dissolved in methane/ethane serves as an anti-freezer (Atreya et al. 2006; Wang et al. 2010). Because of this effect, it is expected that methane condenses as a liquid near the surface of Titan and that methane ice clouds only form higher in the atmosphere (~ 20 -30 km) where the temperature falls below the freezing point of the CH₄-N₂ mixture and N₂ exsolves from the mixture (Thompson et al. 1992; Tokano et al. 2006; Wang et al. 2010). This highlights the importance of determining the saturation vapor pressure for mixed species in the laboratory, especially ternary mixtures, see theoretical calculations in (Cordier et al. 2017; Tan & Kargel 2018) and some preliminary experimental works (Chevrier et al. 2015; Hanley et al. 2016).

2.3. Latent heats of organic liquids and ices for species detected on Titan

The latent heat for each condensate (L) can be found using the Clausius-Clapeyron equation (or Equation 7):

$$L_{vap/sub} = T(V_v - V_c) \frac{dP_{sat}(T)}{dT}, \quad (12)$$

where V_c is the volume of the condensed phase (solid or liquid). The sublimation or vaporization latent heat (L_{sub} or L_{vap}) has a unit of $\text{J}\cdot\text{mol}^{-1}$, though it is usually expressed in unit of $\text{kJ}\cdot\text{mol}^{-1}$. When the gas follows ideal gas behavior ($V_v = RT/P$) and the volume of the condensed phase is insignificant compared to the vapor phase ($V_v \gg V_c$), Equation 12 can be reduced to:

$$L_{vap/sub} = \frac{RT^2}{P_{sat}(T)} \frac{dP_{sat}(T)}{dT}. \quad (13)$$

When the vapor phase no longer behaves like an ideal gas law, typically towards low temperature and high pressure where intermolecular forces and the volume of the gas molecules are not negligible, we can use the van der Waals equation of state to calculate the volume of the vapor phase V_v in Equation 12:

$$(P_{sat}(T) + a/V_v^2)(V_v - b) = RT, \quad (14)$$

where a and b are empirical van der Waals constants for each substance. The van der Waals constants of the 18 Titan-relevant species considered in this study are listed in Table 6. Note that the appropriate universal gas constant to be used here, which corresponds with the unit of the van der Waals constants in Table 6, is $0.08314 \text{ L}\cdot\text{bar}\cdot\text{K}^{-1}\cdot\text{mol}^{-1}$. For C_4H_2 , HC_3N , and C_4N_2 , their van der Waals constants are calculated using their critical temperatures (T_{cri}) and pressures (P_{cri}) listed in Table 2:

$$a = \frac{27R^2T_{cri}^2}{64P_{cri}} \quad \text{and} \quad b = \frac{RT_{cri}}{8P_{cri}}. \quad (15)$$

As an example, the ideal gas assumption does not hold for the air on the surface of Titan compared to Earth due to the lower temperature (94 K versus 300 K) and higher pressure (1.5 bar versus 1 bar). The volume of gas near the surface of Titan (assuming it is a mixture of 95 % N_2 and 5 % CH_4 at 94 K, 1.5 bar) calculated using the ideal gas law is 2.87 % higher than the actual gas volume calculated using the van der Waals equation. While for air near the surface of Earth (assuming 80 % N_2 and 20 % O_2 at 300 K, 1 bar), the volume of air assuming ideal gas is only 0.07 % higher than the actual gas volume.

In this work, we calculated latent heats of sublimation ($L_{sub}(T_{tri})$) and vaporization ($L_{vap}(T_{tri})$) at the triple point of each substance. Considering the volume of the condensed phase negligible compared to the vapor phase, we use the following equation and Equation 14 to calculate the latent heats:

$$L_{vap/sub} = TV_v \frac{dP_{sat}(T)}{dT}. \quad (16)$$

The saturation vapor pressure functions, $P_{sat}(T)$ are listed in Table 3 and the van der Waals constants are listed in Table 6 for these calculations. The calculated latent heats values can be found in Table 7. The latent heat values at T_{tri} are used for subsequent surface energy calculations of organic ices in Section 4.2.

Table 6. Van der Waals constants for each Titan-relevant species listed in Table 1. References: [a] Haynes (2014), [b] Weast (1972), [c] this work.

Species	a (L ² ·bar·mol ⁻²)	b (L·mol ⁻¹)	Ref.
CH ₄	2.303	0.0431	[a]
C ₂ H ₆	5.580	0.0651	[a]
C ₂ H ₄	4.612	0.0582	[a]
C ₂ H ₂	4.516	0.0522	[a]
C ₄ H ₂	18.856	0.1639	[c]
C ₆ H ₆	18.82	0.1193	[a]
C ₃ H ₈	9.39	0.0905	[a]
C ₃ H ₆	8.442	0.0824	[a]
C ₃ H ₄ -a	8.235	0.07467	[b]
C ₃ H ₄ -p	8.40	0.0744	[b]
HCN	11.29	0.0881	[a]
HC ₃ N	15.576	0.1053	[c]
CO ₂	3.658	0.0429	[a]
CH ₃ CN	17.89	0.1169	[b]
C ₂ H ₅ CN	21.57	0.1369	[b]
C ₂ H ₃ CN	18.37	0.1222	[b]
C ₂ N ₂	7.803	0.6952	[b]
C ₄ N ₂	10.871	0.0781	[c]

3. PHYSICAL PROPERTIES - DENSITY

Density is an important material property that can shape the physical evolution of substances on Titan, such as settling and buoyancy, etc. Density is also often required to predict other properties of a substance. In the subsequent sections, we summarize the densities of Titan-relevant organic liquids, along the saturation curve, of Titan-relevant organic ices, and of Titan haze analogs.

3.1. Densities of organic liquids for the species detected on Titan

In Table 8, we summarize the saturation liquid densities as a function of temperature for the 18 Titan-relevant organic species listed in Table 1. For some liquids, we adopt existing the liquid density expressions provided in Daubert & Danner (1989); Rumble (2020). For the other liquids, we least-square fit the liquid density (ρ_l) as a function of temperature using the following expression:

$$\rho_l(T) = \rho_l(T_{cri}) + A_0(1 - T/T_{cri})^{0.35} + \sum_{n=1}^i A_n(1 - T/T_{cri})^n. \quad (17)$$

For most of the organic liquids (CH₄, C₂H₆, C₂H₄, C₃H₈, C₃H₆, CO₂), we fit the saturation liquid density data from Rumble (2020). For C₄H₂, we fit the saturation liquid density data from Lespiau & Prevost (1925); Straus & Kollek (1926); Egloff & Kuder (1942). For C₆H₆, we fit the saturation liquid density data from Kroenlein et al. (2011). For C₃H₄-p, we fit the saturation liquid density data

Table 7. Calculated latent heat of sublimation (L_{sub}) and vaporization (L_{vap}) of the condensates at the triple point of each of the 18 species detected on Titan and listed in Table 1.

Species	$L_{sub}(T_{tri})$ (kJ·mol ⁻¹)	$L_{vap}(T_{tri})$ (kJ·mol ⁻¹)
CH ₄	9.569	8.640
C ₂ H ₆	20.75	18.20
C ₂ H ₄	19.69	16.21
C ₂ H ₂	20.72	16.63
C ₄ H ₂	37.28	24.88
C ₆ H ₆	45.51	35.34
C ₃ H ₈	28.30	25.85
C ₃ H ₆	27.60	25.49
C ₃ H ₄ -a	27.47	23.86
C ₃ H ₄ -p	31.59	26.86
HCN	36.44	28.13
HC ₃ N	45.43	27.96
CO ₂	24.87	16.13
CH ₃ CN	42.96	34.79
C ₂ H ₅ CN	47.41	42.36
C ₂ H ₃ CN	43.62	37.39
C ₂ N ₂	34.60	24.69
C ₄ N ₂	50.02	27.50

from Maass & Wright (1921); Morehouse & Maass (1931); Gee et al. (1986); Kroenlein et al. (2011); Rumble (2020). The liquid density data that are used for the fitting and the deviation between the fitting and each experimental data point are summarized in Table 16 in the Appendix section.

3.2. Densities of organic ices for the species detected on Titan

The existing density data for Titan-relevant organic ices are usually more scarce, and the measured values sometimes may also seem inconsistent with each other. The apparent inconsistencies in the measured ice density are mainly caused by the different experimental diagnostic techniques used and how each technique defines the density (see Yu et al. (2017) for all the different density definitions).

There are two main groups of ice density measurement techniques. The first group of techniques measures the intrinsic density or the material density of the ice. This is the highest density that can be measured for a material, i.e., density with no pore space. Techniques that constrain the crystal structure, such as neutron or X-ray diffraction, give the intrinsic density, with the evaluated volume being the crystal of a unit cell with no pore space. The second group of techniques measures the average density. The average density is usually lower than the intrinsic density, as pore space may be included in addition to the volume of the ice itself. Techniques that measure average density include the quartz crystal microbalance (QCM)/double laser interferometry combination technique, estimation from the refractive index of the ice, and pycnometry technique. With the QCM/double laser interferometry technique, the mass of the ice sample is monitored and measured by the QCM,

Table 8. Density expressions of Titan-relevant organic liquids along the saturation line. The “Temp. (K)” column has the same meaning as Table 3. [a] This work; [b] Daubert & Danner (1989); [c] Kroenlein et al. (2011); [d] Dannhauser & Flueckinger (1963); [e] Rumble (2020).

Species	Liquid density, $\rho_l(T)$ ($\text{kg}\cdot\text{m}^{-3}$)	Temp (K)	Ref
CH ₄	$162.70 + 291.23(1 - T/T_{cri})^{0.35} + 142.42(1 - T/T_{cri}) - 121.96(1 - T/T_{cri})^2 + 107.38(1 - T/T_{cri})^3$	$T_{tri}-T_{cri}$	[a]
C ₂ H ₆	$206.20 + 390.80(1 - T/T_{cri})^{0.35} + 161.80(1 - T/T_{cri}) - 90.702(1 - T/T_{cri})^2 + 88.144(1 - T/T_{cri})^3$	$T_{tri}-T_{cri}$	[a]
C ₂ H ₄	$214.20 + 402.42(1 - T/T_{cri})^{0.35} + 177.02(1 - T/T_{cri}) - 99.181(1 - T/T_{cri})^2 + 101.65(1 - T/T_{cri})^3$	$T_{tri}-T_{cri}$	[a]
C ₂ H ₂	$63.816/0.27448^{1+(1-T/T_{cri})^{0.28752}}$	$T_{tri}-T_{cri}$	[b]
C ₄ H ₂	$2165.6 - 5.2315T$	$T_{tri}-278-[T_{cri}]$	[a]
C ₆ H ₆	$304.70 + 596.41(1 - T/T_{cri})^{0.35} + 292.04(1 - T/T_{cri}) - 296.31(1 - T/T_{cri})^2 + 378.24(1 - T/T_{cri})^3$	$T_{tri}-T_{cri}$	[a]
C ₃ H ₈	$220.50 + 429.60(1 - T/T_{cri})^{0.35} + 167.26(1 - T/T_{cri}) - 87.547(1 - T/T_{cri})^2 + 96.621(1 - T/T_{cri})^3$	$T_{tri}-T_{cri}$	[a]
C ₃ H ₆	$229.60 + 447.91(1 - T/T_{cri})^{0.35} + 181.53(1 - T/T_{cri}) - 102.10(1 - T/T_{cri})^2 + 121.01(1 - T/T_{cri})^3$	$T_{tri}-T_{cri}$	[a]
C ₃ H ₄ -a	$243.20 + 508.18(1 - T/T_{cri})^{0.35} + 66.874(1 - T/T_{cri}) + 232.07(1 - T/T_{cri})^2 - 159.04(1 - T/T_{cri})^3$	$T_{tri}-T_{cri}$	[c]
C ₃ H ₄ -p	$244.90 + 469.73(1 - T/T_{cri})^{0.35} + 409.34(1 - T/T_{cri}) - 658.50(1 - T/T_{cri})^2 + 600.71(1 - T/T_{cri})^3$	$T_{tri}-T_{cri}$	[a]
HCN	$195.00 + 451.55(1 - T/T_{cri})^{0.35} + 1249.0(1 - T/T_{cri}) - 3452.1(1 - T/T_{cri})^2 + 3809.9(1 - T/T_{cri})^3$	$T_{tri}-T_{cri}$	[c]
HC ₃ N	$1189.6 - 1.2850T$	$T_{tri}-315.2-[T_{cri}]$	[d]
CO ₂	$467.60 + 925.62(1 - T/T_{cri})^{0.35} + 465.51(1 - T/T_{cri}) - 412.21(1 - T/T_{cri})^2 + 509.61(1 - T/T_{cri})^3$	$T_{tri}-T_{cri}$	[a]
CH ₃ CN	$247.37 + 556.17(1 - T/T_{cri})^{0.35} + 214.71(1 - T/T_{cri}) + 34.189(1 - T/T_{cri})^2 + 34.820(1 - T/T_{cri})^3$	$T_{tri}-T_{cri}$	[c]
C ₂ H ₅ CN	$244.85 + 447.66(1 - T/T_{cri})^{0.35} + 601.25(1 - T/T_{cri}) - 658.21(1 - T/T_{cri})^2 + 497.05(1 - T/T_{cri})^3$	$T_{tri}-T_{cri}$	[c]
C ₂ H ₃ CN	$252.09 + 757.67(1 - T/T_{cri})^{0.35} - 448.60(1 - T/T_{cri}) + 1307.2(1 - T/T_{cri})^2 - 944.27(1 - T/T_{cri})^3$	$T_{tri}-T_{cri}$	[c]
C ₂ N ₂	$352.99 + 734.98(1 - T/T_{cri})^{0.35} + 191.04(1 - T/T_{cri}) + 216.84(1 - T/T_{cri})^2 - 248.71(1 - T/T_{cri})^3$	$T_{tri}-T_{cri}$	[c]
C ₄ N ₂	970.8	298.15	[e]

and the volume is determined by monitoring the thickness of the ice layers using laser interferometry. Therefore, if pore space develops during the ice growth process, the volume calculated using the thickness of the ice inevitably includes pore space. The average density of the ice can also be estimated from the measured refractive index of the ice (n_{vis}) using the Lorentz-Lorenz equation (see Equation 27). Because the measured refractive index correlates with the porosity of the ice, the derived ice density is the average density. The pycnometry technique directly measures the volume of the condensed ice. As a consequence, the measured volume may include pore space, if any develops during the ice growth process. The porosity of the ice can be strongly affected by the growth processes of the ice, the formation temperatures used in the ice production experiments, and the phase of the ice (crystalline or amorphous) (e.g, Loeffler et al. 2016; Satorre et al. 2018). Note that diffraction techniques cannot measure the density of low-temperature amorphous ice as there is no unit cell structure. Thus, techniques such as QCM/interferometry can serve as diagnostic tools to assess the density and porosity of amorphous ices.

To establish relationships that can be easily used by the community (i.e., the ice density variation with temperature), in this section, we use the intrinsic density data with no or minimal pore space that are measured at different temperatures. Here we choose to use the intrinsic density measured by the diffraction techniques, as this technique measures the unit cell structure of ice crystals without pore space. Because visual inspection of pore space (or bubbles) of the ice sample is possible using the pycnometry technique and procedures have been developed to sufficiently reduce porosity (e.g., Heuse 1930), many of the pycnometry-determined densities are also relatively close to the intrinsic density, e.g., Stewart & La Rock (1958) for C₂H₆ and CH₄ ices, Bol’shutkin et al. (1971); Manzhelii & Tolkachev (1964) for CH₄ ices. Thus, we choose to use density data that are measured by diffraction techniques and pycnometry to create fits for ice intrinsic density as a function of temperature. We

Table 9. Adopted intrinsic density expressions as a function of temperature for Titan-relevant organic ices. The “Temp. (K)” column has the same meaning as Table 3. [a] refitted data of [Maynard-Casely et al. \(2020\)](#); [b] [van Nes & Vos \(1978\)](#); [c] fitted, this work; [d] estimated, this work; [e] [Stewart & La Rock \(1958\)](#); [f] [Blanc et al. \(1962\)](#); [g] [Marlin et al. \(2022\)](#); [h] [Shallcross & Carpenter \(1958\)](#); [i] [Yokoyama & Ohashi \(1998\)](#); [j] [Hannan & Collin \(1953\)](#).

Species	Crystal type	Ice intrinsic density, $\rho_s(T)$ ($\text{kg}\cdot\text{m}^{-3}$)	Temp (K)	Ref
CH ₄	I	$1.0624 \times 10^5 / (201.74 - 1.2024 \times 10^{-2}T + 1.8596 \times 10^{-3}T^2)$	$20.509 - T_{tri}$	[a]
	II	$8.4992 \times 10^5 / (1603.6 - 1.1690 \times 10^{-3}T^3 + 9.0131 \times 10^{-5}T^4)$	$[<]8 - 20.509$	[a]
C ₂ H ₆	I, II	669	$89.726 - T_{tri}$	[b]
	III	$737.91 + 0.21576T - 6.1118 \times 10^{-3}T^2$	$(<)5 - 89.726$	[c]
C ₂ H ₄	I	$795.15 - 0.69734T$	$[<]20.4 - T_{tri}$	[c]
C ₂ H ₂	I	$853.63 - 0.64829T$	$[<]77 - 188.15 - [T_{tri}]$	[c]
C ₄ H ₂	I	$1194.3 - 0.63366T$	$[\leq T_{tri}]$	[d]
C ₆ H ₆	I	$1127.8 - 8.1121 \times 10^{-2}T - 1.1497 \times 10^{-3}T^2$	$[<]20.4 - T_{tri}$	[c]
C ₃ H ₈	I	$832.98 - 0.96372T$	$[<]20.4 - T_{tri}$	[c]
C ₃ H ₆	I	806	77	[e]
C ₃ H ₄ -a	I	860	95	[f]
C ₃ H ₄ -p	I	882	90	[g]
HCN	I	$1234.6 - 1.3477T$	$[<]153.15 - 233.15 - [T_{tri}]$	[c]
HC ₃ N	I	1075.3	248.15	[h]
CO ₂	I	$1711.5 - 8.7556 \times 10^{-2}T - 3.3884 \times 10^{-3}T^2$	$[<]20.4 - 194.15 - [T_{tri}]$	[c]
CH ₃ CN	I (or α)	$816.57 + 2.4008T - 6.7142 \times 10^{-3}T^2$	$201 - T_{tri}$	[c]
	II (or β)	$1127.5 - 4.3029 \times 10^{-2}T - 1.5440 \times 10^{-3}T^2$	$[<]5 - 216.9$	[c]
C ₂ H ₅ CN	I	$1060.7 - 0.46187T$	$[<]100 - 150 - [T_{tri}]$	[c]
C ₂ H ₃ CN	I	1027.4	153	[i]
C ₂ N ₂	I	$1285.9 - 0.20032T$	$[<]15 - 178.15 - [T_{tri}]$	[c]
C ₄ N ₂	I	1230	278	[j]

summarize all the density measurements we used to fit for the intrinsic density-temperature relationships in Table 17. Since ice under different growth conditions may have different porosity, the measured average density may span a range of values, even at the same temperature. For example, the measured average density of crystalline C₂H₄ ice at 60 K is almost 30 % higher in [Yarnall & Hudson \(2022\)](#) (796 $\text{kg}\cdot\text{m}^{-3}$) than in [Satorre et al. \(2017\)](#) (629 $\text{kg}\cdot\text{m}^{-3}$). Thus, in this work, we choose to only present all the existing average density measurements, as shown in Table 18.

In Table 9, we summarize the fitted intrinsic density expressions as a function of temperature for all Titan-relevant ices (cf. compounds listed in Table 1). For most ices, we have generated fits using all the published diffraction and pycnometry data that we could find. For methane ice, however, even though there have been many studies to determine its density using diffraction techniques, the results are not always in agreement – possibly due to differences in the purity of the ice. We choose to only present the fit using the recent measurements by [Maynard-Casely et al. \(2020\)](#) from 8-88 K because they cover the largest temperature range among all the CH₄ ice densities we found. For CH₃CN ice, it is important to note that even though the transition temperature is at 216.9 K (see Table 2), the crystal I or the β form of CH₃CN ice is found to grow below the transition temperature ([Enjalbert & Galy 2002](#)), thus there is an overlap of the temperature range for the expressions in Table 9.

For a full list of intrinsic density data that are used to create fittings in Table 9 (i.e., measured by diffraction and pycnometry), see Table 17 in the Appendix section. All the ice densities measured in Table 17 are for crystalline ices. The rest of the average density measurements that are not used to create the fittings can be found in Table 18 (i.e., measured by QCM or estimated using refractive index of the ice). Note that for amorphous ices, the average density values tend to be much lower compared to the adopted intrinsic density fit, indicating high porosity. Specifically, the porosity can be as high as 40-50 % for amorphous C₂H₆, C₂H₄, CO₂, and C₂H₅CN ices, 30-35 % for amorphous HCN and CH₃CN ices, and 20 % for amorphous C₃H₈ ice. While crystalline ices tend to have much lower porosity, from just a few percent to 20 %, depending on the growth process of the ices (Loeffler et al. 2016; Yarnall & Hudson 2022).

C₄H₂ is the only organic ice for which we could not find any published density measurement. Future laboratory work is required to directly determine the intrinsic density of C₄H₂ ice. In this work, we estimate the density of C₄H₂ ice ($\rho_s(T)$) using a simple solid-liquid density relationship. We use the liquid density expression of C₄H₂ in Table 8 to first calculate its liquid density value at the triple point ($\rho_l(T_{tri})$). Then we can use the relationship determined by Goodman et al. (2004), which is found to be accurate within 6 % for most organics:

$$\rho_s(T) = \left(1.28 - 0.16 \frac{T}{T_{tri}} \right) \rho_l(T_{tri}), \quad (18)$$

where both $\rho_l(T_{tri})$ and $\rho_s(T)$ have units of kg·m⁻³.

As shown in Table 9, many organic ices only have ice intrinsic density measurements at one temperature (C₃H₆, C₃H₄-a, C₃H₄-p, HC₃N, C₂H₃CN). More laboratory density measurements performed at different temperatures are needed to create fits for ice density variation as a function of temperature.

3.3. Densities of Titan haze analogs

Laboratory-made tholins have been serving as the model material for the refractory haze particles in Titan’s atmosphere. Out of the many laboratories that have synthesized tholins, the four groups that have measured the densities of their tholin samples (see a summary in Table 10) are: the University of Colorado Boulder group (UC Boulder, setup name: “Tolbert setup” – named after the PI), NASA Ames Research Center group 1 (NASA ARC 1, setup name: tholin-Radio frequency (RF) system), Johns Hopkins University group (JHU, setup name: Planetary Haze Research (PHAZER)), and Laboratoire Atmosphères, Milieux, Observations Spatiales (LATMOS, setup name: Production d’Aérosols en Microgravité par Plasma REactif (PAMPRE)). The densities obtained by these groups are summarized in Table 10, along with some experimental parameters specific of each sample (setup name, energy source, gas mixture, pressure, type of density measurement). For a list of the general experimental parameters (pressure, temperature, reaction time, gas irradiation time, gas flow rate) that are used for each setup, please refer to Table 19.

Note that only two methods have been used to characterize the densities of tholins produced in various laboratories. The UC Boulder group used a combination system including an aerosol mass spectrometer (AMS) and a scanning mobility particle sizer (SMPS) that measure the average density of the produced tholin particles in-situ. With this method, the volume in the density determination could include volume larger than the material itself if the particles are not spherical and have internal pores. The measured average density of these tholin samples ranges from 400-1130 kg·m⁻³. The other three groups all used helium pycnometry to measure the densities of their tholin sample collected

Table 10. Measured densities of Titan haze analogs, including the type of density measured, the setup in which the sample were produced, and some experimental parameters (energy source and gas mixture composition). §: The UV lamp emits continuously from 115-400 nm. References: [a] Hörst & Tolbert (2013); [b] Trainer et al. (2006); [c] Sekine et al. (2008); [d] Imanaka et al. (2012); [e] He et al. (2017); [f] Lethuillier et al. (2018); [g] Brouet et al. (2016).

Laboratory location (Setup)	Energy source	Gas mixture	Pressure (mbar)	Density, ρ_s ($\text{kg}\cdot\text{m}^{-3}$)	Measured density definition	Ref.
UC Boulder (Tolbert setup)	UV lamp [§]	N ₂ :CH ₄ (99.99:0.01)	830 – 850	480±70		[a]
		N ₂ :CH ₄ (99.9:0.1)	830 – 850	650±110		[a]
		N ₂ :CH ₄ (99.9:0.1)	800	790±90		[b]
		N ₂ :CH ₄ (99:1)	830 – 850	950±150	Average density	[a]
		N ₂ :CH ₄ (98:2)	830 – 850	760±150	(AMS & SMPS)	[a]
		N ₂ :CH ₄ (95:5)	830 – 850	740±130		[a]
	Spark discharge	N ₂ :CH ₄ (90:10)	830 – 850	500±100		[a]
		N ₂ :CH ₄ (99.9:0.1)			820±230	
		N ₂ :CH ₄ (99:1)			980±220	
		N ₂ :CH ₄ (98:2)	830 – 850	1130±100	Average density	[a]
NASA ARC 1 (tholin-RF system)	RF cold plasma irradiation	N ₂ :CH ₄ (90:10)	0.4	1380		[c]
			1.5	1270	Average density	[c]
			0.26	1386.6	(Pycnometry)	[d]
			1.6	1311.3		[d]
JHU (PHAZER)	AC plasma discharge	N ₂ :CH ₄ :CO (94.95:5:0.05)	2.67	N ₂ :CH ₄ (95:5)	1343±2	
				N ₂ :CH ₄ :CO (94.8:5:0.2)	1348±2	
				N ₂ :CH ₄ :CO (94.5:5:0.5)	1364±3	Average density
				N ₂ :CH ₄ :CO (94:5:1)	1379±3	(Pycnometry)
				N ₂ :CH ₄ :CO (92.5:5:2.5)	1395±3	[e]
				N ₂ :CH ₄ :CO (90:5:5)	1416±3	
LATMOS (PAMPRE)	DC plasma discharge	N ₂ :CH ₄ (98:2)	0.2–10	N ₂ :CH ₄ (95:5)	1424±3	
				N ₂ :CH ₄ (95:5)	1440±20	Average density
				N ₂ :CH ₄ (92:8)	1440±30	(Pycnometry)
				1440±10	[f]	
				1340±30	[g]	
					[f]	
Recommended density range				400-1450 kg·m⁻³		

from substrates/walls of the setup. Since the helium gas used in pycnometry can fill pores as small as 3 Å (Yu et al. 2017), the volume in the measured density only includes the internal pores that are not connected to the outside. The pycnometry-measured average densities of these tholin samples range from 1270-1450 kg·m⁻³.

It is interesting that there is a clear gap between the average density measured by the UC Boulder group and the other three lab groups. However, it is hard to evaluate whether their density values are lower than the other groups because of the additional volume taken into account in their average density measurements or because their tholin samples are intrinsically different than the ones from the other groups. Previous works proposed that both the deposition technique and the pressure may lead to density differences of the tholin samples. Specifically, depositing particles on substrates/walls may reduce internal voids/porosity to increase density (Hörst & Tolbert 2013; He et al. 2017) and

lower pressure seems to create tholin samples with higher density (Sekine et al. 2008; Imanaka et al. 2012; Cordier & Carrasco 2019). Overall, we recommend using the widest possible density range, from 400–1450 kg·m⁻³, for Titan’s haze particles to account for the uncertainty of the properties of tholins made in different laboratories. For certain processes such as aerosol sedimentation or comparative planetology, this density range is likely sufficient to describe the haze behavior, as the density of hazes is much larger than Titan’s atmosphere and much smaller than most refractory materials on other planets (silicates, metals). For some other processes, we need more laboratory work to help constrain the density values of the actual haze particles on Titan. For example, we still cannot distinguish whether tholin particles would float or sink into the methane-ethane-nitrogen lakes as the density of the hazes (400-1500 kg·m⁻³) overlaps the density range of the lake liquids (\sim 450-700 kg·m⁻³) (Cordier & Carrasco 2019; Yu et al. 2020a).

4. SURFACE PROPERTIES

The surface properties govern the strength of cohesion and adhesion, rising from the intermolecular structures of substances. The surface free energy is the intrinsic material property that characterizes the surface properties of a substance. The surface free energy is defined as the energy needed to create a unit area of the surface or half of the energy needed to separate two surfaces of a unit area. On the one hand, the surface free energies can affect interactions between the same substances through cohesion. Thus, it is important for atmospheric processes including haze formation through particle coagulation, and also surface processes including sediment transport, as wind shear stress has to overcome sediment cohesion to initiate sediment transport (Yu et al. 2017, 2020a). On the other hand, the surface free energies can affect interactions between two different substances through adhesion. In order to assess processes such as cloud formation through condensate-haze interactions and lake-haze interactions on Titan (Yu et al. 2020a), the surface free energies are therefore an important parameter to consider in order to understand how these substances interact with each other.

Note that the surface free energies are often referred to differently for a liquid and a solid. For a liquid, its surface free energy is often referred to as the surface tension (γ_l), with a unit of mN·m⁻¹, while for a solid, its surface free energy is often referred to as the surface energy (γ_s), with a unit of mJ·m⁻² (equivalent to mN·m⁻¹). In the following sections, we summarize and compute the surface free energies of the Titan-relevant organic liquids, ices, and solids.

4.1. *Surface tensions of Titan-relevant organic liquids*

For liquid condensates, we list their liquid surface tension expressions as a function of temperature ($\gamma_{liq}(T)$) in Table 11. Most surface tension expressions provided in this table are directly taken from Yaws (2014), except for HC₃N, C₄N₂, and C₄H₂, which have no surface tension measurements. Note that Yaws (2014) does provides an estimation of the surface tension of C₄H₂. In this work, we predicted the surface tensions of these three compounds using three methods recommended in Poling (2001): 1) the MacLeod-Sugden method (Macleod 1923; Sugden 1924); 2) the Brock-Bird method (Brock & Bird 1955; Miller & Thodos 1963); and 3) the Pitzer method (Curl & Pitzer 1958; Pitzer 1995).

The MacLeod-Sugden method estimates the surface tension of a material by using its liquid density (ρ_l) (Table 8) and the calculated parachor based on its chemical structure:

$$\gamma_l = \left(\frac{P\rho_l}{M} \right)^4, \quad (19)$$

where the parachor P can be calculated using Table 25 in Quayle (1953) based on the structure of the chemical. P is 148.2 for C_4H_2 , 141.2 for HC_3N , and 192.8 for C_4N_2 . The conventional unit of the parachor is $(\text{mN}\cdot\text{m}^{-1})^{1/4}\times(\text{cm}^3\cdot\text{mol}^{-1})$. M is the molar mass of the chemical (with a unit of $\text{g}\cdot\text{mol}^{-1}$ in Equation 19), and ρ_l is its liquid density (with a unit of $\text{g}\cdot\text{cm}^{-3}$ in Equation 19).

The Brock-Bird method predicts the surface tensions of a material using the critical pressure (P_{cri}) and temperature (T_{cri}) (Table 2) and the boiling point temperature (T_b):

$$\begin{aligned} \gamma_l &= P_{cri}^{2/3} T_{cri}^{1/3} Q (1 - T/T_{cri})^{11/9}, \\ Q &= 0.1196 \left[1 + \frac{T_b/T_{cri} \ln(P_{cri}/1.01325)}{1 - T_b/T_{cri}} \right] - 0.279, \end{aligned} \quad (20)$$

where T_b can be calculated using the SVP equations in Table 3 by equating the pressure to 1 bar.

The Pitzer method predicts the surface tensions of a material using P_{cri} and T_{cri} (Table 2), and the boiling point temperature (T_b):

$$\begin{aligned} \gamma_l &= P_{cri}^{2/3} T_{cri}^{1/3} \frac{1.86 + 1.18\omega}{19.05} \left[\frac{3.75 + 0.91\omega}{0.291 - 0.08\omega} \right]^{2/3} (1 - T/T_{cri})^{11/9}, \\ \omega &= -\log_{10}[P(T = 0.7T_{cri})/P_{cri}] - 1.0, \end{aligned} \quad (21)$$

where ω is the acentric factor, which can be calculated using the vapor pressure at $0.7 T_{cri}$ using Table 3.

In this work, to accommodate for the uncertainty of the different estimation methods, we report an average of the predicted surface tension values. For C_4H_2 , we averaged the predicted surface tension values by all three methods at its triple point, and the averaged value is within 0.4 % of the provided values by Yaws (2014). For HC_3N , we report an average of the surface tensions predicted by all three methods (Equations 19-21). For C_4N_2 , because we do not have data or extrapolations we can use for its liquid density at the triple point, we report an average of the surface tensions predicted by only the latter two methods (Equations 20-21).

We also calculated the surface tensions using all three methods for the rest of the 15 compounds and compared the results to the surface tension values provided by Yaws (2014), see Table 20 in the Appendix section. For some compounds (e.g., C_2H_6 , C_2H_4 , and C_6H_6), the calculated surface tensions are very close to what is provided by Yaws (2014) at the triple point (within 10 %). But for some other compounds, especially triple-bonded substances such as C_3H_4 -a, C_3H_4 -p, and C_2N_2 , the calculated surface tensions are up to 70 % different compared to Yaws (2014) at the triple point. Thus, the estimated surface tension values of C_4H_2 , HC_3N , and C_4N_2 should be considered with caution. More laboratory experiments are needed to accurately determine the surface tensions of these three compounds.

The total surface tension can be divided into different components to reflect specific independent intermolecular forces (Fowkes 1964). This is especially important when considering the interactions

Table 11. Surface tension expressions ($\gamma_l(T)$) as a function of temperature of Titan-relevant organic liquids. The “Temp. (K)” column has the same meaning as Table 3. [a] Yaws (2014); [b] this work.

Species	Surface tension, $\gamma_l(T)$ (mN·m ⁻¹)	Temp (K)	$\gamma_l(T_{tri})$ (mN·m ⁻¹)	Ref.	$\gamma_l^d(T_{tri})$ (mN·m ⁻¹)	$\gamma_l^p(T_{tri})$ (mN·m ⁻¹)	Ref.
CH ₄	$37.432(1 - T/190.564)^{1.09200}$	$T_{tri}-T_{cri}$	18.487	[a]	18.487	0	[a]
C ₂ H ₆	$49.630(1 - T/305.322)^{1.20650}$	$T_{tri}-T_{cri}$	32.500	[a]	32.500	0	[a]
C ₂ H ₄	$53.198(1 - T/282.350)^{1.27840}$	$T_{tri}-T_{cri}$	29.576	[a]	29.576	0	[a]
C ₂ H ₂	$56.510(1 - T/308.39)^{1.13460}$	$T_{tri}-T_{cri}$	18.768	[a]	18.768	0	[a]
C ₄ H ₂	$68.107(1 - T/478.02)^{1.22222}$	$[T_{tri}]-[T_{cri}]$	29.388	[a]	29.388	0	[a]
C ₆ H ₆	$71.970(1 - T/562.02)^{1.23890}$	$T_{tri}-T_{cri}$	30.806	[a]	30.806	0	[a]
C ₃ H ₈	$49.179(1 - T/369.89)^{1.22222}$	$T_{tri}-T_{cri}$	35.681	[a]	35.681	0	[a]
C ₃ H ₆	$53.547(1 - T/364.21)^{1.20580}$	$T_{tri}-T_{cri}$	38.387	[a]	38.387	0	[a]
C ₃ H ₄ -a	$49.123(1 - T/393.9)^{1.16200}$	$T_{tri}-T_{cri}$	29.935	[a]	29.935	0	[a]
C ₃ H ₄ -p	$57.277(1 - T/402.7)^{1.18980}$	$T_{tri}-T_{cri}$	29.845	[a]	29.845	0	[a]
HCN	$52.310(1 - T/456.65)^{1.01980}$	$T_{tri}-T_{cri}$	22.169	[a]	14.5	7.7	[b]
HC ₃ N	25.5±1.9	T_{tri}	25.5±1.9	[b]	24.2	1.3±1.9	[b]
CO ₂	$79.971(1 - T/304.128)^{1.2617}$	$T_{tri}-T_{cri}$	16.616	[a]	16.616	0	[a]
CH ₃ CN	$68.332(1 - T/545.41)^{1.09700}$	$T_{tri}-T_{cri}$	37.557	[a]	23.9	13.7	[b]
C ₂ H ₅ CN	$62.590(1 - T/561.26)^{1.13640}$	$T_{tri}-T_{cri}$	40.284	[a]	27.9	12.4	[b]
C ₂ H ₃ CN	$63.112(1 - T/540.0)^{1.07050}$	$T_{tri}-T_{cri}$	39.718	[a]	27.5	12.2	[b]
C ₂ N ₂	$73.193(1 - T/397.1)^{1.20100}$	$T_{tri}-T_{cri}$	23.064	[a]	23.064	0	[a]
C ₄ N ₂	46.2±2.5	T_{tri}	46.2±2.5	[b]	46.2±2.5	0	[b]

between two compounds, because only the surface tension components from the same intermolecular forces would interact with each other. The most commonly used model, the Owens, Wendt, Rabel, and Kaelble (OWRK) model (Owens & Wendt 1969; Kaelble 1970; Rabel 1971), divides the surface tension into a dispersive (γ_l^d) and a polar component (γ_l^p):

$$\gamma_l = \gamma_l^d + \gamma_l^p. \quad (22)$$

The dispersive component includes non-polar London dispersive forces between molecules, and the polar component includes polar dipole-dipole and H-bonding interactions.

Most of the organic liquids on Titan are completely non-polar, thus, their polar components of the surface tensions (γ_l^p) are zero, and the dispersive components of the surface tensions are equal to their total surface tensions ($\gamma_l^d = \gamma_l^{tot}$). These non-polar substances include CH₄, C₂H₆, C₂H₄, C₂H₂, C₄H₂, C₆H₆, C₃H₈, C₃H₆, C₃H₄-a, C₃H₄-p, CO₂, C₂N₂, and C₄N₂. Some of the nitriles do have polar intermolecular force contributions, including HCN, CH₃CN, HC₃N, C₂H₅CN, and C₂H₃CN. Thus, they have non-zero surface tension polar components. To calculate their surface tension partitioning pattern, we need to know one of the surface tension compounds, and then the other component is the remainder of the total surface tension. Here, we estimate the dispersive surface tension components of these five organic liquids using the Lifshitz theory (Lifshitz & Hamermesh 1992; Israelachvili

2011), see also Yu et al. (2021):

$$\gamma_l^d = \frac{kT}{32\pi d_0^2} \left(\frac{\varepsilon - 1}{\varepsilon + 1} \right)^2 + \frac{h\nu_e}{128\sqrt{2}\pi d_0^2} \frac{(n_{vis}^2 - 1)^2}{(n_{vis}^2 + 1)^{3/2}}, \quad (23)$$

where k is the Boltzmann constant, T is the temperature of the system (here all the calculations are performed at the triple point temperature of each substance), d_0 is the equilibrium separation distance for two surfaces at contact and is found to be around 0.157 ± 0.009 nm for most materials (van Oss 2006), ε is the static dielectric constants of the liquid, h is Planck's constant, ν_e is the main electronic absorption frequency of the molecule, and n_{vis} is the refractive index of the liquid at the visible wavelengths.

Table 12 lists all the required values (ν_e , ε , and n_{vis}) for this calculation for the five organic liquids. The main electronic absorption frequency of the molecule (ν_e , in Hz) can be calculated using $n_e = \text{ionization potential}/h$, where the molecule's ionization potential is in eV and is 4.1357×10^{-15} eV·Hz⁻¹. For the organic liquids, we assume $n_{vis} = n_D$, where n_D is the refractive index at the sodium D line (589 nm). We use n_D because, for most materials, it is the only wavelength where measurements are available in the literature.

4.2. Surface energies of Titan-relevant organic ices

For the organic ices, because there lack direct laboratory measurements of their solid surface energy (γ_s), we estimate their total surface energies by using some of their known properties through two empirical approaches (Guez et al. 1997). The first empirical approach uses the surface tension of the compound in the liquid phase ($\gamma_l(T_{tri})$), and its latent heats of sublimation ($L_{sub}(T_{tri})$) and vaporization ($L_{vap}(T_{tri})$) at the triple point temperature to compute the solid surface energy (Pruppacher & Klett 1978):

$$\gamma_s = \left(\frac{L_{sub}(T_{tri})}{L_{vap}(T_{tri})} \right)^2 \gamma_l(T_{tri}). \quad (24)$$

The second method estimates the surface energy of the ice using the following equation (McDonald 1953):

$$\gamma_s = \frac{1}{4} \frac{L_{sub}(T_{tri})}{N_A} \sigma_s - \left(\frac{1}{4} \frac{L_{vap}(T_{tri})}{N_A} \sigma_s - \gamma_l \right) \frac{L_{vap}(T_{tri})}{L_{sub}(T_{tri})}, \quad (25)$$

where N_A is Avogadro's constant. In addition to $\gamma_l(T_{tri})$, $L_{sub}(T_{tri})$, and $L_{vap}(T_{tri})$, the second method also uses the surface density of molecules of the ice (σ_s), which is a function of the density (ρ_s) and molar mass (M) of the ice:

$$\sigma_s = \frac{1}{d^2}, \text{ where } d^3 = \frac{M}{N_A \rho_s}. \quad (26)$$

We summarize the calculated total surface energy values of organic ices using both methods through Equation 24 and 25 in Table 13. Similar to the organic liquids, the non-polar organic ices have zero polar surface energy components ($\gamma_s^p = 0$) and their non-polar surface energy components are equal to their total surface energy ($\gamma_s^d = \gamma_s^{tot}$). For the organic ices with polar intermolecular contributions, we can also estimate their dispersive components of the surface energies using the Lifshitz theory (Equation 23) and their bulk properties (the static dielectric constants of ices and the refractive index

Table 12. The main electronic absorption frequency (ν_e) and the ionization potential, static dielectric constant (ϵ), and refractive index at the visible wavelength (n_{vis}) for the Titan-relevant organic liquids and ices with polar intermolecular force contribution. [a] Lias (2023); [b] Rumble (2020); [c] Krause & Friedrich (1972); [d] Smyth & McNeight (1936), [e] this work, estimated, [f] Würflinger (1980), [g] Wohlfarth et al. (1996), [h] Kroenlein et al. (2011). †: Note that for HCN, Smyth & McNeight (1936) measured its dielectric constants up to its melting point. However, we discard the data above 100 K due to the presence of impurities in the sample, which causes a sharp increase in the measured dielectric constant near the melting point.

Species	Main electronic absorption frequency, ν_e (10^{15} Hz)	Ionization potential (eV)	Ref.
HCN	3.288	13.60	
HC ₃ N	2.810	11.62	
CH ₃ CN	2.950	12.20	[a]
C ₂ H ₅ CN	2.865	11.85	
C ₂ H ₃ CN	2.638	10.91	
Species	Static dielectric constant, ϵ	Temp (K)	Ref.
HCN (liquid)	$3733.1 - 23.18T + 3.6963 \times 10^{-2}T^2$	T_{tri} -299	[b]
HCN (solid)	2.33 [†]	87	[c, d]
HC ₃ N (liquid)	$918.03 - 4.9149T + 6.9104 \times 10^{-3}T^2$	T_{tri} -314	[b]
HC ₃ N (solid)	4	N/A	[e]
CH ₃ CN (liquid)	$297.24 - 1.5508T + 2.2591 \times 10^{-3}T^2$	280-333	[b]
CH ₃ CN (solid)	4	$217 - T_{tri}$	[f]
C ₂ H ₅ CN (liquid)	$82.222 - 0.22937T + 1.7424 \times 10^{-4}T^2$	213-473	[b]
C ₂ H ₅ CN (solid)	4	N/A	[e]
C ₂ H ₃ CN (liquid)	$111.09 - 0.36806T + 3.4879 \times 10^{-4}T^2$	233-413	[b]
C ₂ H ₃ CN (solid)	4	N/A	[e]
Species	Refractive index at the visible wavelength, n_{vis}	Temp (K)	Ref.
HCN (liquid)	1.2614	293	[b]
HCN (solid)	1.3425	T_{tri}	[e]
HC ₃ N (liquid)	1.38699	290	[g]
HC ₃ N (solid)	1.5320	T_{tri}	[e]
CH ₃ CN (liquid)	$1.49138 - 5.0236 \times 10^{-4}T$	278-328	[h]
CH ₃ CN (solid)	1.4612	T_{tri}	[e]
C ₂ H ₅ CN (liquid)	$1.5114 - 4.9622 \times 10^{-4}T$	292-327	[h]
C ₂ H ₅ CN (solid)	1.4719	T_{tri}	[e]
C ₂ H ₃ CN (liquid)	$1.5241 - 4.5398 \times 10^{-4}T$	293-308	[h]
C ₂ H ₃ CN (solid)	1.5176	T_{tri}	[e]

of the ice at the visible wavelengths, see also Table 12). The dielectric constants of HC_3N , $\text{C}_2\text{H}_5\text{CN}$, and $\text{C}_2\text{H}_3\text{CN}$ ices have never been measured in the laboratory and future work is needed to determine the properties of these ices. Because the first term of Equation 23, where the dielectric constant ε is used, contributes only $\sim 1\%$ of the total dispersive surface energy, the exact selection of ε is not so important. Here, we assume the dielectric constants of HC_3N , $\text{C}_2\text{H}_5\text{CN}$, and $\text{C}_2\text{H}_3\text{CN}$ to be the same as CH_3CN , given their similar n_{vis} and thus similar dielectric constants at high frequency $\varepsilon_\infty = n_{vis}^2$.

There are some existing measurements on the refractive indices for these organic ices with polar intermolecular contributions (Moore et al. 2010; Nna-Mvondo et al. 2019; Hudson 2020; Yarnall & Hudson 2022). However, most of the ices measured in those works include porosity to some extent (see discussion in Section 3.2), which will make the measured refractive indices lower than that for the ices without porosity. Here we choose to estimate the refractive index of all the polar ices using the Lorentz-Lorenz equation with the known density of the liquid phase (Table 8), the known refractive index of the liquid phase (Table 12), and the known intrinsic density of the ice phase (Table 9):

$$\frac{n_s^2 - 1}{n_s^2 + 2} \frac{1}{\rho_s} = \frac{n_l^2 - 1}{n_l^2 + 2} \frac{1}{\rho_l}, \quad (27)$$

where n_s and n_l are the refractive indices of the material in the solid and the liquid phase, and ρ_s and ρ_l are the densities of the solid and the liquid, respectively. Note that the Lorentz-Lorenz equation was originally developed for nonpolar molecules but has been found to be applicable to polar molecules (Domingo et al. 2021).

4.3. Surface energies of Titan haze analogs

Three laboratories have characterized the surface energies of their laboratory-made Titan haze analogs, including the JHU group (setup name: PHAZER), another NASA Ames Research Center group (NASA ARC 2, setup name: COSMIC), and the University of Northern Iowa group (UNI, setup name: Photochemical Aerosol Chamber, PAC). Two methods have been used to measure the surface energies of tholins: an indirect method called the sessile drop contact angle method (CA method), which probes the surface energy of the material through liquids with known surface tensions, and a direct method called the surface force apparatus (SFA method), which directly measures the cohesion force between the material to derive its surface energy. In Table 14, we list the measured surface energy values of the tholin samples from each setup, the measurement technique, and some of the experimental parameters associated with the production of each tholin sample (setup name, energy source, and gas mixture). The additional experimental parameters can be found in Table 19. In general, tholins have higher surface energies compared to common polymers (20-50 $\text{mJ}\cdot\text{m}^{-2}$, e.g., Owens & Wendt 1969). In addition to the experimental conditions that make the tholin samples, the measuring environment is found to be important in determining the measured surface energy values of the samples (Li et al. 2022). For example, the surface properties of the samples may deviate from their true values if the measurements are performed in ambient air over an inert atmosphere/vacuum, where water vapor and other containment like hydrocarbons/oils adsorb on the surface of samples. Here, the recommended surface energy values of tholins are taken from Li et al. (2022), compiled using surface energy data of the four samples made with 5% CH_4 /95% N_2 , where the measurements were conducted in a dry nitrogen environment to avoid water adsorption and contamination from the ambient atmosphere.

Table 13. Calculated solid surface energy (γ_s) of Titan-relevant organic ices using the two empirical approaches (Equations 24 and 25) and their associated surface energy partitioning components.

Species	Method 1 (Equation 24)			Method 2 (Equation 25)		
	$\gamma_s(T_{tri})$ (mJ·m ⁻²)	$\gamma_s^d(T_{tri})$ (mJ·m ⁻²)	$\gamma_s^p(T_{tri})$ (mJ·m ⁻²)	$\gamma_s(T_{tri})$ (mJ·m ⁻²)	$\gamma_s^d(T_{tri})$ (mJ·m ⁻²)	$\gamma_s^p(T_{tri})$ (mJ·m ⁻²)
CH ₄	22.676	22.676	0	21.820	21.820	0
C ₂ H ₆	42.245	42.245	0	39.715	39.715	0
C ₂ H ₄	43.638	43.638	0	40.734	40.734	0
C ₂ H ₂	29.135	29.135	0	35.194	35.194	0
C ₄ H ₂	65.981	65.981	0	65.979	65.979	0
C ₆ H ₆	51.088	51.088	0	53.503	53.503	0
C ₃ H ₈	42.765	42.765	0	41.776	41.776	0
C ₃ H ₆	45.005	45.005	0	44.054	44.054	0
C ₃ H ₄ -a	39.679	39.679	0	41.427	41.427	0
C ₃ H ₄ -p	41.282	41.282	0	45.729	45.729	0
HCN	37.202	21.6	15.6	61.707	21.6	40.1
HC ₃ N	67.3±5.0	40.0	27.3±5.0	79.4±3.1	40.0	39.4±3.1
CO ₂	39.501	39.501	0	56.284	56.284	0
CH ₃ CN	57.268	32.9	24.4	67.543	32.9	34.6
C ₂ H ₅ CN	50.462	33.2	17.3	55.252	33.2	22.1
C ₂ H ₃ CN	54.056	35.7	18.4	58.744	35.7	23.0
C ₂ N ₂	45.294	45.294	0	58.020	58.020	0
C ₄ N ₂	153±8	153±8	0	91.5±4.5	91.5±4.5	0

Table 14. Measured surface energies (γ_s) of Titan haze analogs and the associated experimental setup with some experimental tholin production parameters (energy source and gas mixture composition) and the measuring environment (“air” stands for ambient air environment, and “inert” stands for inert atmosphere such as dry nitrogen). †: Note that the actual surface energy of tholin sample measured by surface force apparatus may vary between 50-100 mJ·m⁻² (Yu et al. 2020a). References: [a] Yu et al. (2020a); [b] Li et al. (2022).

Laboratory location (Setup)	Energy source	Gas mixture	γ_s^{tot} (mJ·m ⁻²)	γ_s^d (mJ·m ⁻²)	γ_s^p (mJ·m ⁻²)	Measurement technique	Measurement environment	Ref.
JHU (PHAZER)	AC plasma discharge	N ₂ :CH ₄ (95:5)	68.1±2.5	39.6±1.4	28.5±2.2	Contact angle	air	[a]
			73.3±1.3	37.3±1.5	36.0±1.5		inert	[b]
	UV lamp	N ₂ :CH ₄ (95:5)	66†	N/A	N/A	SFA	inert	[a]
			66.0±4.7	41.1±0.9	24.9±4.7		air	[a]
NASA ARC 2 (COSMIC)	DC plasma discharge	N ₂ :CH ₄ (95:5)	47.0±2.9	31.8±1.8	15.2±2.9	Contact angle	inert	[b]
		N ₂ :CH ₄ :C ₂ H ₂ (94.5:5:0.5)	65.8±1.9	45.7±2.1	20.1±1.8		inert	[b]
UNI (PAC)	UV lamp	N ₂ :CH ₄ (95:5)	53.4±5.2	44.4±1.0	9.0±5.1	Contact angle	inert	[b]
Recommended average surface energy, γ_{avg}			59.0	37.2	21.8			
Recommended low-end surface energy, γ_{low}			47.0	31.8	15.2			
Recommended high-end surface energy, γ_{high}			81.7	45.7	36.0			

5. CONCLUSION

In this work, we summarize and calculate the following important material properties of Titan-relevant organic liquids, ices, and Titan haze analogs:

- The thermodynamic properties of the organic liquids and ices for the species detected on Titan, including triple point and critical point temperatures and pressures, crystalline ice phase transition temperatures, sublimation and vaporization saturation vapor pressures as functions of temperature, and sublimation and vaporization latent heats at the triple point of each species.
- Intrinsic densities for the Titan-relevant organic liquids and organic ices as functions of temperature, all previously measured intrinsic and average density data for the Titan-relevant organic liquids and organic ices, and all previously measured density values for Titan haze analogs, “tholins”.
- The surface properties of Titan-relevant organic liquids and ices, and Titan haze analogs, including the surface tensions of organic liquids as functions of temperature, the surface energies of organic ices at the triple point temperature, and the surface energy of the haze analogs.

These fundamental material properties could not only be applicable to materials on Titan, but also to icy bodies in the solar system, ices in the interstellar medium, protoplanetary disks, and exoplanets. Other material properties such as the crystal structures of these compounds, the thermal diffusion coefficient of these species in relevant Titan-lake-like solvents, and parameters for clathrates would also be very useful for Titan’s context (see for instance [Cordier et al. \(2021\)](#)), which we would like to include in future works. Because the field is evolving rapidly with more laboratory measurements being conducted, this database will change. Thus, we have created a publicly available database website to serve as a repository for all the data presented in this study: <https://titanmaterials.sites.ucsc.edu/>. We will keep updating this database for the community, taking into account any new laboratory measurements in the future.

6. ACKNOWLEDGEMENTS

X.Y. and J. G., are supported by the 51 Pegasi b Postdoctoral Fellowship from the Heising-Simons Foundation. Y.Y and J. L. is supported by the summer research support offered by the Other Worlds Laboratory at UC Santa Cruz. X.Y. and J.L. are also supported by the NASA Cassini Data Analysis Program Grant 80NSSC21K0528. X.Y., E.S.O, and A.H. are supported by the NASA Cassini Data Analysis Program Grant 80NSSC22K0633. E.S.O acknowledges the support of the “NASA Center for Optical Constants” ISFM. X.Z. is supported by NASA Solar System Workings grant 80NSSC19K0791. We thank the librarians at UC Santa Cruz for providing excellent and extensive interlibrary loan services that make the literature search in this work possible. We also thank Allen (Boshu) Qiao at UT San Antonio for performing data check for our public-accessible website.

7. DATA AVAILABILITY

In addition to the public-accessible website (<https://titanmaterials.sites.ucsc.edu/>) we built to archive the database, we also archived all the data on Zenodo: <https://doi.org/10.5281/zenodo.7539342>. The tables that have only numbers are archived as .csv files. The tables that include functions are archived as Jupyter notebook files (.ipynb).

8. APPENDIX

Table 15. Additional saturation vapor pressure expressions that are evaluated in this work. References: [a] Fray & Schmitt (2009); [b] Kroenlein et al. (2011); [c] Dykyj et al. (1999); [d] Yaws (2015); [e] Dubois et al. (2021); [f] Ružička et al. (2014); [g] Hudson et al. (2022); [h] this work; [i] Sinozaki et al. (1926); [j] Dannhauser & Flueckinger (1963); [k] Onken et al. (1989); [l] Sevrugova et al. (1964); [m] Stull (1947). Notations are the same as Table 3.

Species	Type	Saturation vapor pressure expressions P_{sat} (bar)	Temp. (K)	Ref.
CH ₄	s-g	$e^{10.51-1110/T-4341/T^2+1.035\times 10^5/T^3-7.91\times 10^5/T^4}$	[20.509]-48.15-90.686 (T_{tri})	[a]
	s-g	$e^{7.134-1109.5/T+0.65607\ln(T)}$	[20.509]-49.55-90.686 (T_{tri})	[b]
	l-g	$10^{3.7687-395.744/(T-6.469)}$	[90.686]-92-115	[c]
	l-g	$10^{3.7687-395.744/(T-6.469)+0.43429[(T-115)/T_{cri}]^{2.51347}-6.0941[(T-115)/T_{cri}]^8+369.43[(T-115)/T_{cri}]^{12}}$	115.0-190.564 (T_{cri})	[c]
C ₂ H ₆	s-g	$e^{15.11-2207/T-2.411\times 10^4/T^2+7.744\times 10^5/T^3-1.161\times 10^7/T^4+6.763\times 10^7/T^5}$	[<]83.35-88.75-[90.3560] (T_{tri})	[a]
	s-g	$e^{18.7925-2706.8/T}$	[<]80.808-89.726-[90.3560] (T_{tri})	[b]
	l-g	$10^{4.0567-687.3/(T-14.46)}$	90.35-133	[c]
	l-g	$10^{3.95405-663.72/(T-16.469)}$	133-190	[c]
	l-g	$10^{3.95405-663.72/(T-16.469)+0.43429[(T-190)/T_{cri}]^{2.79768}-55.054[(T-190)/T_{cri}]^8+2992.1[(T-190)/T_{cri}]^{12}}$	190-305.322 (T_{cri})	[c]
C ₂ H ₄	s-g	$e^{14.752-2305.9/T+0.15361\ln(T)}$	[<] 77.5-103.966 (T_{tri})	[b]
	l-g	$10^{4.0936-649.806/(T-10.42)}$	103.966-282.350 (T_{cri})	[d]
C ₂ H ₂	s-g	$10^{6.08413-1148.97/(T-0.31)}$	[<]138.0-191.66 (T_{tri})	[c]
	s-g	$e^{60.618-3951.8/T-7.574\ln(T)}$	[<]133.0-191.66 (T_{tri})	[b]
	l-g	$10^{3.67374-528.67/(T-44.36)}$	191.66-211-[308.39] (T_{cri})	[c]
C ₄ H ₂	s-g	$10^{8.22178-2707.52/(T+59.54)}$	[<]188.0-237.7 (T_{tri})	[c]
	s-g	$e^{16.074-4308.6/T}$	[<]194.045-237.7 (T_{tri})	[b]
	l-g	$10^{3.33975-707.254/(T-71.198)}$	237.7-285-[410] (T_{cri})	[c]
	l-g	$10^{3.6154-754.853/(T-74.882)}$	237.7-303.0-[410] (T_{cri})	[d]
C ₆ H ₆	s-g	$e^{17.35-5663/T}$	[<]184.3-278.6877 (T_{tri})	[a]
	s-g	$e^{60.797-7273.7/T-6.7019\ln(T)}$	[<]183.012-278.6877 (T_{tri})	[b]
	s-g	$10^{6.015-2042/T}$	146.0-157.6-[278.6877] (T_{tri})	[e]
	s-g	$10^{6.345-2150/T}$	[<]134.8-146	[e]
	s-g	$0.04785e^{(1-278.674/T)\exp(3.064696-1.907097\times 10^{-4}T-5.468886\times 10^{-7}T^2)}$	[<]150-278.6877 (T_{tri})	[f]
	s-g	$e^{18.98-5978.2/T}$	[<]134.8-157.6-[278.6877] (T_{tri})	[g]
	l-g	$10^{3.9392-1090.43/(T-76.004)}$	278.6877-376.0-[562.02]	[d]
C ₃ H ₈	l-g	$e^{6.673-574.5/T-2.96\times 10^5/T^2+1.795\times 10^7/T^3-4.463\times 10^8/T^4}$	85.400-231.05-[369.89] (T_{cri})	[h]
	l-g	$10^{4.6956-1030.7/(T-7.79)}$	85.400-167	[c]
	l-g	$10^{3.92828-803.997/(T-26.108)}$	167-237	[c]
	l-g	$10^{3.92828-803.997/(T-26.108)+0.43429[(T-237)/T_{cri}]^{2.55753}+50.655[(T-237)/T_{cri}]^8-1408.9[(T-237)/T_{cri}]^{12}}$	237-369.89 (T_{cri})	[c]
C ₃ H ₆	l-g	$e^{6.527-461.46/T-3.022\times 10^5/T^2+1.823\times 10^7/T^3-4.593\times 10^8/T^4}$	87.850-225.4-[364.21] (T_{cri})	[h]
	l-g	$10^{4.48447-934.227/(T-14)}$	[87.850]-89-163	[c]
	l-g	$10^{3.95606-789.624/(T-25.57)}$	163-240	[c]
	l-g	$10^{3.95606-789.624/(T-25.57)+0.43429[(T-240)/T_{cri}]^{2.67417}+22.1292[(T-240)/T_{cri}]^8-199.34[(T-240)/T_{cri}]^{12}}$	240-364.21 (T_{cri})	[c]
C ₃ H ₄ -a	s-g	$e^{16.026-3393.3/T+0.041846\ln(T)}$	[<]127-136.70 (T_{tri})	[b]
	l-g	$10^{4.3495-971.15/(T-16.5)}$	136.70-174	[c]
	l-g	$10^{3.6752-734.57/(T-38.41)}$	174-253	[c]
	l-g	$10^{3.6752-734.57/(T-38.41)+0.43429[(T-253)/T_{cri}]^{1.136}-265[(T-253)/T_{cri}]^8+1.6325\times 10^4[(T-253)/T_{cri}]^{12}}$	253-393.9 (T_{cri})	[c]
	l-g	$10^{3.6695-674.848/(T-55.808)}$	[136.70]-177.5-393.9 (T_{cri})	[d]
C ₃ H ₄ -p	l-g	$10^{4.24555-935.09/(T-29.57)}$	[169.87]-175-276-402.7 (T_{cri})	[c]
HCN	s-g	$e^{13.93-3624/T-1.325\times 10^5/T^2+6.314\times 19^6/T^3-1.128\times 10^8/T^4}$	[<]235.2-259.871 (T_{tri})	[a]
	l-g	$10^{4.67417-1340.79/(T-11.592)}$	259.871-319.4-[456.65] (T_{cri})	[i]
	l-g	$49.7e^{T_{cri}/T[-9.2183(1-T/T_{cri})+4.846(1-T/T_{cri})^{1.5}-5.2(1-T/T_{cri})^{2.5}+4.1085(1-T/T_{cri})^5]}$	259.871-456.65 (T_{cri})	[b]
	l-g	$10^{5.1309-1602.88/(T+13.743)}$	259.871-456.65 (T_{cri})	[d]
HC ₃ N	s-g	$e^{13.01-4426/T}$	[50.0]-164.9-201.5-[280] (T_{tri})	[a]
	s-g	$10^{7.30-2210/T}$	[<]247-280 (T_{tri})	[j]
	s-g	$52e^{T_{cri}/T[-7.3158(1-T/T_{cri})+1.7462(1-T/T_{cri})^{1.5}-2.2814(1-T/T_{cri})^{2.5}-2.7759(1-T/T_{cri})^5]}$	[<]160-280 (T_{tri})	[b]
	l-g	$10^{3.3419-712.924/(T-102.005)}$	280-336.89-527 (T_{tri})	[d]
	l-g	$52e^{T_{cri}/T[-7.3158(1-T/T_{cri})+1.7462(1-T/T_{cri})^{1.5}-2.2814(1-T/T_{cri})^{2.5}-2.7759(1-T/T_{cri})^5]}$	280-527 (T_{cri})	[b]
CO ₂	s-g	$e^{14.76-2571/T-7.781\times 10^4/T^2+4.325\times 10^6/T^3-1.207\times 10^8/T^4+1.350\times 10^9/T^5}$	[<]69.69-194.7-[216.5890] (T_{tri})	[a]
	l-g	$10^{4.6571-836.06/(T-4.927)}$	216.5890-304.128 (T_{cri})	[k]
CH ₃ CN	l-g	$48.66e^{T_{cri}/T[-8.027(1-T/T_{cri})+1.9887(1-T/T_{cri})^{1.5}-1.5119(1-T/T_{cri})^{2.5}-2.5934(1-T/T_{cri})^5]}$	229.349-545.41 (T_{cri})	[b]
C ₂ H ₅ CN	l-g	$10^{4.1883-1275.05/(T-65.154)}$	[180.4]-275.44-561.26 (T_{cri})	[d]
C ₂ H ₃ CN	l-g	$10^{4.06661-1255.94/(T-41.853)}$	[189.642]-222-351-[540.0] (T_{cri})	[l]
	l-g	$46.5e^{T_{cri}/T[-8.2647(1-T/T_{cri})+3.119(1-T/T_{cri})^{1.5}-2.962(1-T/T_{cri})^{2.5}-2.3068(1-T/T_{cri})^5]}$	[189.642]-222-540.0 (T_{cri})	[b]
C ₂ N ₂	s-g	$e^{26.335-4336.5/T-1.628\ln(T)}$	[<]179.979-245.29 (T_{tri})	[b]
	l-g	$10^{4.51661-1041.52/(T-21.288)}$	245.29-397.1 (T_{tri})	[m]
	l-g	$10^{4.0691-779.237/(T-60.228)}$	245.29-397.1 (T_{tri})	[d]

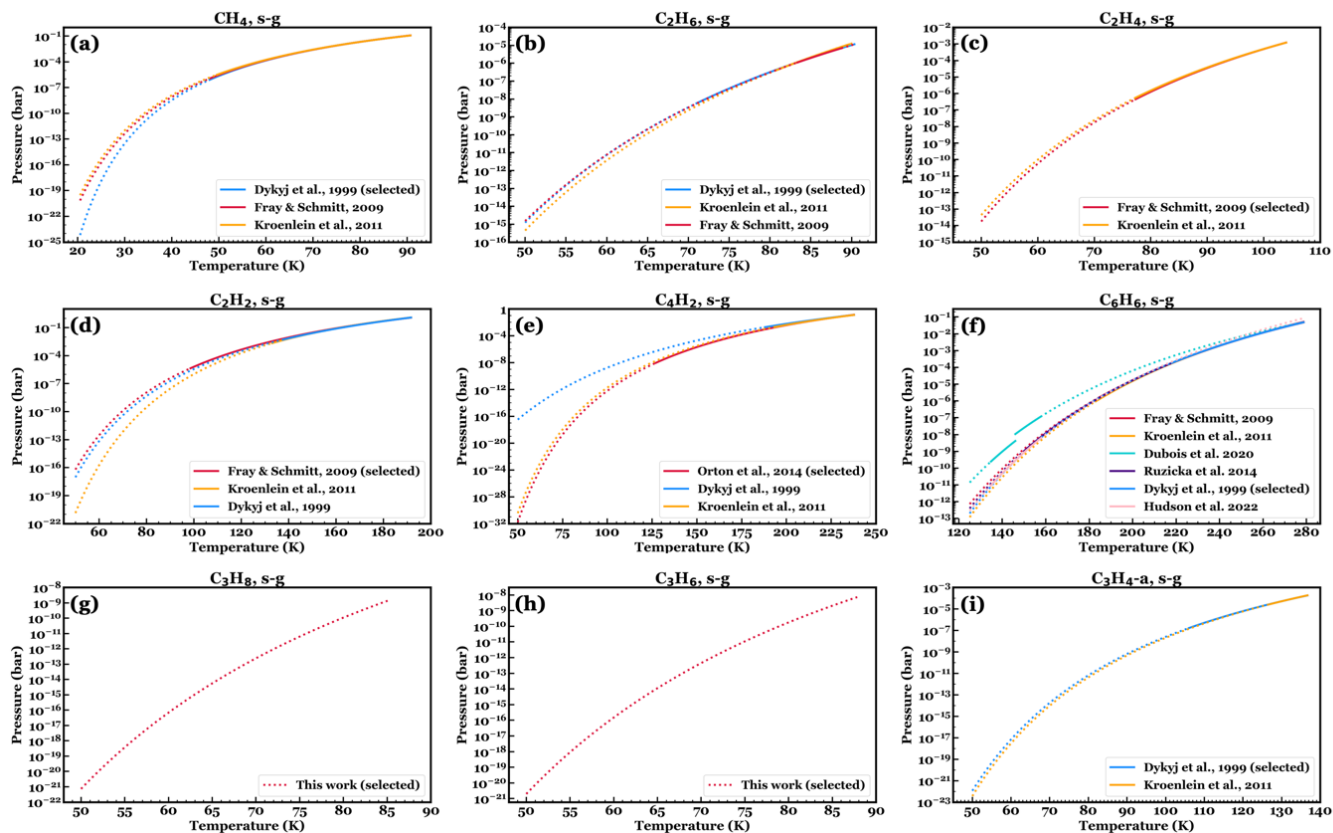


Figure 3. Comparison of the selected solid-gas (s-g) saturation vapor pressure (SVP) functions in Table 3 to the other evaluated s-g SVP functions in Table 15, for the first half of the species in Table 1. The solid lines represent the applicable temperature range (or the temperature without brackets in Table 3 and 15). The different SVP functions agree relatively well for the applicable temperature range. The dotted lines represent the extrapolated temperature range for each SVP function (or the temperature without brackets in Table 3 and 15). The different SVP functions start to deviate from each other for the extrapolated temperature range. Note that for benzene, we plot the unadjusted low-temperature s-g SVP expressions in Dubois et al. (2021), the adjusted s-g SVP expressions of Dubois et al. (2021) in Hudson et al. (2022) are similar to the independently measured SVP expressions in Hudson et al. (2022).

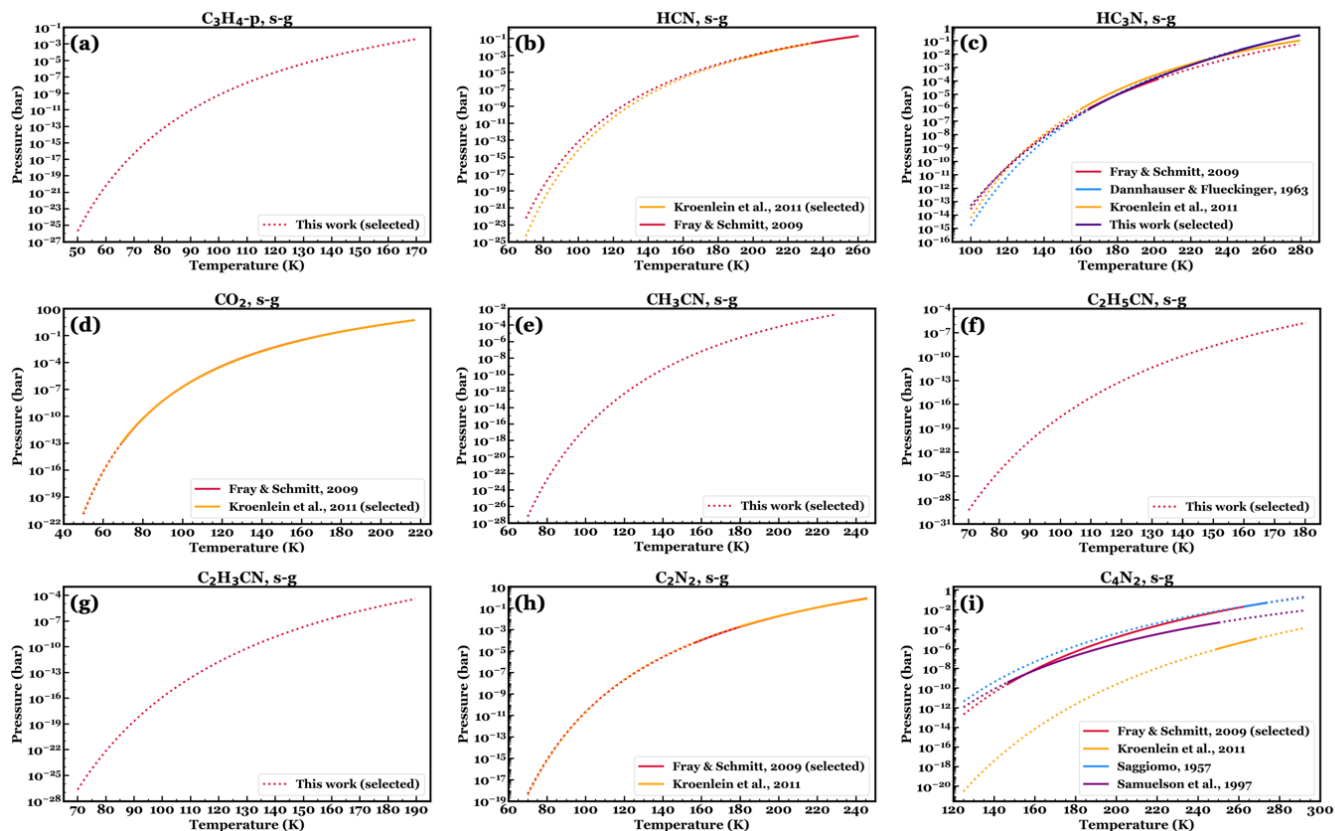


Figure 4. Comparison of the selected solid-gas (s-g) saturation vapor pressure (SVP) functions in Table 3 to the other evaluated s-g SVP functions in Table 15, for the second half of the species in Table 1. Notations are the same as Figure 3. The different SVP functions agree relatively well for the applicable temperature range, except for C_4N_2 , which has one outlier s-g SVP. Similar to Figure 3, the different SVP functions start to deviate from each other for the extrapolated temperature range.

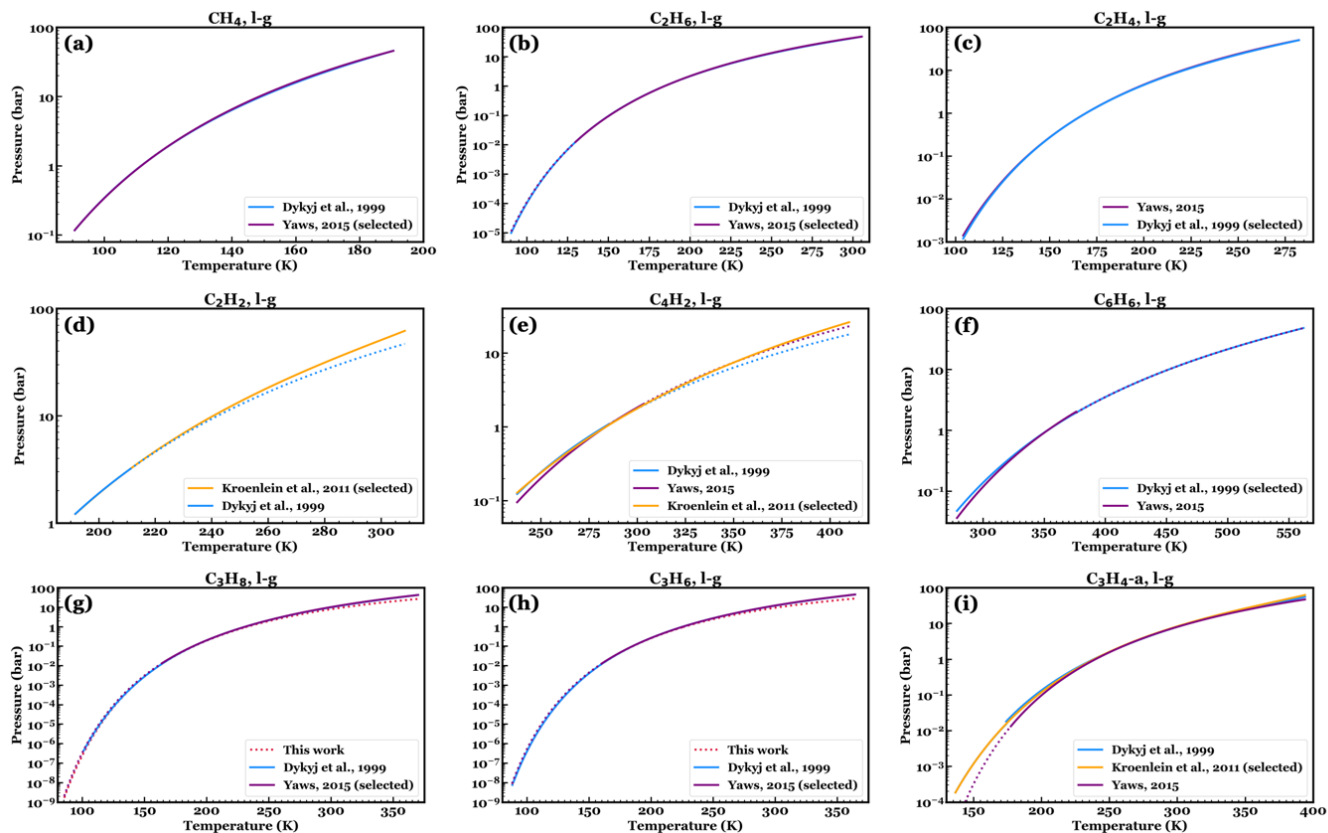


Figure 5. Comparison of the selected liquid-gas (l-g) saturation vapor pressure (SVP) functions in Table 3 to the other evaluated l-g SVP functions in Table 15, for the first half of the species in Table 1. Notations are the same as Figure 3. Similar to Figure 3, the different SVP functions agree relatively well for the applicable temperature range, and they start to deviate from each other for the extrapolated temperature range.

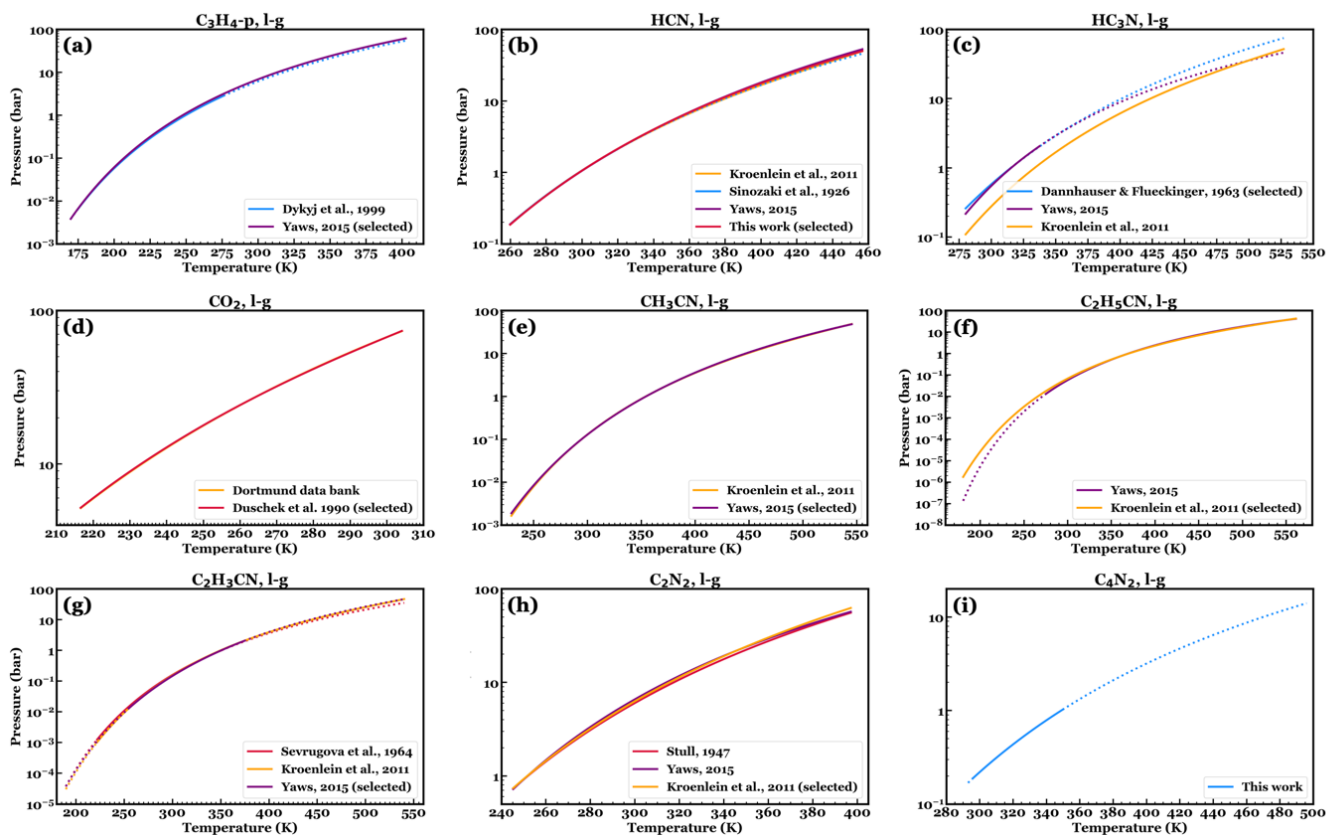


Figure 6. Comparison of the selected liquid-gas (l-g) saturation vapor pressure (SVP) functions in Table 3 to the other evaluated l-g SVP functions in Table 15, for the second half of the species in Table 1. Notations are the same as Figure 3. The different SVP functions agree relatively well for the applicable temperature range, except HC_3N , which has one outlier l-g SVP. Similar to Figure 3, the different SVP functions start to deviate from each other for the extrapolated temperature range.

Table 16. Organic liquid density data, references, adopted density using expressions in Table 8, and the deviation of the fitting to the experimental data in percentage, defined as the absolute difference in percentage between the experimental data and the model fit.

CH₄	Temp (K)	Density (kg·m ⁻³)	Adopted density (kg·m ⁻³)	Deviation (%)
Rumble (2020)	90.6941	451.5	451.6	0.02
	100.0	438.9	438.8	0.01
	110.0	424.8	424.7	0.03
	120.0	409.9	409.9	0.01
	130.0	394.0	394.1	0.02
	140.0	376.9	377.0	0.02
	150.0	357.9	358.0	0.02
	160.0	336.3	336.3	0.01
	170.0	310.5	310.4	0.04
	180.0	276.2	276.1	0.05
	190.0	200.8	201.1	0.13
190.564	162.7	162.7	0.00	
C₂H₆	Temp (K)	Density (kg·m ⁻³)	Adopted density (kg·m ⁻³)	Deviation (%)
Rumble (2020)	90.368	651.5	651.5	0.01
	100.0	640.9	640.9	0.00
	120.0	618.9	618.8	0.01
	140.0	596.6	596.5	0.02
	160.0	573.6	573.4	0.01
	180.0	549.5	549.6	0.01
	200.0	524.0	524.1	0.02
	220.0	496.3	496.4	0.02
	240.0	465.3	465.3	0.01
	260.0	429.1	429.0	0.03
	280.0	382.7	382.5	0.04
	300.0	303.5	303.7	0.07
	305.322	206.2	206.2	0.00
C₂H₄	Temp (K)	Density (kg·m ⁻³)	Adopted density (kg·m ⁻³)	Deviation (%)
Rumble (2020)	103.986	654.6	654.7	0.02
	120.0	634.2	634.1	0.02
	140.0	608.0	607.9	0.02
	160.0	580.9	580.9	0.01
	180.0	552.2	552.3	0.02
	200.0	521.2	521.4	0.03

Continued on the next page

Table 16. Organic liquid density data (cont.)

	220.0	486.7	486.7	0.01
	240.0	446.1	446.0	0.02
	260.0	393.5	393.3	0.06
	280.0	290.7	291.0	0.09
	282.350	214.2	214.2	0.00
C₄H₂	Temp	Density	Adopted	Deviation
	(K)	(kg·m ⁻³)	density (kg·m ⁻³)	(%)
Egloff & Kuder (1942)	236.75	927.1	926.9	0.02
Straus & Kollek (1926)	273.15	736.4	736.5	0.02
Lespieau & Prevost (1925)	278.15	710.7	710.4	0.05
C₆H₆	Temp	Density	Adopted	Deviation
	(K)	(kg·m ⁻³)	density (kg·m ⁻³)	(%)
Rumble (2020)	278.674	894.0	894.4	0.04
	280.0	892.6	892.9	0.04
	300.0	871.6	871.4	0.02
	320.0	850.4	849.8	0.07
	340.0	828.6	828.0	0.07
	360.0	806.2	805.8	0.04
	380.0	783.1	783.0	0.01
	400.0	758.9	759.2	0.04
	420.0	733.6	734.2	0.08
	440.0	706.7	707.5	0.11
	460.0	677.8	678.4	0.09
	480.0	646.1	646.3	0.03
	500.0	610.1	609.6	0.09
	520.0	567.0	565.7	0.24
	540.0	508.9	507.6	0.25
	560.0	385.7	388.9	0.84
	562.02	304.7	304.7	0.00
C₃H₈	Temp	Density	Adopted	Deviation
	(K)	(kg·m ⁻³)	density (kg·m ⁻³)	(%)
Rumble (2020)	85.5	733.1	733.1	0.00
	100.0	718.1	718.2	0.01
	120.0	697.8	697.8	0.00
	140.0	677.6	677.6	0.01
	160.0	657.3	657.2	0.02
	180.0	636.6	636.5	0.01
	200.0	615.4	615.4	0.00
	220.0	593.4	593.5	0.11

Continued on the next page

Table 16. Organic liquid density data (cont.)

240.0	570.4	570.5	0.01	
260.0	545.8	545.9	0.02	
280.0	519.2	519.2	0.00	
300.0	489.4	488.6	0.00	
320.0	454.9	454.8	0.03	
340.0	411.8	411.6	0.05	
360.0	345.6	345.8	0.07	
369.89	220.5	220.5	0.00	
<hr/>				
C₃H₆	Temp	Density	Adopted	Deviation
	(K)	(kg·m ⁻³)	density (kg·m ⁻³)	(%)
<i>Rumble (2020)</i>	87.9	768.1	768.0	0.02
	100.0	754.0	754.1	0.01
	120.0	731.2	731.3	0.02
	140.0	708.8	708.9	0.01
	160.0	686.4	686.4	0.00
	180.0	663.9	663.8	0.02
	200.0	640.8	640.7	0.01
	220.0	616.9	616.8	0.01
	240.0	591.8	591.8	0.00
	260.0	565.0	565.1	0.01
	280.0	535.8	535.9	0.02
	300.0	503.1	503.1	0.00
	320.0	464.5	464.5	0.01
	340.0	414.7	414.7	0.01
	360.0	325.7	325.7	0.00
	364.21	229.6	229.6	0.00
<hr/>				
C₃H₄-p	Temp	Density	Adopted	Deviation
	(K)	(kg·m ⁻³)	density (kg·m ⁻³)	(%)
<i>Kroenlein et al. (2011)</i>	273	650	644.5	0.85
	276	650	640.6	1.45
	282	637	632.7	0.67
	288	628	624.6	0.54
	294	618	616.2	0.28
	300	608	607.6	0.07
	306	599	598.6	0.06
	312	589	589.3	0.06
	318	578	579.6	0.28
	324	568	569.5	0.26
	330	557	558.9	0.34

Continued on the next page

Table 16. Organic liquid density data (cont.)

	336	546	547.7	0.31
	342	534	535.9	0.36
	348	522	523.4	0.27
	354	509	510.1	0.21
	360	495	495.8	0.16
	366	480	480.3	0.06
	372	464	463.4	0.14
	378	446	444.5	0.34
	384	425	423.0	0.48
	390	400	397.3	0.68
	396	365	363.5	0.40
	402	290	296.4	2.21
	402.7	244.90	244.9	0.00
Rumble (2020)	298.15	607.0	610.3	0.54
Gee et al. (1986)	246.0	675.0	677.4	0.36
	217.0	710.0	710.8	0.11
	185.0	749.0	747.4	0.21
Maass & Wright (1921)	217.85	712.6	709.8	0.39
	221.15	709.1	706.1	0.43
	222.3	707.4	704.8	0.37
	232.8	694.1	692.8	0.19
	240.85	684.1	683.5	0.09
	247.85	675.9	675.3	0.09
	253.85	668.0	668.1	0.02
	260.25	659.8	660.4	0.09
Morehouse & Maass (1931)	216.15	710.9	711.8	0.12
	220.05	706.5	707.3	0.12
	221.25	703.9	706.0	0.29
	225.75	699.2	700.8	0.23
	230.75	693.6	695.1	0.22
	232.25	691.1	693.4	0.33
	236.35	687.3	688.7	0.20
	240.15	681.4	684.3	0.42
	240.65	682.7	683.7	0.15
	246.65	675.9	676.7	0.12
	248.95	671.1	674.0	0.43
	250.45	671.0	672.2	0.18
	255.65	665.2	666.0	0.12
	258.75	661.7	662.2	0.08

Continued on the next page

Table 16. Organic liquid density data (cont.)

	260.45	658.2	660.1	0.30
	272.65	644.7	644.9	0.03
CO₂	Temp	Density	Adopted	Deviation
	(K)	(kg·m ⁻³)	density (kg·m ⁻³)	(%)
Rumble (2020)	216.6 (T_{tri})	1178.0	1178.2	0.01
	220.0	1166.0	1165.9	0.01
	230.0	1129.0	1128.7	0.03
	240.0	1089.0	1089.0	0.00
	250.0	1046.0	1046.2	0.02
	260.0	998.9	999.0	0.01
	270.0	945.8	945.8	0.00
	280.0	883.6	883.5	0.01
	290.0	804.7	804.5	0.02
	300.0	679.2	679.4	0.03
	304.128	467.8	467.6	0.00

Table 17. Organic ice density data that are used for the intrinsic density expression fittings in Table 9 (including diffraction and pycnometry data), references, adopted intrinsic density fits using expressions in Table 9, and the deviation of the fitting to the experimental data in percentage. All the ices measured in this table are in their crystalline form.

CH₄	Temp (K)	Density (kg·m ⁻³)	Technique	Adopted density (kg·m ⁻³)	Deviation (%)
Heuse (1930)	20.4	522.5	Pycnometry	528.1	1.08
Mooy (1931)	20.5	521.41	X-ray diffraction	528.1	1.28
Schallamach (1939)	13.9	534.9	X-ray diffraction	529.9	0.93
	14.25	540.4		529.9	1.95
	14.3	540.4		529.9	1.95
	15.0	557.5		529.8	4.97
	17.0	557.5		529.4	5.04
	18.5	533.5		529.0	0.86
	20.35	530.8		528.2	0.50
	20.35	551.7		528.2	4.27
	22.0	532.2		525.0	1.36
	27.5	533.5		523.8	1.82
	35.0	521.4		521.8	0.08
Manzhelii & Tolkachev (1964)	77.4	494.2	Pycnometry	501.3	1.43
	85.4	489.2		495.8	1.35
Tolkachev & Manzhelii (1966)	20.4	522.5	Pycnometry	528.1	1.08
Greer & Meyer (1969)	4.0	528.1	X-ray diffraction	530.0	0.36
	5.0	526.2		530.0	0.73
	17.0	521.9		529.4	1.43
	20.0	519.0		528.3	1.79
	21.0	517.4		525.1	1.49
	25.0	516.9		524.4	1.44
	31.0	515.6		523.0	1.42
	35.0	511.7		521.8	1.98
	40.0	510.7		520.2	1.86
	50.0	508.4		516.3	1.56
	55.0	502.7		514.0	2.23
	58.0	500.2		512.5	2.45
	61.0	497.7		511.0	2.66
	65.0	490.3		508.8	3.77
	70.0	492.8		505.9	2.66
	75.0	485.4		502.8	3.57
Bol'shutkin et al. (1971)	11.0	524.5	X-ray diffraction	530.1	1.06
	12.0	524.4		530.1	1.08

Continued on the next page

Table 17. Organic ice density data (cont.)

	13.0	524.1		530.0	1.13
	14.0	523.8		529.9	1.17
	15.0	523.2		529.8	1.26
	16.0	522.3		529.6	1.40
	17.0	521.5		529.4	1.52
	18.0	520.6		529.1	1.64
	19.0	519.7		528.8	1.75
	20.0	518.5		528.3	1.90
	21.0	517.5		525.1	1.48
	22.0	517.4		525.0	1.46
	25.0	516.8		524.4	1.47
	30.0	515.2		523.2	1.56
	35.0	513.0		521.8	1.72
	40.0	511.3		520.2	1.74
	45.0	510.0		518.3	1.63
	50.0	507.0		516.3	1.83
	55.0	504.0		514.0	1.98
	60.0	500.0		511.5	2.29
	65.0	497.0		508.8	2.37
	70.0	494.0		505.9	2.40
Aadsen (1975)	2.5	527.9	X-ray Diffraction	530.0	0.39
	4.3	528.0		530.0	0.38
	5.7	528.0		530.0	0.39
	7.0	528.0		530.1	0.38
	7.9	528.0		530.1	0.39
	8.9	528.1		530.1	0.38
	9.8	528.0		530.1	0.39
	10.6	528.1		530.1	0.38
	11.9	528.0		530.1	0.40
	13.1	527.9		530.0	0.40
	13.9	527.8		529.9	0.40
	14.7	527.7		529.8	0.40
	15.2	527.6		529.8	0.40
	15.5	527.6		529.7	0.40
	16.1	527.4		529.6	0.41
	16.9	527.2		529.5	0.42
	17.6	527.1		529.2	0.41
	18.5	526.7		529.0	0.43
	19.0	526.4		528.8	0.45

Continued on the next page

Table 17. Organic ice density data (cont.)

19.4	526.2	528.6	0.46
19.7	525.9	528.5	0.50
19.8	525.8	528.4	0.50
19.9	525.7	528.4	0.51
20.0	525.6	528.3	0.52
20.1	525.5	528.3	0.53
20.2	525.4	528.3	0.55
20.3	525.1	528.2	0.58
20.4	524.7	528.2	0.65
20.5	523.8	528.1	0.82
20.6	523.1	525.2	0.41
20.7	523.0	525.2	0.41
20.8	523.0	525.2	0.41
20.9	523.0	525.2	0.41
21.1	522.9	525.1	0.42
21.2	522.9	525.1	0.42
21.4	522.9	525.1	0.42
21.5	522.8	525.1	0.42
21.8	522.7	525.0	0.43
21.9	522.7	525.0	0.43
22.0	522.7	525.0	0.44
22.3	522.6	524.9	0.44
22.6	522.6	524.9	0.44
23.1	522.5	524.8	0.44
24.1	522.1	524.6	0.46
25.1	521.9	524.4	0.46
26.0	521.7	524.2	0.48
27.1	521.4	523.9	0.49
28.1	521.1	523.7	0.50
30.1	520.5	523.2	0.52
32.1	519.8	522.6	0.54
34.1	519.2	522.1	0.56
36.0	518.5	521.5	0.59
38.1	517.7	520.8	0.60
40.0	517.0	520.2	0.62
42.0	516.2	519.5	0.63
44.0	515.3	518.7	0.65
46.1	514.4	517.9	0.67
48.1	513.5	517.1	0.69

Continued on the next page

Table 17. Organic ice density data (cont.)

	50.2	512.5		516.2	0.72
	52.1	511.6		515.3	0.72
	54.2	510.7		514.4	0.72
	55.9	509.7		513.5	0.74
	58.1	508.6		512.4	0.75
	60.1	507.6		511.4	0.76
	62.2	506.4		510.3	0.77
	64.4	505.3		509.1	0.76
	66.3	504.2		508.0	0.76
	68.4	502.9		506.8	0.78
	70.7	501.6		505.5	0.77
	73.0	500.1		504.1	0.79
	74.9	498.9		502.8	0.79
	76.8	497.7		501.7	0.80
	78.9	496.4		500.2	0.78
	81.0	495.0		498.9	0.79
	82.9	493.6		497.6	0.81
	84.8	492.3		496.2	0.79
	86.2	491.3		495.2	0.80
Prokhvatilov & Isakina (1983)	10.0	529.9	X-ray diffraction	530.1	0.04
	12.0	529.8		530.1	0.05
	14.0	529.6		529.9	0.07
	16.0	529.2		529.6	0.09
	18.0	528.5		529.1	0.12
	19.0	527.9		528.8	0.16
	20.0	527.1		528.3	0.23
	20.3	526.7		528.2	0.29
	20.6	524.9		525.2	0.06
	20.8	524.7		525.2	0.10
	21.0	524.5		525.1	0.13
	21.5	524.0		525.1	0.19
	22.0	523.8		525.0	0.23
	23.0	523.4		524.8	0.26
	24.0	523.1		524.6	0.28
	26.0	522.5		524.2	0.31
	28.0	521.9		523.7	0.34
	30.0	521.3		523.2	0.37
	35.0	519.7		521.8	0.40
	40.0	517.8		520.2	0.46

Continued on the next page

Table 17. Organic ice density data (cont.)

	45.0	515.8		518.3	0.49
	50.0	513.6		516.3	0.52
	55.0	511.2		514.0	0.54
	60.0	508.7		511.5	0.55
	65.0	506.0		508.8	0.55
	70.0	503.1		505.9	0.55
	75.0	500.1		502.8	0.54
	80.0	496.9		499.5	0.53
	85.0	493.7		496.1	0.49
	88.0	491.4		493.9	0.52
	89.0	490.6		493.2	0.53
	90.0	489.8		492.5	0.54
Maynard-Casely et al. (2020)	8.0	530.09	Neutron diffraction	530.1	0.00
	10.0	530.11		530.1	0.00
	12.0	530.05		530.1	0.00
	14.0	529.89		529.9	0.01
	16.0	529.62		529.6	0.00
	18.0	529.2		529.1	0.01
	20.0	528.31		528.3	0.01
	22.0	525.41		525.0	0.08
	24.0	524.76		524.6	0.03
	26.0	524.24		524.2	0.01
	28.0	523.64		523.7	0.01
	30.0	523.06		523.2	0.03
	32.0	522.59		522.7	0.02
	34.0	521.85		522.1	0.05
	36.0	521.35		521.5	0.03
	38.0	520.57		520.9	0.06
	40.0	519.93		520.2	0.05
	42.0	518.98		519.5	0.09
	44.0	518.53		518.7	0.04
	46.0	518.05		517.9	0.02
	48.0	517.6		517.1	0.09
	50.0	516.58		516.3	0.06
	52.0	515.58		515.4	0.04
	54.0	514.55		514.4	0.02
	56.0	513.33		513.5	0.03
	58.0	512.49		512.5	0.00
	60.0	511.4		511.5	0.01

Continued on the next page

Table 17. Organic ice density data (cont.)

	62.0	510.62		510.4	0.04
	64.0	509.66		509.3	0.06
	66.0	508.73		508.2	0.10
	68.0	506.26		507.1	0.16
	70.0	505.54		505.9	0.07
	72.0	504.67		504.7	0.00
	74.0	503.09		503.4	0.07
	76.0	502.91		502.2	0.15
	78.0	500.64		500.9	0.04
	80.0	499.7		499.5	0.03
	82.0	497.98		498.2	0.04
	84.0	497.49		496.8	0.14
	86.0	495.31		495.4	0.02
	88.0	493.37		493.9	0.12
Drobyshev et al. (2017)	16.0	510.0	Pycnometry	529.6	3.85
	30.0	520.0		523.2	0.62
C_2H_6	Temp (K)	Density ($\text{kg}\cdot\text{m}^{-3}$)	Technique	Adopted density ($\text{kg}\cdot\text{m}^{-3}$)	Deviation (%)
Mark & Pohland (1925)	88.0	708.0	X-ray diffraction	709.6	0.22
Heuse (1930)	20.4	751.9	Pycnometry	739.8	1.61
Stewart & La Rock (1958)	77.0	713.0	Pycnometry	718.3	0.74
van Nes & Vos (1978)	90.0	669.0	X-ray diffraction	669.0	0.00
	85.0	719.0		712.1	0.96
Klimenko et al. (2008)	5.0	740.2	X-ray diffraction	738.8	0.18
	10.0	740.1		739.5	0.09
	15.0	739.7		739.8	0.01
	20.0	739.2		739.8	0.08
	25.0	738.6		739.5	0.12
	30.0	737.8		738.9	0.15
	35.0	737.1		738.0	0.12
	40.0	735.9		736.8	0.12
	45.0	734.8		735.2	0.06
	50.0	733.4		733.4	0.00
	55.0	731.7		731.3	0.06
	60.0	729.8		728.9	0.13
	65.0	727.5		726.1	0.19
	70.0	724.6		723.1	0.21
	75.0	721.5		719.7	0.25
	80.0	717.4		716.1	0.19

Continued on the next page

Table 17. Organic ice density data (cont.)

	82.0	715.5		714.5	0.14
	84.0	713.3		712.9	0.05
	86.0	710.8		711.3	0.07
	88.0	707.9		709.6	0.24
	89.5	704.4		708.3	0.55
	90.0	656.2		669.0	1.95
C₂H₄	Temp (K)	Density (kg·m ⁻³)	Technique	Adopted density (kg·m ⁻³)	Deviation (%)
Heuse (1930)	20.4	780.7	Pycnometry	780.9	0.03
Clusius & Weigand (1940)	103.97	717.8	Pycnometry	722.6	0.68
Stewart & La Rock (1958)	77.0	732.0	Pycnometry	741.5	1.29
van Nes & Vos (1979)	85.0	750.4	X-ray diffraction	735.9	1.94
C₂H₂	Temp (K)	Density (kg·m ⁻³)	Technique	Adopted density (kg·m ⁻³)	Deviation (%)
McIntosh (1097)	188.15	730.0	Pynometry	731.7	0.23
Sugawara & Kanda (1952)	156.0	747.2	X-ray diffraction	752.5	0.70
Amamchyan & Moroz (1965)	77.0	810.0	Pynometry	803.7	0.78
	90.0	790.0		795.3	0.67
van Nes & van Bolhuis (1979)	160.0	752.0	X-ray diffraction	749.9	0.28
	170.0	750.5		743.4	0.95
	141.0	765.4		762.2	0.42
McMullan et al. (1992)	131.0	764.3	Neutron diffraction	768.7	0.58
	141.0	760.2		762.2	0.27
C₆H₆	Temp (K)	Density (kg·m ⁻³)	Technique	Adopted density (kg·m ⁻³)	Deviation (%)
Heuse (1930)	20.4	1125.5	Pycnometry	1125.7	0.01
Cox et al. (1958)	270.15	1023.0	X-ray diffraction	1022.0	0.09
Bacon et al. (1964)	218.15	1055.0	Neutron diffraction	1055.4	0.02
	138.15	1094.0		1094.7	0.02
Kohzin (1954)	77.0	1115.0	X-ray diffraction	1114.7	0.02
Richards et al. (1921)	278.7	1015.1	Pycnometry	1015.9	0.08
C₃H₈	Temp (K)	Density (kg·m ⁻³)	Technique	Adopted density (kg·m ⁻³)	Deviation (%)
Heuse (1930)	20.4	813.7	Pycnometry	813.5	0.00
Stewart & La Rock (1958)	77.0	763.0	Pycnometry	759.5	0.50
Boese et al. (1999)	30.0	803.0	X-ray diffraction	804.4	0.20
	90.0	743.0		747.1	0.60
C₃H₆	Temp	Density	Technique	Adopted	Deviation

Continued on the next page

Table 17. Organic ice density data (cont.)

	(K)	($\text{kg}\cdot\text{m}^{-3}$)		density ($\text{kg}\cdot\text{m}^{-3}$)	(%)
Stewart & La Rock (1958)	77.0	806.0	Pycnometry	806.0	0.00
C₃H₄-a	Temp	Density	Technique	Adopted	Deviation
	(K)	($\text{kg}\cdot\text{m}^{-3}$)		density ($\text{kg}\cdot\text{m}^{-3}$)	(%)
Blanc et al. (1962)	95.0	860.0	Lattice structure model	860.0	0.00
C₃H₄-p	Temp	Density	Technique	Adopted	Deviation
	(K)	($\text{kg}\cdot\text{m}^{-3}$)		density ($\text{kg}\cdot\text{m}^{-3}$)	(%)
Marlin et al. (2022)	90.0	882.0	X-ray diffraction	882.0	0.00
HCN	Temp	Density	Technique	Adopted	Deviation
	(K)	($\text{kg}\cdot\text{m}^{-3}$)		density ($\text{kg}\cdot\text{m}^{-3}$)	(%)
Dulmage & Lipscomb (1951)	153.15	1032.8	X-ray diffraction	1028.2	0.45
	193.15	965.1		974.3	0.96
Werner (1929)	233.15	925.0	Pycnometry	920.4	0.50
HC₃N	Temp	Density	Technique	Adopted	Deviation
	(K)	($\text{kg}\cdot\text{m}^{-3}$)		density ($\text{kg}\cdot\text{m}^{-3}$)	(%)
Shallcross & Carpenter (1958)	248.15	1075.3	X-ray diffraction	1075.3	0.00
CO₂	Temp	Density	Technique	Adopted	Deviation
	(K)	($\text{kg}\cdot\text{m}^{-3}$)		density ($\text{kg}\cdot\text{m}^{-3}$)	(%)
Heuse (1930)	20.4	1702.1	Pycnometry	1708.3	0.36
Behn (1900)	194.15	1560.0	Pycnometry	1566.8	0.43
De Smedt & Keesom (1924)	78.8	1638.7	X-ray diffraction	1683.6	2.74
Maass & Barnes (1926)	191.65	1569.0	Pycnometry	1570.3	0.08
	189.55	1573.0		1573.2	0.01
	187.65	1575.0		1575.8	0.05
	177.85	1589.0		1588.8	0.02
	167.95	1600.0		1601.2	0.08
	157.95	1610.0		1613.1	0.19
	144.35	1621.0		1628.3	0.45
	90.15	1663.0		1676.1	0.79
	193.55	1565.0		1567.6	0.17
	185.25	1582.0		1579.0	0.19
	178.05	1590.0		1588.5	0.09
	168.05	1602.0		1601.1	0.06
	158.25	1611.0		1612.8	0.11
	147.95	1623.0		1624.4	0.08
	137.95	1630.0		1634.9	0.30
	90.15	1674.0		1676.1	0.12
Keesom & Köhler (1934a)	83.15	1687.6	X-ray diffraction	1680.8	0.41

Continued on the next page

Table 17. Organic ice density data (cont.)

Keesom & Köhler (1934b)	20.0	1718.0	X-ray diffraction	1708.4	0.56		
	35.0	1714.3		1704.3	0.58		
	65.0	1701.3		1691.5	0.58		
	86.0	1688.6		1678.9	0.57		
	94.0	1682.2		1673.3	0.53		
	111.0	1667.8		1660.0	0.47		
	114.0	1663.4		1657.5	0.35		
	Mueller (1969)	77.0		1670.0	Pycnometry	1684.7	0.88
	Seiber et al. (1971)	82.0		1670.0	Pycnometry	1681.5	0.69
	Simon & Peters (1980)	150.0		1643.9	X-ray diffraction	1622.1	1.33
	Mangan et al. (2017)	80.0		1684.6	X-ray diffraction	1682.8	0.10
		85.0		1681.4		1679.6	0.11
		90.0		1678.3		1676.2	0.13
		95.0		1674.0		1672.6	0.08
100.0		1670.4	1668.9	0.09			
105.0		1667.4	1664.9	0.15			
110.0		1662.4	1660.9	0.09			
115.0		1658.7	1656.6	0.13			
120.0		1653.4	1652.2	0.07			
110.0		1664.1	1660.9	0.19			
115.0	1658.4	1656.6	0.11				
120.0	1654.0	1652.2	0.11				
125.0	1649.9	1647.6	0.14				
130.0	1646.3	1642.9	0.21				
<hr/>							
CH₃CN-α	Temp (K)	Density (kg·m ⁻³)	Technique	Adopted density (kg·m ⁻³)	Deviation (%)		
Barrow (1981)	215.0	1022.4	X-ray diffraction	1022.4	0.00		
Brackmeyer et al. (1997)	208.0	1025.3	X-ray diffraction	1025.5	0.01		
Enjalbert & Galy (2002)	201.0	1027.9	X-ray diffraction	1027.9	0.01		
Torrie & Powell (1989)	229.0	1016.5	Neutron diffraction	1014.3	0.22		
Choi et al. (2020)	225.0	1016.5		1016.8	0.03		
	230.0	1011.7		1013.6	0.19		
	235.0	1010.0	1010.0	0.01			
<hr/>							
CH₃CN-β	Temp (K)	Density (kg·m ⁻³)	Technique	Adopted density (kg·m ⁻³)	Deviation (%)		
Antson et al. (1987)	100.0	1104.5	Neutron diffraction	1107.8	0.30		
Enjalbert & Galy (2002)	206.0	1058.2	X-ray diffraction	1053.1	0.48		
Torrie & Powell (1989)	12.0	1131.0	Neutron diffraction	1126.8	0.37		
	60.0	1125.6		1119.4	0.56		

Continued on the next page

Table 17. Organic ice density data (cont.)

	110.0	1107.3		1104.1	0.29
	170.0	1075.8		1075.6	0.02
	220.0	1044.5		1043.3	0.11
Choi et al. (2020)	5.0	1125.1	Neutron diffraction	1127.2	0.19
	10.0	1125.2		1126.9	0.15
	15.0	1124.9		1126.5	0.14
	20.0	1125.0		1126.0	0.09
	25.0	1124.7		1125.5	0.07
	30.0	1124.2		1124.8	0.05
	35.0	1123.9		1124.1	0.02
	40.0	1123.2		1123.3	0.01
	45.0	1122.6		1122.4	0.01
	50.0	1121.7		1121.5	0.02
	55.0	1120.7		1120.5	0.02
	60.0	1119.5		1119.4	0.01
	65.0	1118.4		1118.2	0.02
	70.0	1117.2		1116.9	0.02
	75.0	1115.6		1115.6	0.01
	80.0	1114.2		1114.2	0.00
	85.0	1112.7		1112.7	0.00
	90.0	1111.0		1111.1	0.01
	95.0	1109.2		1109.5	0.02
	100.0	1107.4		1107.8	0.03
	105.0	1105.6		1106.0	0.03
	110.0	1103.7		1104.1	0.04
	115.0	1101.7		1102.1	0.04
	120.0	1099.6		1100.1	0.05
	125.0	1097.6		1098.0	0.04
	130.0	1095.5		1095.8	0.03
	135.0	1093.0		1093.6	0.05
	140.0	1090.8		1091.2	0.04
	145.0	1088.7		1088.8	0.01
	150.0	1085.9		1086.3	0.04
	155.0	1083.3		1083.7	0.04
	160.0	1080.8		1081.1	0.02
	165.0	1078.0		1078.4	0.03
	170.0	1075.4		1075.6	0.02
	175.0	1072.5		1072.7	0.02
	180.0	1069.3		1069.7	0.04

Continued on the next page

Table 17. Organic ice density data (cont.)

	185.0	1066.0		1066.7	0.06
	190.0	1063.1		1063.6	0.05
	195.0	1059.7		1060.4	0.07
	200.0	1056.4		1057.1	0.07
	205.0	1053.0		1053.8	0.08
	210.0	1049.4		1050.4	0.09
	215.0	1045.8		1046.9	0.10
C₂H₅CN	Temp (K)	Density (kg·m ⁻³)	Technique	Adopted density (kg·m ⁻³)	Deviation (%)
Brand et al. (2020)	100.0	1014.0	X-ray diffraction	1014.5	0.01
	110.0	1010.0		1009.9	0.01
	120.0	1005.0		1005.3	0.02
	130.0	1001.0		1000.7	0.03
	140.0	996.0		996.0	0.03
	150.0	991.0		991.4	0.05
C₂H₃CN	Temp (K)	Density (kg·m ⁻³)	Technique	Adopted density (kg·m ⁻³)	Deviation (%)
Yokoyama & Ohashi (1998)	153.0	1027.4	X-ray diffraction	1027.4	0.00
C₂N₂	Temp (K)	Density (kg·m ⁻³)	Technique	Adopted density (kg·m ⁻³)	Deviation (%)
Parkes & Hughes (1963)	178.15	1250.2	X-ray diffraction	1250.2	0.00
Torrie & Powell (1989)	15.0	1282.9	Neutron diffraction	1282.9	0.00
C₄N₂	Temp (K)	Density (kg·m ⁻³)	Technique	Adopted density (kg·m ⁻³)	Deviation (%)
Hannan & Collin (1953)	278.15	1229.5	X-ray diffraction	N/A	N/A

Table 18. Organic ice average density data that are not used for the fittings in Table 9, the associated references, adopted intrinsic density fits using expressions in Table 9, and the phase of ice. The quartz crystal microbalance (QCM)/double laser interferometry combination technique is abbreviated as QCM in the table.

CH₄	Temp (K)	Density (kg·m ⁻³)	Technique	Adopted density (kg·m ⁻³)	Phase
Roux et al. (1980)	20.0	426.0	QCM	528.3	Undetermined
Satorre et al. (2008)	10.0	471.5	QCM	530.1	Undetermined
Shinbayeva et al. (2017)	16.0	480.0	Estimated using n_{vis}	529.6	Crystalline
	30.0	490.0		523.2	Crystalline
Yarnall & Hudson (2022)	30.0	508.0	QCM	523.2	Crystalline
C₂H₆	Temp (K)	Density (kg·m ⁻³)	Technique	Adopted density (kg·m ⁻³)	Phase (%)
Molpeceres et al. (2016)	30.0	539.0	QCM	738.9	Amorphous
	18.0	414.0		739.8	Amorphous
Satorre et al. (2017)	13.0	411.0	QCM	739.7	Amorphous
	18.0	413.0		739.8	Amorphous
	20.0	441.0		739.8	Amorphous
	25.0	474.0		739.5	Amorphous
	30.0	530.0		738.9	Amorphous
	35.0	541.0		738.0	Amorphous
	40.0	600.0		736.8	Amorphous
	45.0	602.0		735.2	Crystalline
65.0	604.0	726.1	Crystalline		
Yarnall & Hudson (2022)	60.0	778.0	QCM	728.9	Crystalline
C₂H₄	Temp (K)	Density (kg·m ⁻³)	Technique	Adopted density (kg·m ⁻³)	Phase
Molpeceres et al. (2017)	30.0	580.0	QCM	774.2	Metastable crystalline
Satorre et al. (2017)	13.0	463.0	QCM	786.1	Amorphous
	16.0	507.0		784.0	Amorphous
	18.0	530.0		782.6	Amorphous
	20.0	564.0		781.2	Amorphous
	22.0	570.0		779.8	Metastable crystalline
	26.0	584.0		777.0	Metastable crystalline
	28.0	588.0		775.6	Metastable crystalline
	30.0	580.0		774.2	Metastable crystalline
	33.0	620.0		772.1	Metastable crystalline
	35.0	643.0		770.7	Metastable crystalline
	40.0	634.0		767.3	Crystalline
	45.0	650.0		763.8	Crystalline

Continued on the next page

Table 18. Organic ice density data (cont.)

	50.0	629.0		760.3	Crystalline
	55.0	636.0		756.8	Crystalline
	60.0	629.0		753.3	Crystalline
	65.0	630.0		749.8	Crystalline
Yarnall & Hudson (2022)	60.0	796.0	QCM	753.3	Crystalline
C₆H₆	Temp (K)	Density (kg·m ⁻³)	Technique	Adopted density (kg·m ⁻³)	Phase
Romanescu et al. (2010)	100.0	952.0	Estimated using n_{vis}	1108.2	Crystalline
Yarnall & Hudson (2022)	100.0	1085.0	QCM	1108.2	Crystalline
C₃H₈	Temp (K)	Density (kg·m ⁻³)	Technique	Adopted density (kg·m ⁻³)	Phase
Hudson et al. (2021)	15.0	653.0	QCM	818.7	Amorphous
	65.0	797.0		771.0	Crystalline
Yarnall & Hudson (2022)	65.0	797.0	QCM	771.0	Crystalline
C₃H₆	Temp (K)	Density (kg·m ⁻³)	Technique	Adopted density (kg·m ⁻³)	Phase
Hudson et al. (2021)	15.0	663.0	QCM	N/A	Amorphous
	65.0	782.0		N/A	Crystalline
C₃H₄-p	Temp (K)	Density (kg·m ⁻³)	Technique	Adopted density (kg·m ⁻³)	Phase
Hudson et al. (2021)	15.0	705.0	QCM	N/A	Amorphous
	80.0	866.0		N/A	Crystalline
HCN	Temp (K)	Density (kg·m ⁻³)	Technique	Adopted density (kg·m ⁻³)	Phase
Hudson (2020)	15.0	808.0	QCM	1214.4	Amorphous
Yarnall & Hudson (2022)	120.0	1037.0	QCM	1072.9	Crystalline
CO₂	Temp (K)	Density (kg·m ⁻³)	Technique	Adopted density (kg·m ⁻³)	Phase
Schulze & Abe (1980)	4.1	1088.0	Estimated using n_{vis}	1712.5	Undetermined
	6.0	1066.0		1712.3	Undetermined
	7.2	1035.0		1712.1	Undetermined
	8.1	1028.0		1712.0	Undetermined
	9.7	1013.0		1711.7	Undetermined
	12.0	1013.0		1711.4	Undetermined
	14.9	1016.0		1710.9	Undetermined
	17.1	1030.0		1710.4	Undetermined
	18.2	1042.0		1710.2	Undetermined
	20.2	1069.0		1709.8	Undetermined

Continued on the next page

Table 18. Organic ice density data (cont.)

	23.0	1101.0		1709.1	Undetermined
	25.2	1135.0		1708.6	Undetermined
	28.1	1197.0		1707.8	Undetermined
	29.7	1224.0		1707.3	Undetermined
	31.3	1245.0		1706.9	Undetermined
	33.1	1268.0		1706.3	Undetermined
	35.2	1307.0		1705.6	Undetermined
	36.5	1324.0		1705.2	Undetermined
	37.8	1362.0		1704.7	Undetermined
	40.8	1399.0		1703.7	Undetermined
	44.9	1465.0		1702.1	Undetermined
	48.7	1499.0		1700.6	Undetermined
	56.8	1588.0		1696.9	Undetermined
	60.4	1652.0		1695.2	Undetermined
	65.1	1664.0		1692.7	Undetermined
	69.7	1711.0		1690.2	Undetermined
	73.4	1747.0		1688.0	Undetermined
	76.9	1763.0		1685.9	Undetermined
	79.5	1762.0		1684.3	Undetermined
	81.9	1769.0		1682.8	Undetermined
	84.9	1769.0		1680.8	Undetermined
	88.0	1776.0		1678.7	Undetermined
Wood & Roux (1982)	20.0	1080.0	QCM	1709.8	Undetermined
	80.0	1670.0		1684.0	Undetermined
Loeffler et al. (2016)	14.0	1190-1370	QCM	1711.0	Predominantly crystalline
	20.0	1270-1450		1709.8	Predominantly crystalline
	30.0	1330-1560		1707.2	Predominantly crystalline
	40.0	1520-1640		1704.0	Predominantly crystalline
	50.0	1630-1700		1700.0	Predominantly crystalline
	60.0	1670-1710		1695.4	Predominantly crystalline
	70.0	1670-1700		1690.0	Predominantly crystalline
Satorre et al. (2008)	10.0	990.0	QCM	1711.7	Amorphous
	12.0	985.0		1711.4	Amorphous
	15.0	985.0		1710.8	Amorphous
	20.0	1030.0		1709.8	Partially amorphous
	30.0	1160.0		1707.2	Crystalline
	31.0	1160.0		1706.9	Crystalline
	34.0	1190.0		1706.0	Crystalline
	42.0	1250.0		1703.2	Crystalline

Continued on the next page

Table 18. Organic ice density data (cont.)

	46.0	1350.0		1701.7	Crystalline
	50.0	1455.0		1700.0	Crystalline
	58.0	1485.0		1696.3	Crystalline
	66.0	1485.0		1692.2	Crystalline
	73.0	1480.0		1688.3	Crystalline
	77.0	1560.0		1685.9	Crystalline
	80.0	1540.0		1684.0	Crystalline
	84.0	1510.0		1681.4	Crystalline
	90.0	1470.0		1677.3	Crystalline
Yarnall & Hudson (2022)	70.0	1666.0	QCM	1690.0	Crystalline
Domingo et al. (2015)	10.0	986.0	QCM	1711.7	Undetermined
	12.0	983.0		1711.4	Undetermined
	14.0	983.0		1711.0	Undetermined
	18.0	1032.0		1710.2	Undetermined
	29.0	1161.0		1707.5	Undetermined
	33.0	1183.0		1706.3	Undetermined
	40.0	1255.0		1704.0	Undetermined
	44.0	1345.0		1702.5	Undetermined
	48.0	1455.0		1700.9	Undetermined
	55.0	1485.0		1697.8	Undetermined
	63.0	1484.0		1693.8	Undetermined
	70.0	1480.0		1690.0	Undetermined
	74.0	1559.0		1687.7	Undetermined
	77.0	1532.0		1685.9	Undetermined
	80.0	1513.0		1684.0	Undetermined
	86.0	1468.0		1680.0	Undetermined
CH₃CN-β	Temp (K)	Density (kg·m ⁻³)	Technique	Adopted density (kg·m ⁻³)	Phase
Hudson (2020)	15.0	778.0	QCM	1126.5	Amorphous
Yarnall & Hudson (2022)	130.0	1073.0	QCM	1095.8	Crystalline
C₂H₅CN	Temp (K)	Density (kg·m ⁻³)	Technique	Adopted density (kg·m ⁻³)	Phase
Hudson (2020)	15.0	703.0	QCM	1053.8	Amorphous
Yarnall & Hudson (2022)	110.0	992.0	QCM	1009.9	Crystalline

Table 19. Additional experimental parameters for each tholin production facility included in this work. The unit for the gas flow rate is standard cubic centimeters per minute (sccm). *: Reaction time is 72 h for the samples made with cold plasma discharge and 144 h for the samples made with UV lamp. References: [a] Trainer et al. (2006); [b] Hörst & Tolbert (2013); [c] Sekine et al. (2008); [d] Imanaka et al. (2004); [e] Imanaka et al. (2012); [f] He et al. (2017); [g] Li et al. (2022); [h] Szopa et al. (2006); [i] Sciamma-O’Brien et al. (2017).

Laboratory location (Setup)	Pressure (mbar)	Temperature (K)	Reaction time (h)	Irradiation time	Gas flow rate (sccm)	Ref.
UC Boulder (Tolbert setup)	800-850	300	N/A	N/A	100	[a, b]
NASA ARC 1 (tholin-RF system)	0.26-1.6	300	31-65	N/A	24-41	[c, d, e]
JHU (PHAZER)	2.67	100-300	72-144*	3 s	10	[f, g]
LATMOS (PAMPRE)	0.2-10	300	8-32	N/A	N/A	[h]
UNI (PAC)	670	300	72	3 min	20	[g]
NASA ARC 2 (COSmIC)	30	150	5-13	3.5 μ s	2000	[g, i]

Table 20. Calculated total surface tension (γ_l) of Titan-relevant organic liquids using the three empirical approaches (Equations 19, 20, and 21) at the triple point of each species and the accuracy (the “Acc” column) of the calculated values compared to Yaws (2014).

Species	MacLeod-Sugden method (Equation 19)			Brock-Bird method (Equation 20)		Pitzer method (Equation 21)	
	Parachor ($\text{mN}\cdot\text{m}^{-1}$) ^{1/4} × ($\text{cm}^3\cdot\text{mol}^{-1}$)	$\gamma_l(T_{tri})$ ($\text{mN}\cdot\text{m}^{-1}$)	Acc. (%)	$\gamma_l(T_{tri})$ ($\text{mN}\cdot\text{m}^{-1}$)	Acc. (%)	$\gamma_l(T_{tri})$ ($\text{mN}\cdot\text{m}^{-1}$)	Acc. (%)
CH ₄	71.0	15.97	13.63	16.24	12.17	18.05	2.37
C ₂ H ₆	111.0	33.46	2.96	31.94	1.73	34.27	5.45
C ₂ H ₄	99.1	28.63	3.19	27.55	6.85	29.80	0.75
C ₂ H ₂	89.6	20.46	9.03	20.11	7.13	20.91	11.40
C ₄ H ₂	148.2	55.53	N/A	16.10	N/A	16.91	N/A
C ₆ H ₆	205.7	30.70	0.35	29.83	3.15	31.34	1.73
C ₃ H ₈	151.0	39.72	11.33	36.88	3.35	39.16	9.76
C ₃ H ₆	139.1	41.56	8.26	37.62	1.99	39.97	4.11
C ₃ H ₄ -a	129.6	40.40	34.95	41.25	37.81	44.03	47.08
C ₃ H ₄ -p	129.6	37.58	25.91	33.95	13.76	35.04	17.41
HCN	82.6	25.22	13.78	26.76	20.72	28.04	26.50
HC ₃ N	141.2	27.75	N/A	24.11	N/A	24.76	N/A
CO ₂	68.1	11.05	33.52	19.41	16.80	17.11	2.96
CH ₃ CN	122.6	41.44	10.34	39.12	4.15	41.01	9.19
C ₂ H ₅ CN	162.6	48.93	21.46	44.20	9.72	46.34	15.02
C ₂ H ₃ CN	150.7	43.58	9.71	42.68	7.45	44.60	12.28
C ₂ N ₂	134.2	38.98	69.02	24.80	7.54	25.86	12.13
C ₄ N ₂	192.8	36.67	N/A	44.48	N/A	48.01	N/A

REFERENCES

- Aadsen, D. R. 1975, Ph.D. Thesis
- Amamchyan, R. G. & Moroz, A. I. 1965, Tr. Vses. Nauchn.-Issled. Inst. Kislородn. Mashinostr., 10, 150.
- Amey, R. L. & Cole, R. H. 1964, JChPh, 40, 146. doi:10.1063/1.1724850
- Anderson, C. M. & Samuelson, R. E. 2011, Icarus, 212, 762. doi:10.1016/j.icarus.2011.01.024
- Anderson, C. M., Samuelson, R. E., Achterberg, R. K., et al. 2014, Icarus, 243, 129. doi:10.1016/j.icarus.2014.09.007
- Anderson, C. M., Samuelson, R. E., Yung, Y. L., et al. 2016, Geophys. Res. Lett., 43, 3088. doi:10.1002/2016GL067795
- Anderson, C. M., Samuelson, R. E., & Nna-Mvondo, D. 2018, SSRv, 214, 125. doi:10.1007/s11214-018-0559-5
- Antoine, C. 1888, C. R. Acad. Sci., 107, 681.
- Antson, O. K., Tilli, K. J., & Andersen, N. H. 1987, Acta Cryst., 43(3). 296. doi: 10.1107/S0108768187097866.
- Atreya, S. K., Adams, E. Y., Niemann, H. B., et al. 2006, Planet. Space Sci., 54, 1177. doi:10.1016/j.pss.2006.05.028
- Bacon, G. E., Curry, N. A., & Wilson, S. A. 1964, Proceedings of the Royal Society of London Series A, 279, 98. doi:10.1098/rspa.1964.0092
- Barnes, J. W., Bow, J., Schwartz, J., et al. 2011, Icarus, 216, 136. doi:10.1016/j.icarus.2011.08.022
- Barnes, J. W., Turtle, E. P., Trainer, M. G., et al. 2021, PSJ, 2, 130. doi:10.3847/PSJ/abfdcf
- Barrow, M. J., 1981, Acta Cryst. B, 37, 2239. doi:10.1107/S0567740881008510
- Barth, E. L. & Toon, O. B. 2003, Icarus, 162, 94. doi:10.1016/S0019-1035(02)00067-2

- Barth, E. L. & Toon, O. B. 2006, *Icarus*, 182, 230. doi:10.1016/j.icarus.2005.12.017
- Barth, E. L. 2017, *Planet. Space Sci.*, 137, 20. doi:10.1016/j.pss.2017.01.003
- Barth, E. L. 2019, EPSC-DPS Joint Meeting 2019
- Barth, E. L. submitted.
- Behn, U. 1900, *Annalen der Physik*, 308, 733. doi:10.1002/andp.19003081209
- Benilan, Y., Bruston, P., Raulin, F., et al. 1994, *J. Geophys. Res.*, 99, 17069. doi:10.1029/94JE01087
- Benkoski, J. J., Luedeman, W. L., Teehan, J. O., et al. 2019, *Planet. Space Sci.*, 179, 104721. doi:10.1016/j.pss.2019.104721
- Blanc, J., Brecher, C., & Halford, R. S. 1962, *JChPh*, 36, 2654. doi:10.1063/1.1732348
- Boese, R., Weiss, H. C., & Bläser, D. 1999, *Angewandte Chemie International Edition*, 38(7), 988. doi:10.1002/(SICI)1521-3773(19990401)38:7:988::AID-ANIE988;3.0.CO;2-0
- Bol'shutkin, D. N., Gasan, V. M., Prokhvatilov, A. I. 1971, *Journal of Structural Chemistry*, 12(4), 670. doi:10.1007/BF00743694
- Bouchez, A. H. & Brown, M. E. 2005, *ApJL*, 618, L53. doi:10.1086/427693
- Brackmeyer, T., Erker, G., Fröhlich, R., Prigge, J. & Peuchert, U. 1997, *Chem. Ber. Rec*, 130, 899.
- Brand, H. E, Gu, Q., Kimpton, J. A., Auchetl, R. & Ennis, C. 2020, *Journal of synchrotron radiation*, 27(1), 212. doi:10.1107/S1600577519015911
- Bredig, G. & Teichmann, L. 1925, *Zeitschrift für Elektrochemie und angewandte physikalische Chemie*, 31(8), 449. doi:10.1002/bbpc.19250310821
- Brock, J. R. & Bird, R. B 1955, *AICHe Journal*, 1(2), 174. doi:10.1002/aic.690010208
- Brouet, Y., Lévassieur-Regourd, A. C., Sabouroux, P., et al. 2016, *MNRAS*, 462, S89. doi:10.1093/mnras/stw2151
- Brown, G. N. & Ziegler, W. T. 1980, *Adv. Cryog. Eng.*, 25, 662. doi:10.1007/978-1-4613-9856-1_76
- Brown, M. E., Bouchez, A. H., & Griffith, C. A. 2002, *Nature*, 420, 795. doi:10.1038/nature01302
- Brown, M. E., Roberts, J. E., & Schaller, E. L. 2010, *Icarus*, 205, 571. doi:10.1016/j.icarus.2009.08.024
- Brunetto, R., Caniglia, G., Baratta, G. A., et al. 2008, *ApJ*, 686, 1480. doi:10.1086/591509
- Cable, M. L., Hörst, S. M., Hodyss, R., et al. 2012, *Chemical Reviews*, 112(3), 1882. doi:10.1021/cr200221x
- Cable, M. L., Runčevski, T., Maynard-Casely, H. E., et al. 2021, *Accounts of Chemical Research*, 54(15), 3050. doi:10.1021/acs.accounts.1c00250
- Chen, J.-P., Hazra, A., & Levin, Z. 2008, *Atmospheric Chemistry & Physics*, 8, 7431. doi:10.5194/acp-8-7431-2008
- Chevrier, V. F., Luspay-Kuti, A., & Singh, S. 2015, 46th Annual Lunar and Planetary Science Conference
- Chickos, J. S., Braton, C. M., Hesse, D. G., & Liebman, J. F. 1991, *The Journal of Organic Chemistry*, 56(3), 927. doi:10.1021/jo00003a007
- Choi, K. Y., Duyker, S. G., Maynard-Casely, H. E., et al. 2020, *ACS Earth and Space Chemistry*, 4, 1324. doi:10.1021/acsearthspacechem.0c00105
- Clusius, K. & Weigand, K. 1940, *Zeitschrift für Physikalische Chemie*, 46(1), 1. doi:10.1515/zpch-1940-4602
- Comola, F., Kok, J. F., Lora, J. M., et al. 2022, *Geophys. Res. Lett.*, 49, e97913. doi:10.1029/2022GL097913
- Cordier, D., Mousis, O., Lunine, J. I., et al. 2009, *ApJL*, 707, L128. doi:10.1088/0004-637X/707/2/L128
- Cordiner, M. A., Palmer, M. Y., Nixon, C. A., et al. 2015, *ApJL*, 800, L14. doi:10.1088/2041-8205/800/1/L14
- Cordier, D., García-Sánchez, F., Justo-García, D. N., et al. 2017, *Nature Astronomy*, 1, 0102. doi:10.1038/s41550-017-0102
- Cordier, D., Bonhommeau, D. A., Vu, T. H., et al. 2021, *A&A*, 653, A80. doi:10.1051/0004-6361/202140789
- Cordier, D. & Carrasco, N. 2019, *Nature Geoscience*, 12, 315. doi:10.1038/s41561-019-0344-4
- Coustenis, A., Schmitt, B., Khanna, R. K., et al. 1999, *Planet. Space Sci.*, 47, 1305. doi:10.1016/S0032-0633(99)00053-7
- Coustenis, A., Salama, A., Schulz, B., et al. 2003, *Icarus*, 161, 383. doi:10.1016/S0019-1035(02)00028-3
- Coustenis, A., Jennings, D. E., Nixon, C. A., et al. 2010, *Icarus*, 207, 461. doi:10.1016/j.icarus.2009.11.027

- Coustenis, A., Jennings, D. E., Achterberg, R. K., et al. 2016, *Icarus*, 270, 409. doi:10.1016/j.icarus.2015.08.027
- Coustenis, A., Jennings, D. E., Achterberg, R. K., et al. 2020, *Icarus*, 344, 113413. doi:10.1016/j.icarus.2019.113413
- Cox, E. G., Cruickshank, D. W. J., & Smith, J. A. S. 1958, *Proceedings of the Royal Society of London Series A*, 247, 1. doi:10.1098/rspa.1958.0167
- Curl, R. F & Pitzer, K. 1958, *Industrial & Engineering Chemistry*, 50(2), 265. doi:10.1142/9789812795960_0046
- Curtis, D. B., Glandorf, D. L., Toon, O. B., et al. 2005, *Journal of Physical Chemistry A*, 109, 1382. doi:10.1021/jp045596h
- Curtis, D. B., Hatch, C. D., Hasenkopf, C. A., et al. 2008, *Icarus*, 195, 792. doi:10.1016/j.icarus.2008.02.003
- Dannhauser, W. & Flueckinger, A. F. 1963, *JChPh*, 38, 69. doi:10.1063/1.1733497
- Dannhauser, W. & Flueckinger, A. F. 1964, *J. Phys. Chem.*, 68(7), 1814. doi:10.1021/j100789a024
- Daubert, T. E. & Danner, R. P. 1989, *Physical and thermodynamic properties of pure chemicals: data compilation* (1st ed.; Washington, DC: Taylor & Francis)
- de Kok, R. J., Teanby, N. A., Maltagliati, L., et al. 2014, *Nature*, 514, 65. doi:10.1038/nature13789
- De Smedt, J. & Keesom, W. H. 1924, In *Proceedings of the Koninklijke Akademie Van Wetenschappen Te Amsterdam*, 27, 839.
- Domingo, M., Luna, R., Satorre, M. A., et al. 2015, *Journal of Low Temperature Physics*, 181, 1. doi:10.1007/s10909-015-1326-6
- Domingo, M., Luna, R., Satorre, M. Á., et al. 2021, *ApJ*, 906, 81. doi:10.3847/1538-4357/abc5c5
- Drobyshev, A., Aldiyarov, A., Sokolov, D., et al. 2017, *Low Temperature Physics*, 43, 724. doi:10.1063/1.4985981
- Dubois, D., Iraci, L. T., Barth, E. L., et al. 2021, *PSJ*, 2, 121. doi:10.3847/PSJ/ac06d5
- Dulmage, W. J. & Lipscomb, W. N. 1951, *Acta Cryst.*, 4(4), 330. doi:10.1107/S0365110X51001070
- Duncan, N. E. & Janz, G. J. 1955, *JChPh*, 23, 434. doi:10.1063/1.1742007
- Duschek, W., Kleinrahm, R., & Wagner, W., 1990, *The Journal of Chemical Thermodynamics*, 22(9), 841. doi:10.1016/0021-9614(90)90173-N
- Dykyj, J., Svoboda, J., Wilhoit, R. C., et al. 1999, *Vapor Pressure of Chemicals, Subvol. A* (1st ed.; Verlag, Germany: Springer)
- Egloff, G. & Kuder, R. C. 1942, *J. Phys. Chem.*, 46(2), 296. doi:10.1021/j150416a008
- Enjalbert, R. & Galy, J. 2002, *Acta Crystallographica Section B: Structural Science*, 58(6), 1005. doi:10.1107/S0108768102017603
- Finke, H. L., Messerly, J. F., & Todd, S. S., 1972, *The Journal of Chemical Thermodynamics*, 4(3), 359. doi:10.1016/0021-9614(72)90019-5
- Flasar, F. M., Kunde, V. G., Abbas, M. M., et al. 2004, *The Cassini-Huygens Mission*, 169. doi:10.1007/1-4020-3874-7_4
- Flasar, F. M., Achterberg, R. K., Conrath, B. J., et al. 2005, *Science*, 308, 975. doi:10.1126/science.1111150
- Fray, N. & Schmitt, B. 2009, *Planet. Space Sci.*, 57, 2053. doi:10.1016/j.pss.2009.09.011
- Fowkes, F. M. 1964, *Industrial & Engineering Chemistry*, 56, 40. doi: 10.1021/ie50660a008
- Fulchignoni, M., Ferri, F., Angrilli, F., et al. 2005, *Nature*, 438, 785. doi:10.1038/nature04314
- Gee, N., Shinsaka, K., Dodelet, J. P. & Freeman, G. R., 1986, *The Journal of Chemical Thermodynamics*, 18(3), 221. doi:10.1016/0021-9614(86)90050-9
- Goodman, B. T., Wilding, W. V., Oscarson, J. L., et al. 2004, *Journal of Chemical & Engineering Data*, 49(6), 1512. doi:10.1021/je034220e
- Greer, S. C., & Meyer, L. 1969, *Zeitschrift für angewandte Physik*, 27(3), 198.
- Griffith, C. A., Owen, T., Miller, G. A., et al. 1998, *Nature*, 395, 575. doi:10.1038/26920
- Griffith, C. A., Hall, J. L., & Geballe, T. R. 2000, *Science*, 290, 509. doi:10.1126/science.290.5491.509
- Griffith, C. A., Penteadó, P., Baines, K., et al. 2005, *Science*, 310, 474. doi:10.1126/science.1117702
- Griffith, C. A., Penteadó, P., Rannou, P., et al. 2006, *Science*, 313, 1620. doi:10.1126/science.1128245
- Grima, C., Mastrogiuseppe, M., Hayes, A. G., et al. 2017, *Earth and Planetary Science Letters*, 474, 20. doi:10.1016/j.epsl.2017.06.007

- Guez, L., Bruston, P., Raulin, F., et al. 1997, *Planet. Space Sci.*, 45, 611. doi:10.1016/S0032-0633(97)00018-4
- Gunn, A. & Jerolmack, D. J. 2022, *Nat. Astron.*, 6, 923. doi: 10.1038/s41550-022-01669-0.
- Hanel, R., Conrath, B., Flasar, F. M., et al. 1981, *Science*, 212, 192. doi:10.1126/science.212.4491.192
- Hanley, J., Thompson, G. L., Roe, H. G., et al. 2016, AAS/DPS Meeting Abstracts
- Hannan, R. B., & Collin, R. L. 1953, *Acta. Cryst.*, 6(4), 350. doi:10.1107/S0365110X53000922
- Haynes, W. M. 2014, Haynes, W. M., ed. 2014, *CRC Handbook of Chemistry and Physics*, 95th edn. (Boca Raton, FL: CRC Press), ISBN 9781482208689.
- He, C., Hörst, S. M., Riemer, S., et al. 2017, *ApJL*, 841, L31. doi:10.3847/2041-8213/aa74cc
- Heuse, W. 1930, *Zeitschrift für Physikalische Chemie*, 147, 266. doi:10.1515/zpch-1930-14723
- Hill, W. W., Rosenzweig, S., & Franck, E. U., 1990, *Berichte der Bunsengesellschaft für physikalische Chemie*, 94(5), 564. doi:10.1002/bbpc.19900940506
- Hörst, S. M. & Tolbert, M. A. 2013, *ApJL*, 770, L10. doi:10.1088/2041-8205/770/1/L10
- Hörst, S. M. 2017, *Journal of Geophysical Research (Planets)*, 122, 432. doi:10.1002/2016JE005240
- Hudson, R. L. 2020, *Icarus*, 338, 113548. doi:10.1016/j.icarus.2019.113548
- Hudson, R. L., Gerakines, P. A., Yarnall, Y. Y., et al. 2021, *Icarus*, 354, 114033. doi:10.1016/j.icarus.2020.114033
- Hudson, R. L., Yarnall, Y. Y., & Gerakines, P. A. 2022, *PSJ*, 3, 120. doi:10.3847/PSJ/ac67a5
- Imanaka, H., Khare, B. N., Elsila, J. E., et al. 2004, *Icarus*, 168, 344. doi:10.1016/j.icarus.2003.12.014
- Imanaka, H., Cruikshank, D. P., Khare, B. N., et al. 2012, *Icarus*, 218, 247. doi:10.1016/j.icarus.2011.11.018
- Israelachvili, J. N. 2011, *Intermolecular and Surface Forces* (3rd ed.; New York: Academic)
- Jolly, A., Cottini, V., Fayt, A., et al. 2015, *Icarus*, 248, 340. doi:10.1016/j.icarus.2014.10.049
- Kaelble, D. H. 1970, *The Journal of Adhesion*, 2, 66. doi:10.1080/0021846708544582
- Keesom, W. H. & Köhler, J. W. L. 1934, *Physica*, 1, 655. doi:10.1016/S0031-8914(34)80253-4
- Keesom, W. H. & Köhler, J. W. L. 1934, *Physica*, 1, 167. doi:10.1016/S0031-8914(34)90021-5
- Khanna, R. K., Perera-Jarmer, M. A., & Ospina, M. J. 1987, *Spectrochimica Acta Part A: Molecular Spectroscopy*, 43, 421. doi:10.1016/0584-8539(87)80128-9
- Khanna, R. K. 2005, *Icarus*, 177, 116. doi:10.1016/j.icarus.2005.02.014
- Khanna, R. K. 2005, *Icarus*, 178, 165. doi:10.1016/j.icarus.2005.03.011
- Kirchhoff, G. 1858, *Annalen der Physik*, 180, 612. doi:10.1002/andp.18581800806
- Klimenko, N. A., Gal'tsov, N. N., & Prokhvatilov, A. I. 2008, *Low Temperature Physics*, 34, 1038. doi:10.1063/1.3029759
- Köhler, H. 1936, *The nucleus in and the growth of hygroscopic droplets*, 32, 1152. doi:10.1039/TF9363201152
- Kozhin, V. M. 1954, *Zh. Fiz. Khim.*, 28, 566.
- Krause, P. F. & Friedrich, H. B. 1972, *J. Phys. Chem.*, 76(8), 1140. doi:10.1021/j100652a009
- Krishna Pillai, M. G. & Cleveland, F. F. 1961, *Journal of Molecular Spectroscopy*, 5, 212. doi:10.1016/0022-2852(61)90084-4
- Kroenlein, K., Muzny, C., Kazakov, A., et al. 2011, NIST/TRC Web Thermo Tables (WTT) NIST Standard Reference Subscription Database 3 - Professional Edition Version 2, NIST/TRC Web Thermo Tables (WTT) - Professional Edition, [online], <http://wtt-pro.nist.gov/> (Accessed May 28, 2022).
- Kunde, V. G., Aikin, A. C., Hanel, R. A., et al. 1981, *Nature*, 292, 686. doi:10.1038/292686a0
- Lapôtre, M. G. A., Malaska, M. J., & Cable, M. L. 2022, *Geophys. Res. Lett.*, 49, e97605. doi:10.1029/2021GL097605
- Lavvas, P., Griffith, C. A., & Yelle, R. V. 2011, *Icarus*, 215, 732. doi:10.1016/j.icarus.2011.06.040
- Lavvas, P., Lellouch, E., Strobel, D. F., et al. 2021, *Nat. Astron.*, 5, 289. doi:10.1038/s41550-020-01270-3
- Lespieau, R., & Prevost, C., 1925, *C.R. Hebd. Seances Acad. Sci.*, 180, 676.
- Lethuillier, A., Le Gall, A., Hamelin, M., et al. 2018, *Journal of Geophysical Research (Planets)*, 123, 807. doi:10.1002/2017JE005416
- Li, J., Yu, X., Sciamma-O'Brien, E., et al. 2022, *PSJ*, 3, 2. doi:10.3847/PSJ/ac3d27

- Lias, S. G., 2023, in NIST Chemistry WebBook, Eds. P. J. Linstrom & W. G. Mallard (Gaithersburg, MD: National Institute of Standards and Technology), 20899. doi:10.18434/T4D303.
- Lifshitz, E. M., & Hamermesh, M., 1992, The theory of molecular attractive forces between solids. In *Perspectives in Theoretical Physics*, Pergamon.
- Lellouch, E., Bézard, B., Flasar, F. M., et al. 2014, *Icarus*, 231, 323. doi:10.1016/j.icarus.2013.12.016
- Loeffler, M. J., Moore, M. H., & Gerakines, P. A. 2016, *ApJ*, 827, 98. doi:10.3847/0004-637X/827/2/98
- Lombardo, N. A., Nixon, C. A., Greathouse, T. K., et al. 2019, *ApJL*, 881, L33. doi:10.3847/2041-8213/ab3860
- Lorenz, R. D., Wall, S., Radebaugh, J., et al. 2006, *Science*, 312, 724. doi:10.1126/science.1123257
- Maass, O. & Wright, C. H. 1921, *Journal of the American Chemical Society*, 43(5), 1098. doi:10.1021/ja01438a013
- Maass, O. & Barnes, W. H. 1926, *Proceedings of the Royal Society of London Series A*, 111, 224. doi:10.1098/rspa.1926.0065
- MacKenzie, S. M., Barnes, J. W., Sotin, C., et al. 2014, *Icarus*, 243, 191. doi:10.1016/j.icarus.2014.08.022
- Macleod, D. B. 1923, *Transactions of the Faraday Society*, 19, 38. doi:10.1039/TF9231900038
- Maguire, W. C., Hanel, R. A., Jennings, D. E., et al. 1981, *Nature*, 292, 683. doi:10.1038/292683a0
- Mahata, P. C. & Alofs, D. J. 1975, *Journal of Atmospheric Sciences*, 32, 116. doi:10.1175/1520-0469(1975)032<0116:ICNTEO>2.0.CO;2
- Mangan, T. P., Salzmann, C. G., Plane, J. M. C., et al. 2017, *Icarus*, 294, 201. doi:10.1016/j.icarus.2017.03.012
- Manzhelii, V. G. & Tolkachev, A. M. 1964, *Soviet Physics-Solid State*, 5(12), 2506.
- Marlin, T. C., Cable, M. L., Vu, T., et al. 2022, *LPI Contributions*, 2678, 2321
- Mark, H. & Pohland, E. 1925, *Zeitschrift für Kristallographie-Crystalline Materials*, 62(1-6), 103. doi:10.1524/zkri.1925.62.1.103.
- Maynard-Casely, H. E., Hester, J. R., & Brand, H. E. 2020, *IUCrJ*, 7(5), 844. doi:10.1107/S2052252520007460
- Mayo, L. A. & Samuelson, R. E. 2005, *Icarus*, 176, 316. doi:10.1016/j.icarus.2005.01.020
- McDonald, J. E. 1953, *Journal of Atmospheric Sciences*, 10, 416. doi:10.1175/1520-0469(1953)010<0416:HNOSWD>2.0.CO;2
- McDonald, J. E. 1964, *Journal of Atmospheric Sciences*, 21, 76. doi:10.1175/1520-0469(1964)021<0076:OACGTM>2.0.CO;2
- McIntosh, D. 1907, *J. Phys. Chem.*, 11(4), 306. doi:10.1021/j150085a005
- McMullan, R. K. Kvick, Å., & Popelier P., 1992, *Acta Cryst. Section B: Structural Science*, 48(5), 726. doi:10.1107/S0108768192004774
- Miller, D. G. & Thodos, G. 1963, *Ind. Eng. Chem. Fundamentals*, 2(1), 78. doi:10.1021/i160005a015
- Molpeceres, G., Satorre, M. A., Ortigoso, J., et al. 2016, *ApJ*, 825, 156. doi:10.3847/0004-637X/825/2/156
- Molpeceres, G., Satorre, M. A., Ortigoso, J., et al. 2017, *MNRAS*, 466, 1894. doi:10.1093/mnras/stw3166
- Moore, M. H., Ferrante, R. F., Moore, W. J., et al. 2010, *ApJS*, 191, 96. doi:10.1088/0067-0049/191/1/96
- Mooy, H. H. 1931, *Nature*, 127, 707. doi:10.1038/127707c0
- Morehouse, F. R. & Maass, O. 1931, *Canadian Journal of Research*, 5, 306. doi:10.1139/cjr31-070
- Moses, J. I., Allen, M., & Yung, Y. L. 1992, *Icarus*, 99, 318. doi:10.1016/0019-1035(92)90149-2
- Mueller, P. R. 1969, Ph.D. Thesis
- Niemann, H. B., Atreya, S. K., Demick, J. E., et al. 2010, *Journal of Geophysical Research (Planets)*, 115, E12006. doi:10.1029/2010JE003659
- Nixon, C. A., Jennings, D. E., Bézard, B., et al. 2013, *ApJL*, 776, L14. doi:10.1088/2041-8205/776/1/L14
- Nixon, C. A., Thelen, A. E., Cordiner, M. A., et al. 2020, *AJ*, 160, 205. doi:10.3847/1538-3881/abb679
- Nna-Mvondo, D., Anderson, C. M., & Samuelson, R. E. 2019, *Icarus*, 333, 183. doi:10.1016/j.icarus.2019.05.003
- Onken, U., Rarey-Nies, J., & Gmehling, J. 1989, *International Journal of Thermophysics*, 10, 739. doi:10.1007/BF00507993

- Orton, G. S., Fletcher, L. N., Moses, J. I., et al. 2014, *Icarus*, 243, 494. doi:10.1016/j.icarus.2014.07.010
- Owens, D. K., & Wendt, R. C. 1969, *Journal of Applied Polymer Science*, 13, 1741. doi:10.1002/app.1969.070130815
- Palmer, M. Y., Cordiner, M. A., Nixon, C. A., et al. 2017, *Science Advances*, 3, e1700022. doi:10.1126/sciadv.1700022
- Parkes, A. S., & Hughes, R. E. 1963, *Acta Cryst.*, 16, 734. doi:10.1107/S0365110X63001924
- Perry, J. H., & Porter, F. 1926, *Journal of the American Chemical Society*, 48(2), 299. doi:10.1021/ja01413a001
- Pitzer, K. S., 1995, *J. Phys. Chem.*, 99(35), 13070. doi:10.1021/j100035a006
- Poggiali, V., Hayes, A. G., Mastrogiuseppe, M., et al. 2020, *Journal of Geophysical Research (Planets)*, 125, e06558. doi:10.1029/2020JE006558
- Poling, B. E., 2002, *Properties of gases and liquids*. McGraw-Hill Education.
- Porco, C. C., Baker, E., Barbara, J., et al. 2005, *Nature*, 434, 159. doi:10.1038/nature03436
- Prokhvatilov, A. I., & Isakina, A. P. 1983, *Fizika nizkikh temperatur*, 9(4), 419.
- Pruppacher, H. R., & Klett, J. D. 1978, *Microphysics of Clouds and Precipitation* (1st ed.; Cham: Springer)
- Putnam, W. E., Marvin McEachern, D., & Kilpatrick, J. E. 1965, *JChPh*, 42, 749. doi:10.1063/1.1696002
- Quayle, O. R. 1953, *Chemical Reviews*, 53(3), 439. doi:10.1021/cr60166a003
- Rabel, W. 1971, *Farbe und Lack*, 77, 997.
- Rankine, W. M. 1866, *Proc. R. Soc. Edinb.*, 5, 449. doi:10.1017/S0370164600041201
- Richards, T. W., Bartlett, E. P., & Hodges, J. H., 1921, *J. Am. Chem. Soc.*, 43(7), 1538. doi:10.1021/ja01440a014
- Rodriguez, S., Le Mouélic, S., Rannou, P., et al. 2011, *Icarus*, 216, 89. doi:10.1016/j.icarus.2011.07.031
- Roe, H. G., de Pater, I., Macintosh, B. A., et al. 2002, *ApJ*, 581, 1399. doi:10.1086/344403
- Romanescu, C., Marschall, J., Kim, D., et al. 2010, *Icarus*, 205, 695. doi:10.1016/j.icarus.2009.08.016
- Roux, J. A., Wood, B. E., Smith, A. M., et al. 1980, Final Report, 1 Oct. 1978 - 1 Sep. 1979 ARO, Inc., Arnold Air Force Station, TN.
- Rumble, J. R. 2020, Boca Raton: CRC Press, 2020, 102nd ed., edited by Rumble, J. R.
- Růžička, K., Fulem, M., Červinka, C., 2014, *The Journal of Chemical Thermodynamics*, 68, 40. doi:10.1016/j.jct.2013.08.022.
- Sagan, C. & Thompson, W. R. 1984, *Icarus*, 59, 133. doi:10.1016/0019-1035(84)90018-6
- Saggiomo, A. J. 1957, *J. Org. Chem.*, 22(10), 1171. doi:10.1021/jo01361a009
- Samuelson, R. E., Mayo, L. A., Knuckles, M. A., et al. 1997, *Planet. Space Sci.*, 45, 941. doi:10.1016/S0032-0633(97)00088-3
- Samuelson, R. E., Smith, M. D., Achterberg, R. K., et al. 2007, *Icarus*, 189, 63. doi:10.1016/j.icarus.2007.02.005
- Satorre, M. Á., Domingo, M., Millán, C., et al. 2008, *Planet. Space Sci.*, 56, 1748. doi:10.1016/j.pss.2008.07.015
- Satorre, M. Á., Millán, C., Molpeceres, G., et al. 2017, *Icarus*, 296, 179. doi:10.1016/j.icarus.2017.05.005
- Satorre, M. Á., Luna, R., Millán, C., et al. 2018, *Astrophysics and Space Science Library*, 451, 51. doi:10.1007/978-3-319-90020-9_4
- Sciamma-O'Brien, E., Upton, K. T., & Salama, F. 2017, *Icarus*, 289, 214. doi:10.1016/j.icarus.2017.02.004
- Schallamach, A. 1939, *Proceedings of the Royal Society of London Series A*, 171, 569. doi:10.1098/rspa.1939.0084
- Schaller, E. L., Brown, M. E., Roe, H. G., et al. 2006, *Icarus*, 182, 224. doi:10.1016/j.icarus.2005.12.021
- Schaller, E. L., Brown, M. E., Roe, H. G., et al. 2006, *Icarus*, 184, 517. doi:10.1016/j.icarus.2006.05.025
- Schulze, W. & Abe, H. 1980, *Chemical Physics*, 52, 381. doi:10.1016/0301-0104(80)85240-2
- Schurmeier, L. R. & Dombard, A. J. 2018, *Icarus*, 305, 314. doi:10.1016/j.icarus.2017.10.034
- Sebree, J. A., Roach, M. C., Shipley, E. R., et al. 2018, *ApJ*, 865, 133. doi:10.3847/1538-4357/aadba1
- Seiber, B. A., Smith, A. M., Wood, B. E., et al. 1971, *ApOpt*, 10, 2086. doi:10.1364/AO.10.002086

- Seinfeld, J. H. & Pandis, P. N. 2014, John Wiley & Sons
- Sekine, Y., Imanaka, H., Matsui, T., et al. 2008, *Icarus*, 194, 186.
doi:10.1016/j.icarus.2007.08.031
- Sevrugova, N., Sokorskii, V., & Zhavoronkov, N., 1964, *Zh. Prikl. Khim*, 37, 1989.
- Shallcross, F. V. & Carpenter, G. B. 1958, *Acta Crystallographica*, 11(7), 490.
doi:10.1107/S0365110X58001365
- Shinbayeva, A. K., Drobyshev, A. S., Ramos, M., & Sokolov, D. Y., 2017, *Bulletin of the Al-Farabi Kazakh National University*, 60(1), 28.
- Simon, A. & Peters, K. 1980, *Acta Cryst. B*, 36, 2750. doi:10.1107/S0567740880009879
- Singh, S., McCord, T. B., Combe, J.-P., et al. 2016, *ApJ*, 828, 55.
doi:10.3847/0004-637X/828/1/55
- Sinozaki, H., Hara, R., & Mitsukuri, S. 1926, *Bulletin of the Chemical Society of Japan*, 1(4), 59. doi:10.1246/bcsj.1.59
- Smyth, C. P. & McNeight, S. A. 1936, *Journal of the American Chemical Society*, 58(9), 1723.
doi:10.1021/ja01300a065
- Soderblom, L. A., Kirk, R. L., Lunine, J. I., et al. 2007, *Planet. Space Sci.*, 55, 2025.
doi:10.1016/j.pss.2007.04.014
- Steffens, B. L., Nixon, C. A., Sung, K., et al. 2022, *PSJ*, 3, 59. doi:10.3847/PSJ/ac53ad
- Stewart, J. W. & La Rock, R. I. 1958, *JChPh*, 28, 425. doi:10.1063/1.1744150
- Straus, F. & Kollek, L. 1926, *Berichte der deutschen chemischen Gesellschaft (A and B Series)*, 59(8), 1664.
doi:10.1002/cber.19260590804
- Stull, D. R. 1947, *Industrial & Engineering Chemistry*, 39(4), 517. doi:10.1021/ie50448a022
- Sugawara, T. & Kanda, E. 1952, *Sci. Rep. Res. Inst., Tohoku Univ., Ser. A*, 4, 607.
doi:10.50974/00041629.
- Sugden, S. 1924, *Journal of the Chemical Society, Transactions*, 125, 1177.
doi:10.1039/CT9242501177
- Sylvestre, M., Teanby, N. A., Dobrijevic, M., et al. 2020, *AJ*, 160, 178.
doi:10.3847/1538-3881/abafb2
- Szopa, C., Cernogora, G., Boufendi, L., et al. 2006, *Planet. Space Sci.*, 54, 394.
doi:10.1016/j.pss.2005.12.012
- Tan, S. P., & Kargel, J. S. 2018, *Fluid Ph. Equilibria.*, 458, 153.
doi:10.1016/j.fluid.2017.11.020
- Teanby, N. A., Sylvestre, M., Sharkey, J., et al. 2019, *Geophys. Res. Lett.*, 46, 3079.
doi:10.1029/2018GL081401
- Thelen, A. E., Nixon, C. A., Chanover, N. J., et al. 2019, *Icarus*, 319, 417.
doi:10.1016/j.icarus.2018.09.023
- Thompson, W. R., Zollweg, J. A., & Gabis, D. H. 1992, *Icarus*, 97, 187.
doi:10.1016/0019-1035(92)90127-S
- Tolkachev, A. M., & Manzhelii V. G. 1966, *Soviet Physics-Solid State*, 7(7), 1711.
- Tokano, T., McKay, C. P., Neubauer, F. M., et al. 2006, *Nature*, 442, 432. doi:10.1038/nature04948
- Tomasko, M. G., Archinal, B., Becker, T., et al. 2005, *Nature*, 438, 765. doi:10.1038/nature04126
- Torrie, B. H. & Powell, B. M. 1989, *Journal of Physics Condensed Matter*, 1, 5827.
doi:10.1088/0953-8984/1/34/001
- Trainer, M. G., Pavlov, A. A., Dewitt, H. L., et al. 2006, *Proceedings of the National Academy of Science*, 103, 18035.
doi:10.1073/pnas.0608561103
- Turtle, E. P., Perry, J. E., McEwen, A. S., et al. 2009, *Geophys. Res. Lett.*, 36, L02204.
doi:10.1029/2008GL036186
- Turtle, E. P., Perry, J. E., Hayes, A. G., et al. 2011, *Science*, 331, 1414.
doi:10.1126/science.1201063
- van Nes, G. V. & Vos, A. 1978, *Acta Cryst. B*, 34(6), 1947. doi:10.1107/S0567740878007037
- van Nes, G. V. & Vos, A. 1979, *Acta Cryst. B*, 35(11), 2593. doi:10.1107/S0567740879009961
- van Nes, G. V. & van Bolhuis, F. 1979, *Acta Cryst. B*, 35, 2580.
doi:10.1107/S056774087900995X
- van Oss, C. J. 2006, *Interfacial Forces in Aqueous Media* (2nd ed.; Boca Raton, FL: CRC press)
- Vinatier, S., Schmitt, B., Bézard, B., et al. 2018, *Icarus*, 310, 89. doi:10.1016/j.icarus.2017.12.040
- Vuitton, V., Yelle, R. V., Klippenstein, S. J., et al. 2019, *Icarus*, 324, 120.
doi:10.1016/j.icarus.2018.06.013
- Wagner, W. 1973, *Cryogenics*, 13, 470.
doi:10.1016/0011-2275(73)90003-9
- Wang, C. C., Atreya, S. K., & Signorell, R. 2010, *Icarus*, 206, 787.
doi:10.1016/j.icarus.2009.11.022

- Wang, C. C., Kathrin Lang, E., & Signorell, R. 2010, *ApJL*, 712, L40. doi:10.1088/2041-8205/712/1/L40
- Weast, R. C. 1972, Weast, R. C., ed. 1972, *CRC Handbook of Chemistry and Physics*, 53th edn. (Boca Raton, FL: CRC Press).
- Weber, L. A. & Kilpatrick, J. E. 1962, *JChPh*, 36, 829. doi:10.1063/1.1732617
- Werner, O., 1929, *Z. Phys. Chem.*, 4(1), 371. doi: 10.1515/zpch-1929-0428
- Willacy, K., Allen, M., & Yung, Y. 2016, *ApJ*, 829, 79. doi:10.3847/0004-637X/829/2/79
- Witek, P. P. & Czechowski, L. 2015, *Planet. Space Sci.*, 105, 65. doi:10.1016/j.pss.2014.11.005
- Wohlfarth, C., Wohlfarth, B., & Lechner, M. D. 1996, *Refractive indices of organic liquids*. Springer-Verlag, Berlin: Springer. doi:10.1007/b85533
- Wood, B. E. & Roux, J. A. 1982, *Journal of the Optical Society of America (1917-1983)*, 72, 720
- Würflinger, A., 1980, *Berichte der Bunsengesellschaft für physikalische Chemie*, 84(7), 653. doi:10.1002/bbpc.19800840709
- Wye, L. C., Zebker, H. A., & Lorenz, R. D. 2009, *Geophys. Res. Lett.*, 36, L16201. doi:10.1029/2009GL039588
- Yaws, C. L., Richmond, P. C. 2014, *Thermophysical Properties of Chemicals and Hydrocarbons*. doi:10.1016/B978-081551596-8.50026-2
- Yaws, C. L., 2015, *The Yaws handbook of vapor pressure: Antoine coefficients*. Gulf Professional Publishing.
- Yarbrough, D. W. & Tsai, C. H. 1978, *Advances in Cryogenic Engineering*, 602-610.
- Yarnall, Y. Y. & Hudson, R. L. 2022, *Icarus*, 373, 114799. doi:10.1016/j.icarus.2021.114799
- Yokoyama, Y., & Ohashi, Y. 1998, *Bulletin of the Chemical Society of Japan*, 71(2), 345. doi: 10.1246/bcsj.71.345
- Yu, X., Hörst, S. M., He, C., et al. 2017, *Icarus*, 297, 97. doi:10.1016/j.icarus.2017.06.034
- Yu, X., Hörst, S. M., He, C., et al. 2018, *Journal of Geophysical Research (Planets)*, 123, 2310. doi:10.1029/2018JE005651
- Yu, X., Hörst, S. M., He, C., et al. 2020, *ApJ*, 905, 88. doi:10.3847/1538-4357/abc55d
- Yu, X., Hörst, S. M., He, C., et al. 2020, *Earth and Planetary Science Letters*, 530, 115996. doi:10.1016/j.epsl.2019.115996
- Yu, X., He, C., Zhang, X., et al. 2021, *Nat. Astron.*, 5, 822. doi:10.1038/s41550-021-01375-3
- Zacny, K., Lorenz, R., Rehnmark, F., et al. 2019, *IEEE Aerospace Conference*, 1. doi:10.1109/AERO.2019.8741887